WIND FORCED CHANGES AND VARIABILITY IN THE EAST AUSTRALIAN CURRENT

by

Katherine L. Hill, M.Sc, B.Sc(hons)

Submitted in fulfilment of the requirements
for the Degree of Doctor of Philosophy in Quantitative Marine Science
(A joint CSIRO and UTas PhD program in Quantitative Marine Science)

Institute of Antarctic and Southern Ocean Studies
University of Tasmania
submit date: August 2009

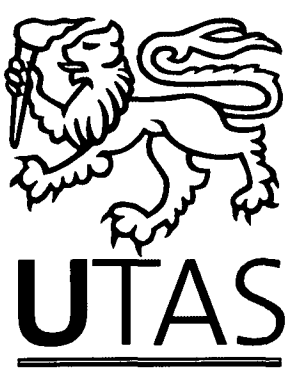

I declare that this thesis contains no material which has been accepted for a degree or diploma by the University or any other institution, except by way of background information and duly acknowledged in the thesis, and that, to the best of my knowledge and belief, this thesis contains no material previously published or written by another person, except where due acknowledgement is made in the text of the thesis.

Signed: K. L. Hill
Katherine L. Hill

Date: 07/09/09

ABSTRACT

The waters off the coast of Tasmania have become gradually warmer and saltier over the past 60 years according to a coast station time series, with sea surface temperatures rising at a rate more than double the global average. I demonstrate that this is related to a strengthening and more southerly reach of the East Australian Current (EAC) extension. The station also shows a strong decadal timescale signal in temperature and salinity. In this thesis, I use a combination of the Maria Island time series and Tasman Box XBT sections, 50 year atmosphere and ocean state estimates, and idealised forcing experiments with a global ocean model to build a picture of how the EAC system is changing, and what is driving it. I find that changes at Maria Island are closely related to changes in the wind stress curl in the South Pacific, with Maria Island lagging the winds by 3 years. This propagation speed is too fast for 1st Mode baroclinic Rossby wave adjustment which would take 10-15 years, so a faster mechanism is needed.

The observed variability at Maria Island is part of a bigger picture of decadal variability in the Southwest Pacific region. The EAC takes one of two paths at the point of separation at 32°S; it either continues down the coast as the EAC Extension, or separates and flows across the Tasman Sea to New Zealand as the Tasman Front. On decadal timescales either the Tasman Front or the EAC Extension is favoured, which form part of two gyre scale states. When the Tasman Front is favoured, a single gyre structure is seen, which mainly sits to the north of New Zealand; whereas when the EAC extension is favoured, a double gyre structure exists, with a second gyre centre east of New Zealand. Analysis of ocean reanalyses suggests that an enhanced wind stress curl maximum in the South Pacific appears to favour the EAC extension over the Tasman Front.

From model forcing experiments, where the wind stress curl maximum is enhanced in a 20°S longitude region for a period of a year, I am able to demonstrate a rapid mechanism by which the EAC can respond to changes in the South Pacific winds. Ocean ridges and islands provide a mechanism for conversion between fast barotropic and slow baroclinic Rossby waves. Due to the position of New Zealand, barotropic Rossby waves can travel across to New Zealand, travel around New Zealand as a coastal Kelvin wave, and then take 3 years to cross to interact with the EAC as a baroclinic Rossby wave. This shows that islands and bathymetry, as well as basin size, can dictate the rate at which oceans respond to changes in wind forcing. In addition intrinsic ocean variability exists, so that decadal variability in the ocean can be set up by a single pulse of wind forcing, due to the multiple ways in which the ocean responds to wind forcing. The model was also able to recreate the anti-correlation between the EAC Extension and the Tasman Front.

This thesis illustrates a very close relationship between the variability in the EAC western boundary current system and basin scale wind stress variability. In addition I identify a rapid mechanism by which the ocean can adjust in the presence of islands and ridges to explain the observed 3 year time lag. This suggests that both barotropic and baroclinic physics are needed to explain the timescales of observed low frequency variability in the ocean.

ACKNOWLEDGEMENTS

My sincere thanks go to my supervisors, Dr Stephen Rintoul and Professor Richard Coleman for their unwaivering support, guidance and patience over the last few years. I will remember Steve for never turning me away when I knocked on his door, and his inspired and broad perspective on the science. Richard has always been a voice of positivity and encouragement, and gives unwaivering support to all students he is involved with, ensuring that our PhD experience runs as smoothly and trouble free as possible. I would also like to thank Dr Peter Oke and Mr Ken Ridgway for their input and guidance.

The QMS PhD program jointly funded by the University of Tasmania and CSIRO Marine and Atmospheric Research, has provided a fabulous environment for a PhD training program. Having one PhD from both sites has meant that we have the resources of two sites at our fingertips. I have been based at CSIRO for the duration of my PhD, and the support provided to students is second to none and it has been a very positive and nurturing environment to study mostly due to genuine interest and enthusiasm of scientists down the corridor. The success of the program is due to the commitment and vision of Richard Coleman with the help of Denbeigh Armstrong.

I would like to thank Armin Koehl and Ben Geise for their time and support in helping me gain access to the vast resources of data which have been produced by the GECCO and SODA reanalysis programs and Russ Fiedler for his support while I embarked on a very steep learning curve in running ocean models. I would also like to thank the two anonymous reviewers for their positive and constructive comments.

Special thanks go to all the staff members of CSIRO who have been involved in collecting and processing data for the Maria Island coast station timeseries over the last 60 years, and also to those who have fought for the continuation of this remarkable resource when simple monitoring programs were not fashionable. Without it, analysis of decadal ocean variability in the South Pacific would have little or no ground truthing.

I would like to thank my mother for never trying to disuade me from following my own path, even when it takes me to the other side of the world. I would also like to thank my brother, who always reminds me that at the end of the day, there are a only a few important things in life, and we really have very little to worry about.

I would like to dedicate this thesis to my father, David John Hill (1947-1989), who taught me to see life as an adventure, and first introduced me to the wonders of the ocean. Without him, I would have probably taken a very different path

PAPERS WHICH FORM PART OF THIS THESIS

A number of articles form are in the process of being published as a result of this work. While these articles have co-authors, the figures and text included in this thesis have been produced my myself.

Some of the results from chapter 3 were published as:

Hill, K.L. and S.R. Rintoul and R. Coleman and K. Ridgway (2008) Wind forced low frequency variability in the East Australian Current *Geophysical Research Letters*,35 doi:10.1029/2007GL0391

Some of the result from chapter 4 will be published as:

Hill, K.L. and S.R. Rintoul and K. Ridgway and P. Oke (2008) Decadal changes in the South Pacific Western Boundary Current system revealed in observations and ocean state estimates. *submitted to Journal of Geophysical Research*,

Some of the results from chapter 6 will be published as:

Hill, K.L. and S.R. Rintoul and P. Oke (2009) A fast mechanism for the EAC to respond to remote wind forcing: Barotropic/Baroclinic Rossby Wave interactions with ridges and Islands. *in prep for submission to Ocean Modelling*

TABLE OF CONTENTS

LIST OF FIGURES

CHAPTER 1

INTRODUCTION

1.1 Motivation

A long term record from Maria Island coast station shows that the waters off the east coast of Tasmania have become warmer over the last 60 years (Ridgway, 2007). The Maria Island record also shows significant decadal variability in both temperature and salinity. Both temperature and salinity increase over this time period, especially in the summer, consistent with a strengthening and poleward extension of the East Australian Current (EAC) (Ridgway, 2007). However, the dynamics driving such a change have not been explained. Changes have also been observed in species distributions over this time period, with many species previously restricted to the coast of the Australian mainland extending their ranges southward off the coast of Tasmania (Edgar, 2000; Thresher et al., 2003; Poloczanska et al., 2007; Johnson et al., 2005; Ling, 2008; Ling et al., 2008). This is likely to have a significant impact on the Tasmanian fisheries, a major contributor to Tasmania's economy.

The goal of this thesis is to describe the patterns of low frequency variability observed in the Maria Island time series, and its relationship with the basin scale circulation of the South Pacific.

1.2 Maria Island Coast Station time series - evidence of change and variability

Maria Island coast station, situated at 42.5°S, 148.2°E is the longest high quality ocean time series in the Southern Hemisphere. Measurements of temperature, salinity and nutrients have been made monthly at the 50 and 100m isobaths since October 1944. Maria Island sits on the equatorial side of the subtropical convergence zone, at the interface of subantarctic and subtropical waters (see Figure 1.1). This means relatively small changes in hemispheric and gyre scale circulation patterns manifest themselves as prominent signals in the Maria Island record. Pronounced seasonal variability can clearly be seen in both temperature and salinity. Harris et al. (1987) identified two main states. In winter and early spring, the temperature/salinity signature was primarily modified subantarctic water (SAW), with a temperature of 14.5°C and salinity of around 35.3 psu with a deep mixed layer of around 300m. In the summer, when there is a subtropical watermass intrusion from the north, Harris et al. (1987) found that the temperature would reach 18.5°C and salinity would typically reach 35.6 psu. Ridgway (2007) and Cresswell (2000) identified distinct austral summer and winter circulation regimes in this region. In the summer, warm salty water is advected polewards along the east coast of Tasmania, by a strengthened EAC. In the winter, there is a reversal in current flow, as cool, fresh subantarctic surface waters are drawn up from further south, also entraining flow from the Zeehan Current. The Zeehan Current flows down the west coast of Tasmania, and extends round the southern tip of Tasmania during winter, when the Leeuwin Current system off Western and Southern Australia is strongest (Cresswell, 2000). To completely understand the drivers for the observed signal at Maria, the relative roles of local forcing in the Tasman Sea area versus the wider gyre scale influence of ocean processes in the central South Pacific require further examination.

In addition to such distinct seasonal variability, Ridgway (2007) also identified trends in temperature and salinity. The region has become both warmer and saltier, with mean trends of 2.28°C and 0.36 psu per century between 1944 and 2002, compared to global average estimates of sea surface temperature change of 0.09-0.14°C ±0.04°C per decade since 1960 (0.9-1.4°C per century) (Casey & Cornillion, 2001) and 0.6±0.2°C per century since 1900 (Smith & Reynolds, 2004). Ridgway (2007) inferred that these trends are not forced by radiative heating but are caused by an increase in the strength of the East Australia Current bringing more warm salty water south, particularly in the summer months.

1.3 Evidence of ecosystem changes

Very few comprehensive studies of relationships between variability in climate and marine ecosystems can be found, particularly in the Southern Hemisphere. Harris et al. (1987, 1988) focused on the Tasman Sea, and were the first to correlate variability in climate with the success of major fisheries (Harris et al., 1988), and the composition of phytoplankton blooms in the region (Harris et al., 1987).

Lyne et al. (2005) gathered anecdotal information on ecosystem changes observed in the South East Australian region. This included evidence that the range of sea urchins *Centrostephanus rodgersii*, previously restricted to the New South Wales coast on the Australian mainland, has expanded southward off the east coast of Tasmania. The salmon aquaculture industry is also sensitive to changes in water temperature, with recent warm summers leading to significant decline in production and profit. Lyne et al. (2005) summarised ecosystem changes seen in the South East Australian region. In the last decade 34 fish species have either become newly established south of the Bass Strait, or exhibited major distributional changes. Similar shifts were seen in plankton distributions. The species composition of phytoplank-

ton blooms off Tasmania has seen an increasing proportion of tropical species, such as *Gefyrocapsa oceanica* over the native *Emiliana huxlei.* Red tides, *Noctiluca scintillans*, have also appeared in Bass Strait and along the Tasmanian coastline since 2001, similar to large scale blooms seen off the coast of New South Wales in 1997 (Lyne et al., 2005). This suggests a southward range extension of species across a broad range of taxa, which broadly correlates with a southward shift in the East Australian current, bringing warm waters further south (Lyne et al., 2005). However, the precise relationships have not been explored, i.e., whether a shift is due to the southward increased advection of larvae/plankton, or due to the expansion of habitat of subtropical species due limited by their viable temperature range.

Further work by Poloczanska et al. (2007) produced a comprehensive study on the impacts of climate change on Australian marine life, from model results and the reviewed literature. In particular, they identified regions most at risk from the effects of climate change. The South East Australian region was defined as one of the regions most at risk from climate change, for a combination of reasons. First, it is dubbed a "Climate Hotspot", as the strengthening of the EAC is expected to continue, bringing warmer water further south. Second, it is a biogeographic transition zone, sitting between subtropical and subantarctic zones, so the region is sensitive to large scale climate shifts. Third, the South East Australian region is the most heavily populated of Australia's coastlines, so most stressed by fishing pressure (Hobday & Hartmann, 2006). The region was identified as particularly at risk, due to its high level of endemism. Polaczanska et al documented impacts of changing temperature and nutrient regimes on a broad spectrum of ecosystems. It was acknowledged that while impacts on individual species are relatively easy to predict, the response at the ecosystem level is much more complex.

The southward range extension of the spiny sea urchin (*Centrostephanus rodgersii*)

along the coast of Tasmania has been discussed in more detail by Ling (2008) and Ling et al. (2008). It was found that a combination of larval advection and temperature controls determine the distribution of the sea urchins, and since the 1960's when urchins were first identified in Tasmanian waters, a transition has been seen from colonisation through larval advection, to a self sustaining community which is able to reproduce in situ (Ling et al., 2008). This is due to an increase in water temperature during August, which is generally when the water temperatures reach a minimum. August coincides with a critical period in the development of urchin larvae, which develop poorly in water temperatures below 12°C. August temperatures above 12°C are becoming increasingly common. The impact of this relatively new addition to the ecosystem is considerable. The macroalgal beds are grazed completely, forming regions known as "barrens". The faunal community of these regions is found to be "overwhelmingly impoverished" relative to the macroalgal beds, with only 72 taxa found in barren regions, compared to 221 within intact macroalgal beds (Ling, 2008). Moreover, these macroalgal beds are the prime habitat for abalone and rock lobster, both of which are multi-million dollar fishery industries. The only effective predator of the urchins are rock lobsters much larger than the minimum catch size, which are very rare outside marine reserves. Ling (2008) highlighted the southward expansion of sea urchins as an example where changes in ocean currents can lead to disproportionately large impacts where key species with the ability to modify a habit either change or extend their range. It is also an example of the combined impacts of fishing and climate variability.

1.4 Regional circulation

The EAC is the western boundary current of the wind driven South Pacific subtropical gyre (Figure 1.1), transporting warm salty water from the tropics southward to

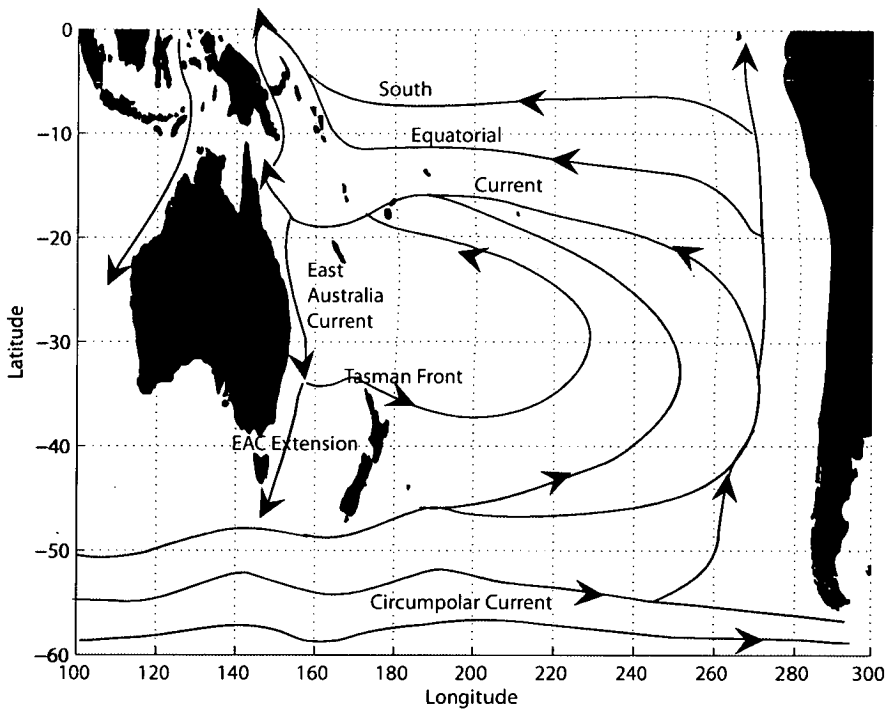

Figure 1.1: A schematic of the South Pacific wind driven circulation

balance the net equatorward transport in the interior of the basin. This transport is driven by the wind stress curl, the gradient of wind stress set up predominantly between the southern hemisphere subtropical westerly winds and the SE trades (Cai et al., 2005). The westward flowing South Equatorial Current (SEC) forms the northern limb of the gyre and can cover a meridional range from 4°N to 30°S in the form of multiple jets (Kessler & Taft, 1987). On reaching the coast of Australia, the SEC bifurcates at around 15°S at the surface and 22°S at depth (Qu & Lindstrom, 2002) and the southern limb forms the EAC. The EAC separates from the coast at around 31-34°S to form the Tasman Front (Ridgway & Dunn, 2003; Mulhearn, 1987). The Tasman Front flows across the Tasman Sea and around the northern tip of New Zealand to form the East Auckland Current. The remainder of the EAC, named the EAC extension, continues south to the east coast of Tasmania, roughly following the shelf edge (which drops off sharply from 200m to around 1500m).

1.5 The East Australian Current

The EAC shows some unique features when compared to other western boundary currents. Firstly, the EAC is weaker than its counterparts, with mean southward transport estimates of 22 Sv at 30°S (Mata et al., 2000) and 27 Sv at 28°S (Ridgway & Godfrey, 1994). A countercurrent runs offshore of the EAC, which is about 17 Sv of northward flow. This gives a net southward transport of 9.5 Sv (Ridgway & Godfrey, 1994, 1997). These transport estimates for the EAC are compared to estimates of 43 Sv - 85 Sv for the Agulhas Current (Matano et al., 2002). Moreover, it is an eddy rich current (Boland & Hamon, 1970; Boland & Church, 1981), so much so, that it is arguable whether it is a single current, as the baroclinic eddy mass transport is several times that of the mean flow. A more recent study, assessing the seasonal cycle of the EAC, suggests larger southward transports and that the seasonal amplitude is also large compared to the mean flow, with a minimum observed southward flow of 27.4 Sv in winter, and a maximum of 36.3 Sv in summer (Ridgway & Godfrey, 1997). The net transport of the EAC (including the northward countercurrent is 9.5 Sv, with a seasonal amplitude of 6 Sv. Compare this to the Florida Current at 26°S, which has a seasonal amplitude of 3 Sv with a background flow of 30 Sv (Schott et al., 1988).

A number of theories have been put forward in the literature to explain the dynamics and position of the separation point of the EAC from the coast of Australia and formation of the Tasman Front. Three main theories exist. Firstly, the coastline curvature and bathymetry around Sugarloaf Point, situated at 32.26°S (Godfrey et al., 1980); secondly, the structure of gyre-scale wind stress curl (Tilburg et al., 2001) and lastly, the blocking of westward propagating Rossby waves by New Zealand (Nilsson & Cresswell, 1980).

However, more recent studies suggest that the location of the separation point can

vary by up to 150km (Ridgway & Dunn, 2003) which means that coastline curvature and Rossby wave blocking by New Zealand are unlikely to provide the complete explanation. Bostock et al. (2006) analysed model data and foraminifera oxygen isotope ratios to infer that the latitude of the separation zone has varied since the last glacial maximum. During the last glacial maximum, the separation zone was further north between 23 and 26°S, compared to its current position around 32°S. Bostock et al suggest that the southward shift was caused by a significant change in the wind stress curl since the last glacial maximum, seemingly corroborating Tilburg et al's hypothesis. The mechanism of separation is likely to influence how the Tasman Front and the EAC extension respond to large scale wind changes and variability.

The dynamics of the regional currents around New Zealand were investigated in a series of global ocean models of increasing complexity (Tilburg et al., 2001). The modelled EAC separates even when New Zealand is removed in a linear model. Tilburg et al. (2001) suggest that the position of the separation point is related to the zonally integrated meridional gradient of wind stress curl. Analysis of two runs of the GFDL coupled climate model by Gnanadesikan et al. (2006) found that the EAC focussed all its transport along the Tasman Front in version 2.0, whereas in version 2.1 of the model , the EAC fed most of its transport into the EAC Extension. A number of changes to the model set up were made between version 2.0 and 2.1, including a reduction in background viscosity in the extratropics to generate stronger boundary currents (Gnanadesikan et al., 2006). In version 2.0, strong positive wind stress curl (more than $0.4*10^{-7}Nm^2$) is only found north of 40-42°S in the South Pacific so the subtropical gyre was positioned to the north of New Zealand. In version 2.1, wind stress curl remains positive down to 55°S so that all of New Zealand was within the subtropical gyre. This suggests that gyre

scale wind stress curl may determine the dynamics of the EAC separation and in particular the relative strength of the EAC and Tasman Front. However, the precise relationship between wind stress curl and the nature of the separation of the EAC and associated frontal systems is not fully understood.

1.6 Variability and change in the South Pacific Gyre

The observed long term trend at Maria Island, documented by Ridgway (2007), forms part of a bigger picture of observed changes in the South Pacific region. Harris et al. (1988) identified correlations between large-scale climate variability and a number of fisheries and ecosystem variables in the Tasmanian waters. They identified the number of days with strong westerly winds as the primary forcing factor, which in turn was linked to large scale climate factors, such as El Niño. Thresher et al. (2004) suggested that cooling at 1000m over the last three centuries, inferred from deep water coral proxies south of Tasmania, reflected an increase in the poleward flow of the EAC along the Tasmanian coast, which was in turn driven by a poleward shift of the westerly wind (Thresher, 2002; Harris et al., 1988; Oke & England, 2004). Roemmich et al. (2007) presented evidence of a spin up of the South Pacific gyre between 1993 and 2004 using altimeter sea surface height (SSH), hydrographic dynamic height and velocity datasets, and related the observations to the Southern Annular Mode (SAM). Roemmich at al. showed that SSH had increased by 12 cm between 1993 and 2004, centered around 40°S, 170°W. Evidence from dynamic height suggested that the geostrophic circulation of the gyre had increased by at least 20% at 1000m during the 1990s, which was confirmed by Argo and WOCE float trajectories. These signals seemed to peak in 2003, and then began to decline. Roemmich et al. (2007) concluded that the subtropical gyre in the South Pacific has spun up in response to increased wind stress curl. Analysis of CSIRO

Mk3 climate model runs showed that an increase/shift south of the wind stress curl can cause an intensification/shift south of the EAC (Cai et al., 2005). Cai (2006) compared the NCEP winds from the 1950s to the 1990's which show a clear increase in the wind stress curl in response to a marked increase in zonal westerly winds. The Sverdrup-Island Rule solution (Godfrey, 1989) suggests a strengthened South Pacific gyre, and EAC transport increases of about 6-8 Sverdrups over 50 years, although these figures have not been compared to the observed volume flow (Cai, 2006). Climate change simulations also suggest that this trend towards a stronger gyre and a stronger EAC will continue in the future due to climate change (Cai et al., 2005). EAC transports are predicted to increase by 5-10 Sv for the mean of years 2055-2085. The change in the EAC is expected to be greater than the western boundary currents of the other subtropical gyres as the southern tip of the land boundary extends into the the zonal strip of strongest curl changes. This generates a warming rate in the Tasman sea that is the largest observed in the Southern Hemisphere in these model runs (Cai et al., 2005).

Observational studies of these long term changes and variability are hampered by a dearth of observations in the region with sufficent spatial or temporal coverage. The longevity of the time series offshore of Maria Island is a notable exception to this. The long term changes and variability in temperature and salinity at Maria Island were related to changes in the strength of the EAC (Ridgway, 2007). However, the scarcity of corresponding observations over a broader region meant that Ridgway could not pinpoint whether a stronger EAC (i.e. a spin up of the gyre), a shift south, or a change in the character of the separation zone caused the observed signal at Maria. While a wealth of observations have come on-line since the 1990's, the short length of the datasets (less than 50 years) make it difficult to distinguish between trends and low frequency variability, and prohibits statistically significant

correlations on decadal timescales (Roemmich et al., 2007).

Low frequency variability in the South Pacific wind stress curl has been related to the Pacific-South America (PSA) pattern, the southern hemisphere atmospheric teleconnection associated with ENSO (Karoly, 1989; Sasaki et al., 2008; Garreaud & Battisti, 1999; Mo, 2000). The South Pacific gyre exhibits decadal timescale variability, related to variability in basin scale wind stress curl (Sasaki et al., 2008). The first empirical orthogonal function (EOF) of 30 years sea level from a global eddy resolving ocean model driven by NCEP-1 winds is strongly inversely correlated with the decadal ENSO index (Sasaki et al., 2008). (Sasaki et al., 2008) also suggested that the spin up of the South Pacific gyre in the 1990s discussed by (Roemmich et al., 2007) is not related to a continuous long term trend, but is part of a decadal variability pattern. On decadal timescales, a stronger gyre and hence stronger wind stress curl was associated with a weaker Tasman Front (Sasaki et al., 2008).

Sprintall et al. (1995) found evidence of a thinning and reduction of warm EAC waters around northern New Zealand during the 1991-1993 El Nino from the World Ocean Circulation Experiment (WOCE) P14C hydrographic data, and the Tasman Box XBT lines, associated with divergence of mass in the upper waters. Sprintall et al. also noted unusually strong southwesterly winds at northern New Zealand coastal sites during this time, and associated the observed anomalous ocean heat transport to the prolonged ENSO episode that began in early 1991. A direct link between the SOI and the strength of subtropical westerlies has been established with changing air pressure fields in the subtropical gyre and Southern Ocean (Gordon, 1986; Karoly, 1989) and eddy driven zonal wind anomalies in mid to high latitudes (L'Heureux & Thompson, 2006). Therefore, the reduction in the tropical trades associated with El Niño events could be dynamically linked to increased subtropical westerlies. The net effect of this on the wind stress curl field was not discussed. Morris et al. (1996)

explored variability in the subtropical gyre using high resolution XBT data from the Fiji to Hawaii (PX09) and Auckland to Fiji (PX06) lines from 1987-1994. They associated interannual variability with ENSO, suggesting that relatively weak gyre scale transport is related to the La Niña event of 1988/89. After 1991, gyre scale transport was more intense. As the trade winds are strengthened during a La Niña event, but the net effect is a weaker gyre, this would suggest that it is the subtropical westerlies which have a stronger influence on the wind stress curl field and hence the strength of the South Pacific gyre.

The inverse relationship between the trades and the westerlies was also articulated by Harris et al. (1988), who linked the position of the westerly wind belt with the position of the continental high pressure over Australia and hence ENSO (as the Southern Oscillation Index is defined by the Darwin-Tahiti pressure gradient). Harris et al. (1988) also identified a clear cyclical pattern in these zonal westerly winds with a mean periodicity of 11 years. Harris et al. (1988) suggested that strong westerlies observed during El Niño events would drive colder, nutrient rich sub-antarctic waters up the east coast of Tasmania in summer. This is likely to reduce both temperature and salinity at Maria Island. Observational evidence from hydrographic and XBT data however, suggests that ENSO has a negligible influence in the EAC region. Hsieh & Hamon (1991) explored ENSO signals in using Empirical Orthogonal Functions (EOFs) from 4 decades of hydrographic data collected off Sydney, and sea level at Sydney. EOF modes were calculated using 50m hydrography data and adjusted sea level, and while the first two modes significantly correlated with ENSO, they found that the amplitude of the ENSO-like signal was small. Hsieh & Hamon (1991) concluded that the connections with ENSO are relatively weak (1/3 - 1/8 of seasonal ranges). Ridgway & Godfrey (1997) explored temperature and circulation changes around South East Australia using XBT data, and concluded

also that there was little evidence of in-phase ENSO related changes found south of about 10°S. Further work is needed to examine the relationship between decadal ENSO, the trade winds and subtropical westerly winds, and the net effect on the wind stress curl and hence the South Pacific gyre strength.

1.7 Mechanisms of decadal variability in the ocean

Timescales of variability in the ocean are generally thought to be dictated by atmospheric and oceanic teleconnections. As discussed above, ENSO-like decadal variability in the Pacific is known by a number of names (see further discussion in section 2.1.4). Essentially the signal in question is the same. In addition to the timescale, the difference between interannual ENSO variability and low frequency decadal ENSO variability is seen in the spatial pattern. Power et al. (1999) describe the Interdecadal Pacific Oscillation as a ENSO type spatial structure with a broader tropical signature, and a stronger extratropical signature.

Latif & Barnett (1996) discusses the origins Pacific decadal climate variability through the analysis of SST and sea level pressure (SLP) in observations and a coupled model. Latif & Barnett (1996) identify a cycle of unstable air-sea interactions between the Aleutian Low and the North Pacific subtropical gyre. The feedback between the atmosphere an ocean is related to variations in the strength of the Kuroshio as a result of variations in the strength of the Gyre. A stronger (weaker) Aleutian Low, strengthens (weakens) the wind stress curl over the South Pacific, resulting in a stronger (weaker) gyre and hence a stronger (weaker) Kuroshio Extension. The stronger (weaker) Kuroshio then produces a positive (negative) SST anomaly in the North Pacific, which then weakens (strengthens) the Aleutian Low (Latif & Barnett, 1996). Schneider et al. (2002) also relate the spatial pattern of decadal variability in the north Pacific to the Aleutian Low, variations in the North

Pacific subtropical gyre and hence variations in the strength of the Kuroshio Extension. However, Schneider et al. (2002) suggests it is stochastic variability in the Aleutian Low which changes the Ekman pumping over the North Pacific, which excites Rossby waves; and it is this Rossby wave propagation which dictates the timescale of variability. No evidence is found for a mid-latitude ocean-atmosphere negative feedback loop.

In the South Pacific, the pattern and timescale of decadal variability has been attributed to atmospheric teleconnections from the Tropics (i.e. ENSO variability) to the extratropics (known as the Pacific-South American Mode), and extratropical oceanic teleconnections propagating westwards in the form of baroclinic Rossby waves. As 1st mode baroclinic Rossby waves take over a decade to cross an ocean at subtropical latitudes, it is these which are thought to dictate the timescale of basin scale decadal variability, and hence the broader spatial pattern of decadal ENSO (Power et al., 2006; Sasaki et al., 2008). As Rossby waves act as "integrators" of wind forcing as they propagate across the Pacific, the reponse of the extratropical ocean has been thought of as a low pass filter of high frequency atmospheric variability (Sasaki et al., 2008). This suggests decadal variability in the Pacific Ocean is a passive response of the extratropical ocean to higher frequency ENSO variability via atmospheric and oceanic (Rossby wave) teleconnections (Schneider & Miller, 2001; Schneider et al., 2002; Schneider & Cornuelle, 2005; Power et al., 2006; Sasaki et al., 2008). In summary, the precise mechanisms which dictate the spatial pattern and timescale of basinwide decadal variability in the ocean are not clear. Decadal variability has been related to a number of processes, including the a midlatitude coupled ocean-atmosphere negative feedback loop, the extratropical ocean's response to stochastic forcing, and the passive response of the ENSO variability. The role of Rossby wave propagation patterns in dictating this timescale

also needs to be articulated.

1.8 The Dynamics of wind driven circulation - local verses remote forcing

Subtropical gyres are a dominant feature of the wind driven circulation of the upper ocean layer. The western boundary currents of the gyres form an important mechanism whereby heat is transported from the tropics to the higher latitudes. It is also the mechanism by which the net equatorward geostrophic flow is balanced (Sverdrup balance). Hence, variations in the wind field over the basin will manifest as variability in the strength of the western boundary current. Understanding the dynamics of this relationship, and the timescales at which the surface ocean responds to such changes are extremely important in deducing the cause of the observed variations in the western boundary currents at timescales from seasonal to multidecadal.

The surface ocean responds almost immediately to changes in wind forcing. Changes in the local wind forcing cause regional changes in ocean currents in the upper few tens of meters within a few hours (Pond & Pickard, 1983). However, basin scale adjustment to a perturbation takes longer and depends on the latitude and distance between the region of forcing and region of interest. The primary mechanism by which such signals are communicated across ocean basins in the extratropics are Rossby waves, which are excited by perturbations in isopycnals and travel westward along isopycnal surfaces. Waves can also have poleward (for short wavelengths) and vertical components (McCreary, 1984). Their propagation speed decreases exponentially with increasing latitude (Killworth et al., 1997; Kilworth & Blundell, 2005; Chelton et al., 1998). In the case of the subtropical South Pacific, it takes around 10 years for baroclinic Rossby waves to travel from the coast of South America to Australia at 30°S and 20 years at 48°S. Qiu & Chen (2006) identified a time lag of 2

years between changes in scatterometer-derived wind stress curl in the South Pacific and the ocean's response in altimetric SSH. Roemmich et al. (2007) also noted a lag between the peak in the wind forcing over the subtropical South Pacific, and the peak in the response of the ocean, in terms of the strength of the subtropical gyre circulation, of about 4-5 years. Schneider & Miller (2001) used wind stress data and a Rossby wave model to demonstrate that variations in wind stress in the central North Pacific manifest as winter SST anomalies in the Kuroshio-Oyashio extension with a 3 year lag. These studies suggest that a faster mechanism than first mode baroclinic Rossby waves is responsible for the observed time lag between wind forcing and the response of western boundary currents. However, both Qiu & Chen (2006) and Schneider & Miller (2001) conclude that the baroclinic Rossby wave dynamics provide the basis for the observed SSH variability in the subtropical gyres of the Pacific on interannual to decadal timescales. This conclusion relies on the integrating nature of Rossby waves along their pathway. As Qiu & Chen (2006) force their linear model with basin scale wind anomalies, it was not possible to isolate the region(s) of forcing which was critical to creating the observed variability in SSH.

The processes affecting the transport of western boundary currents as a result of periodic forcing were explored in detail by Anderson & Corry (1985). They explored the linear response of a two layer ocean model to periodic wind stress curl variations in the presence of bottom topography. It was concluded that for short periods (i.e. much less than the time taken for wind generated baroclinic Rossby waves to pass over topography), the response is strongly modified by topography. For long periods, Rossby Waves compensate for the effect of topography and the non-topographic Sverdrup balance holds. The dominance of the barotropic response increases with latitude, and hence the response to seasonal winds in regions poleward of 30°N/S is

primarily barotropic (Veronis & Stommel, 1956; Gill & Niiler, 1973). Reid (1986) suggested that the barotropic component is small in the subtropical gyre, although Fu & Davidson (1995) found a relatively large response to wind forcing in the south-east Pacific, south of 30°S. North of 29°S, annual SSH variability is influenced by local isopycnal response to Ekman pumping (Roemmich & Cornuelle, 1990; Morris et al., 1996). However, annual variations in the thermocline do not dominate south of 29°S (Roemmich & Cornuelle, 1990).

More recently, model experiments have been used to explore the role of topography in modifying planetary wave propagation, and the consequences for ocean adjustment. Tanaka & Ikeda (2004) explored variability in the Kuroshio region using a regional model with simple ridge topography and an idealised wind stress anomaly. They investigated the interaction of barotropic and baroclinic Rossby waves at different timescales across the ocean ridges and found that on interannual timescales and longer, barotropic waves have very little success in crossing the ridges. Baroclinic waves tend to be transmitted across the ridges, having a net mass transport, and therefore modifying the Kuroshio Current. However, on seasonal and shorter timescales, baroclinic waves forced directly by the winds dissipate quickly. However, barotropic wave energy appears to be effectively transmitted to the west of the ridge, by conversion to baroclinic modes on the ridge within a few years of the wind perturbation. Tanaka & Ikeda (2004) conclude that the balance between baroclinic and barotropic modes is dependant on the frequency of forcing and their modification across the ridge appears to be related to the interaction between the wavelength of forcing and ridge width.

A simple box model was used to explore the Kelvin/Rossby wave dynamics around an island (Liu et al., 1999). Liu et al. (1999) suggest that the circulation is set up in three stages. An SSH anomaly is established by Rossby waves dissipated against

the east coast of the island. The direction of circulation around the island is set up by a coastal Kelvin wave, which propagates around the coast, and the circulation is completed by long Rossby waves, which are initiated on the west coast of the island. Sasaki et al. (2008) suggested that this theory could be applied to the South Pacific, where sea level variability in the Tasman Sea can be explained by changes in the South Pacific wind stress curl field and the signal is then communicated around the New Zealand coast.

The results of Tanaka & Ikeda (2004) and Liu et al. (1999) suggest that wind forcing could initiate variability on the western boundary with a lag of a few years, by the conversion between barotropic and baroclinic modes through interaction with islands or ocean ridges.

1.9 The aims of this thesis

We can say with certainty that the waters off Tasmania have been getting warmer and saltier since 1944. The trend in temperature is double the global average sea surface temperature change over the same time period, and is certainly related to a strengthening of the EAC. There is also distinct decadal timescale variability in the strength of the EAC, and hence temperature and salinity. There is mounting evidence that such changes and variability are causing changes in the distribution of species across a broad range of taxa, resulting in significant ecosystem changes. One particular example is the establishment of spiny sea urchins *Centrostephanus rogersii* in Tasmanian waters, and the related destructive grazing of giant kelp forests.

This thesis explores the causes of observed changes and variability in the EAC system. In particular, I focus on three specific questions:

1. What is the relationship between the changes in the South Pacific winds, the

South Pacific wind driven gyre, and observed changes in the South Tasman Sea?

2. How is observed EAC variability related to the regional current system? Can we build a picture of regional decadal variability using new 50-year ocean reanalysis products?

3. What are the mechanisms by which the ocean communicates remote south Pacific wind forcing to changes in the EAC, and how is this achieved within a few years, when the theoretical first mode baroclinic response would take 10-20 years?

First, I use in situ observations and atmospheric reanalysis data to demonstrate that low frequency temperature and salinity variability observed at Maria Island reflects changes in the position and strength of the subtropical gyre in response to changes in the South Pacific winds. A consistent time lag of 3 years is found between changes in South Pacific winds and changes in temperature and salinity observed at Maria Island. This lag is too fast for a 1st mode baroclinic Rossby wave response, the principle mechanism by which oceans respond to changes in forcing. The data and methods for this section are found in chapter 2, and the results in chapter 3.

I then explore the observed decadal variability in the EAC in detail, by considering the nature of the wind variability, the resultant subtropical gyre variability, and the relationships between different branches of the current system. I exploit results from two different 50-year ocean reanalysis products to further understand the above mentioned relationships over a longer time period. By using a combination of the available observations (namely the Maria Island timeseries and Tasman Box XBT lines) and results from ocean reanalyses, I build a comprehensive picture of wind-forced decadal variability in the South Pacific western boundary current system. In

particular, I identify that the transport of the EAC Extension and the Tasman Front are strongly anticorrelated, and this is representative of changes in the circulation of the gyre driven by changes in South Pacific wind stress curl. The data and methods for this study are found in chapter 2, and the results in chapter 4.

Lastly, I use idealised model forcing experiments to gain an understanding of the mechanisms which govern the short time lag between changes in the winds and changes in EAC transport. It is shown that fast modes of ocean communication can be achieved by the conversion between fast barotropic waves and slower baroclinic waves due to their interaction with ocean (subsurface) ridges and islands. I am able to demonstrate that there are multiple ways in which the ocean can respond to changes in winds depending on the combination of barotropic/baroclinic processes and hence the nature of the regional bathymetry. In addition, I am also able to recreate the observed relationship between the EAC Extension and the Tasman Front by simply enhancing the wind stress curl maximum in a region of the South Pacific. Details of the model and set up of the forcing experiments will be found in chapter 5, and results in chapter 6. Concluding remarks to this thesis are given in chapter 7, wrapping up the contributions of this study and pointing out avenues for future work.

CHAPTER 2

DATA AND METHODS

In this chapter, I outline the datasets and methods of analysis used in chapters 3 and 4.

2.1 Observational Data

2.1.1 Maria Island coast station timeseries

The Maria Island Time Series (Maria) station is situated off the southeast coast of Tasmania at 42.6°S, 148.23°E. It is the longest high quality time series station in the Southern Hemisphere, running from 1944 to the present day. The station is located at the 50 m isobath, approximately 5 km from the edge of the narrow continental shelf. Monthly temperature, salinity and nutrient measurements are taken from the surface to 50 metres, at 10 metre intervals. While most of the EAC separates near 30°S forming the Tasman Front, the remainder of the current continues southward to form the EAC Extension (Cresswell, 2000) (Figure 1.1). The ribbon of warm water carried south by the EAC Extension lies over the upper continental slope, just offshore of Maria Island (Figures 2.1b and c). Ridgway (2007) used satellite measurements of surface temperature to confirm that the Maria temperature record represented the temperature of the EAC Extension and was correlated with surface temperature over a broader region.

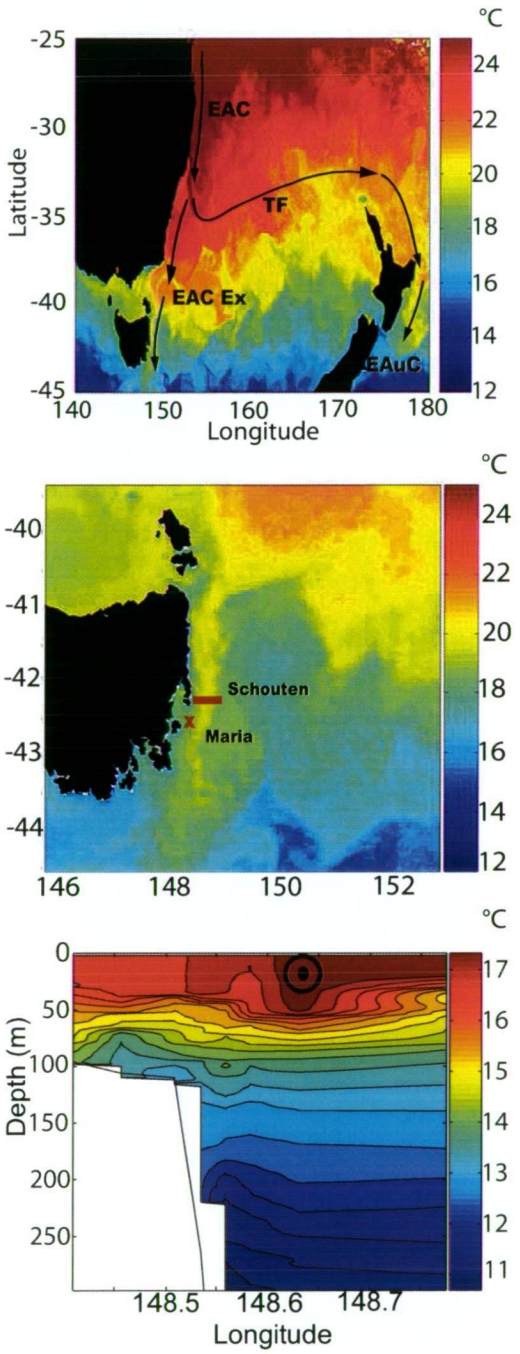

Figure 2.1: (a) Satellite SST of the Tasman Sea for March 2001. Superimposed are arrows showing the main regional currents. The East Australia Current (EAC), EAC Extension (EAC Ex), the Tasman Front (TF), and the East Auckland Current (EAuC); (b) Satellite SST of Tasmanian region. Locations of the Maria Island coast station timeseries and the Schouten Island Transect are marked; (c) A temperature transect offshore from Schouten Island (Cresswell 2000). The narrow shelf means that the waters in the region of the Maria coast station (50m isobath) are representative of the broader offshore oceanographic conditions.

2.1.2 CSIRO Atlas of Regional Seas

The CSIRO Atlas of Regional Seas (CARS 2006) and the CARS coastal (Coast8 2006) datasets were used to compare Maria data with the regional background climatology temperature and salinity (Ridgway et al., 2002; Dunn & Ridgway, 2002). CARS is a digital atlas of seasonal ocean water properties produced from hydrography data taken from the BlueLINK BOA (BLUElink Ocean Archive), which in turn is based on a number of datasets including the World Ocean Database 2001 (WOD01), the World Ocean Circulation Experiment World Hydrographic Program 1 (WOCE-WHP1), CSIRO data holdings, and the Argo float network. Stations such as Maria Island coast station are included in the CARS analysis. CARS initially focused on the seas around Australia, but now extends to the Southern Hemisphere and tropics. Temperature, salinity, oxygen, nitrate, silicate and phosphate are all mapped onto 79 depth levels, with 0.5x0.5 degree resolution in the region 0-360°E, 70°S to 26°N (10°N in the Atlantic). Coast8 is a high resolution version of CARS, at 1/8° resolution for a polygon encompassing the Australian coastal and shelf waters defined within the region 110-155°E, 18-50°S.

2.1.3 Tasman Box XBT data

The Tasman Box consists of 3 XBT lines, which form a closed box in the South West Pacific (Roemmich et al., 2005). These lines are PX06 (Auckland to Fiji), PX30 (Fiji to Brisbane) and PX34 (Sydney to Wellington) (Figure 2.2). This region encompasses the EAC, the South Equatorial Current and the Tasman Front. These lines are occupied quarterly, and XBT's are dropped every 40 km in the open ocean, and every 15-20km inshore. The Fiji to Brisbane and Sydney to Wellington lines have been running since 1991, and the Auckland to Fiji line has been established since 1986. A combined XBT/CTD/altimeter method was used to calculate the

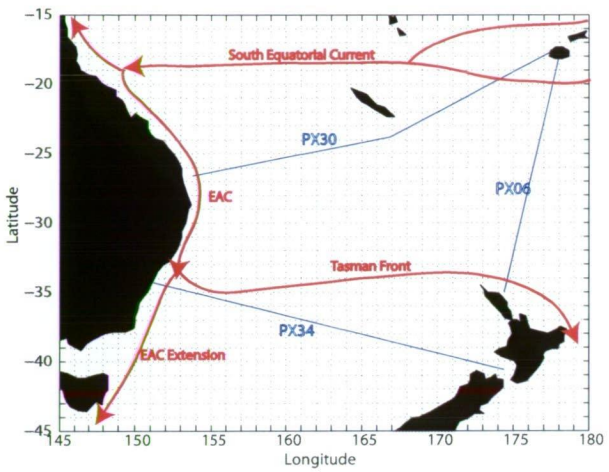

Figure 2.2: A schematic of Tasman Box XBT sections and the currents which cross them

geostrophic transports into and out of the Tasman Box (for full details see Ridgway, 2008). Ekman transport was incorporated to give an estimate of total transport by calculating the Ekman pumping along the XBT sections from ERA-40 wind stress data.

2.1.4 Climate Indices

The Southern Oscillation Index (SOI) and the Southern Annular Mode (SAM) Index were low pass filtered with a 5 year running mean to determine their relationship with the observed low frequency variability in the Maria coast station timeseries. The Southern Oscillation Index is calculated from the Darwin-Tahiti sea level pressure difference (Trenberth, 1984). A number of papers have discussed low frequency variability in the Pacific region, which goes by a number of names and is calculated in a variety of ways. These include the Pacific Decadal Oscillation (PDO) (the first EOF of North Pacific and tropical SST (Mantua et al., 1997)), the Interdecadal Pacific Oscillation (IPO) (first near-global EOF of SST (Folland et al., 1998; Power et al., 1999)) and Decadal ENSO (calculated by projecting the spatial pattern of the first EOF mode of the 7 year low pass filtered SST in the Equatorial Pacific

(20°S-20°N, 120°E-70°W) onto the unfiltered SSH in the same region (Sasaki et al., 2008)). However calculated, the low frequency variability in the ENSO system dominates and Power et al. (1999) demonstrated that a low pass filtered SOI, the PDO and the IPO are highly correlated (r=>0.9) since 1945 (prior to this, differences are likely due to instrument error). Therefore, for simplicity, a 5 year low pass filtered SOI is used to represent the low frequency variability in the ENSO system, and we will call this signal decadal ENSO. The SAM index was obtained from the 1st EOF of Southern Hemisphere NCEP-2 (1979-present) Sea Level Pressure. Prior to 1979, there is not sufficient data in the Southern Hemisphere to give a reliable SAM index (see discussion of trends in NCEP-1 reanalysis in section 2.2.2).

2.2 Reanalysis Data

2.2.1 National Center for Atmospheric Research - National Centre for Environmental Prediction Atmospheric Reanalysis 1 (NCAR/NCEP-1)

NCEP-1 is a 50+ year global atmospheric reanalysis product, covering the period from 01/01/1948-present at 2 degree spatial resolution (Kalnay et al., 1996). We used the monthly mean wind stress data. As noted in secton 1, NCEP-1 reanalysis winds show a general increase in the wind stress curl in the South Pacific, and marked increase in the zonal westerlies, especially south of Australia and New Zealand. Caution must be exercised in interpreting these trends due to inconsistencies related to the evolution of the observing system and reports of an enhanced trend in the polar vortex in the NCEP-1 data (Kistler et al., 2001; Bromwich & Fogt, 2004; Hines et al., 2000; Renwick, 2004; Tennant, 2004). However, the intensification of the polar vortex related to a positive trend in the Southern Annular Mode is well documented from a variety of data sources (Thompson & Solomon, 2002; Kushner et al., 2001). The mean and the trend in zonal winds is shown in Figure 2.3a. By

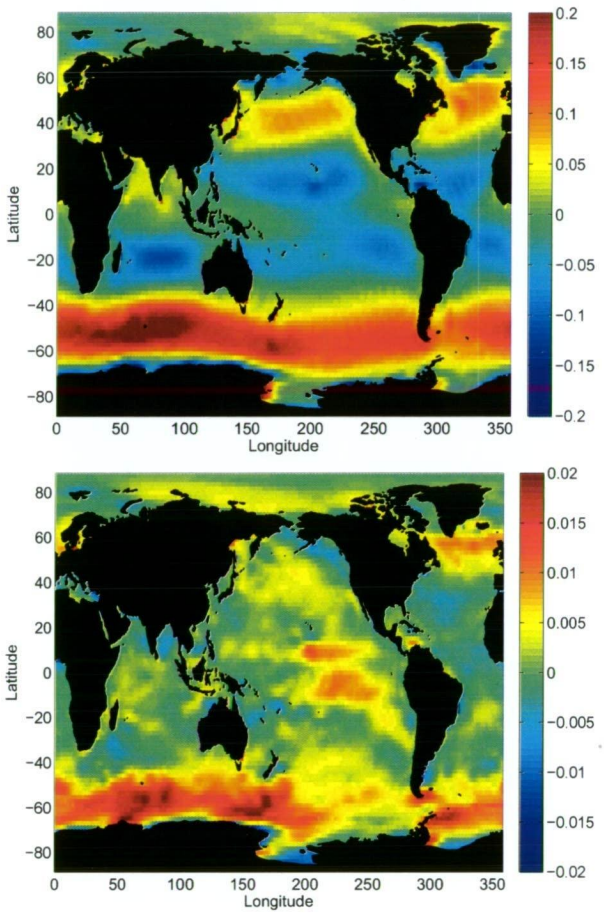

Figure 2.3: NCEP-1 mean zonal wind stress in N/m^2 (top) and trend in N/m^2 per decade (bottom). In both cases easterly is positive.

far the dominant feature of this figure is the strong positive trend in wind stress (0.01-0.02 N/m^2 per decade) in a coherent zonal band between 50 and 70°S. This trend is strongest in the South Indian Ocean sector. A weakening of the trade winds in the tropical Pacific is also apparent (-0.01 N/m^2 per decade).

2.2.2 European Centre for Medium Wave Weather Forecasting - European Atmospheric Reanalysis-40 (ECMWF ERA-40)

ECMWF ERA-40 is a 40 year global reanalysis product, running from 1957-2001, at 2.5 degree resolution (Uppala et al., 2005). Monthly mean wind stress data were

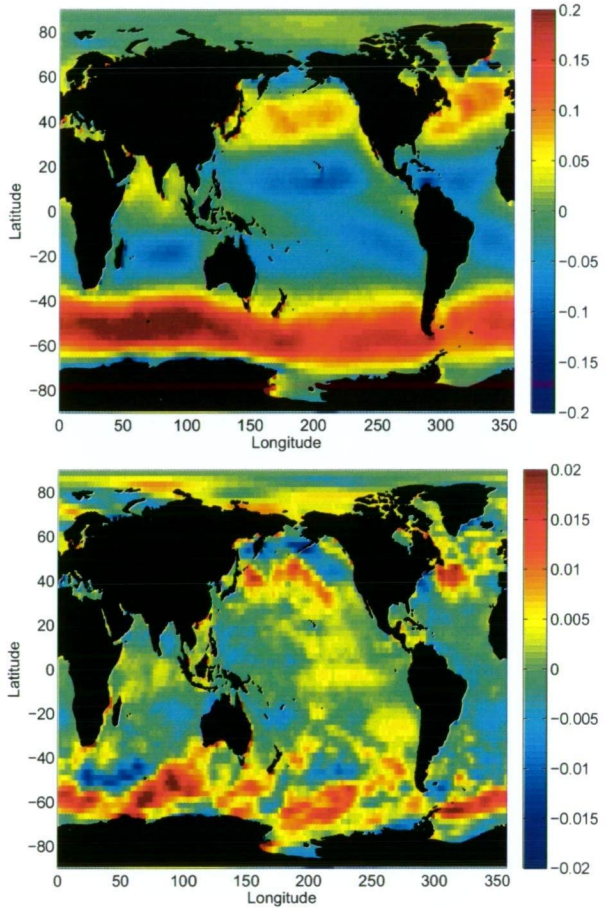

Figure 2.4: ERA-40 mean zonal wind stress in N/m^2 (top) and trend in N/m^2 per decade (bottom). In both cases, easterly is positive.

used. As with NCEP-1, inconsistencies have been noted related to the evolution of the observing system, which impacts the high latitude southern hemisphere in particular (Bromwich & Wang, 2008). The mean and the trend in zonal winds is shown in Figure 2.4. A hemispheric strengthening of winds is seen centred on 60°S albeit patchy. Maximum trend values are around 0.01-0.02 N/m^2 per decade. This trend is strongest in the South Indian Ocean. The weakening of the trade winds is also seen, but is less then 0.005 N/m2 per decade.

2.2.3 Comparing NCAR-NCEP-1 and ECMWF ERA-40

NCEP-1 and ERA-40 represent two approaches to developing atmospheric reanalyses. As discussed above, much attention in the literature has focussed on the enhanced trend in the polar vortex, found in NCEP-1 as discussed above. Analysis suggests that ERA-40 is more accurate during the satellite era (1980 onwards). ERA-40 is more reliant on satellite data than NCEP-1, which relies on station based data, so there are larger inconsistencies in ERA-40 prior to the satellite era (Bromwich & Fogt, 2004; Bromwich & Wang, 2008). Figures 2.3 (NCEP-1) and 2.4 (ERA-40) highlight the differences between the two models in terms of mean zonal winds and trend. Both NCEP and ERA-40 products show a positive trend in the southern hemisphere westerly winds with maximum values of around +0.02 m/s per decade (Figure 2.3 and 2.4). However, the trend in the southern hemisphere westerlies since 1960 appears to be more zonally coherent in NCEP, especially from Southern Africa to south of Australia and New Zealand, whereas the trend in ERA-40 is much more patchy. While much attention has focused on differences and inconsistencies at high latitudes, Grotjan (2008) also identified significant differences in primary circulation and energetics of the two products in the equatorial region. In Figures 2.3 and 2.4, NCEP-1 also shows a more coherent weakening of the trade winds in the tropical Pacific than ERA-40.

The focus of this study is on the role of the winds in driving low frequency variability in the South Pacific gyre and hence the East Australia Current. Figure 2.5 shows a time series of South Pacific regional mean wind stress curl for NCEP and ERA-40 (180-280°E, 20-50°S). While the magnitude of wind stress curl differs (estimates of 4-6*10^{-8} N/m^3, and 5.5-7.5*10^{-8} N/m^3 for NCEP and ERA-40 respectively), the phases and amplitudes of decadal variability are very similar, and it is this low frequency variability, and its connection to regional ocean circulation, which is

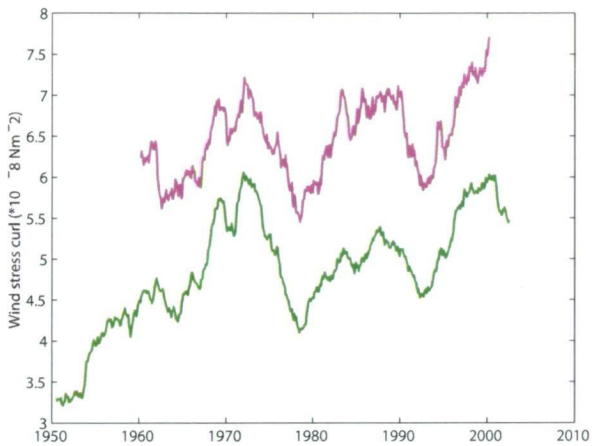

Figure 2.5: South Pacific regional mean wind stress curl 20-50°S, 180-280°E for NCEP-1 (green) and ERA-40 (pink).

the focus of this study. While there are some shortcomings in both of these wind product datasets, they represent the best effort in recreating the structure of the atmosphere over the last 50 years. Results from both reanalyses will be discussed in chapters 3 and 4.

2.2.4 Simple Ocean Data Assimilation (SODA) ocean reanalysis

SODA version 2.0.2 is a 0.5 degree ocean reanalysis product covering the 44 year period between 1958 and 2001 forced by ERA-40 winds (Carton & Giese, 2006). The model uses the Parallel Ocean Program (POP) model with an average resolution of 0.25° and 0.4° in the zonal and meridional directions and has 40 vertical levels. Fields from SODA that are used here have been mapped onto a 0.5 degree grid using optimal interpolation. Because altimeter sea level observations represent such a major change in the observation base, these are excluded from the reanalysis.

SODA employs a sequential data assimilation scheme that uses fields from the numerical model as a background field at the update time (every 10 days). At each assimilation step, an optimal interpolation technique is used to compute an analysis

by combining the background field with an array of observations. The model is initialised with the analysis and integrated forward in time until the next assimilation step. Due to the sequential nature of the adjustments, the reanalysis fields do not generally conserve mass or heat.

Steric sea level rise was assessed by comparing SODA version 1.2 with 20 tide gauge station sea level records from around the world on sub-seasonal timescales (Carton et al., 2005). A positive relationship was found at all selected tide gauge stations, with an average correlation of r=0.7. This represents a substantial improvement on previous versions of the SODA reanalysis. Carton et al. (2005) also compared the SODA dynamic height with altimeter sea level, and found very good spatial agreement in the linear trends with sea level rise concentrated in the western Tropical Pacific, eastern Indian and Southern Ocean. This is promising considering that altimeter data are excluded from the reanalysis.

2.2.5 German-Estimating the Climate and Circulation of the Ocean (GECCO) ocean reanalysis

GECCO is based on the 1 degree ECCO/MIT adjoint ocean model, which is brought into consistency with satellite and in situ observations from 1952-2001 (Koehl et al., 2006). During the optimization, initial temperature and salinity conditions, as well as time dependant fluxes of momentum, heat and freshwater, are adjusted by an adjoint method in order to bring the model into agreement with observations. Background forcing consists of NCEP-1 wind stress, net heat and freshwater fluxes. This approach is therefore mass and energy conserving.

Some of the adjustments made to the fluxes are likely to have been made due to reasons other than errors in the fluxes. For instance, to make up for the low spatial resolution, especially in the equatorial Pacific, the winds in this region were enhanced by the model during the optimisation process, to improve the dynamics

in this region. The first 10 years of GECCO were excluded from this study due to issues with long term adjustment processes to the initial conditions (Koehl et al., 2006).

Comparison of GECCO with observations of the tropical Atlantic circulation suggests that GECCO produces the transports of the major currents well (Rabe et al., 2008). The dynamically consistent assimilation scheme doesn't introduce artificial source or sink terms into the ocean. However, it was found that unresolved processes (in particular, due to coarse model resolution) may project onto the forcing fields during the optimisation process, so winds may not be more realistic in all regions. While these wind perturbations appeared to be an effect on seasonal to interannual timescales, Rabe et al. (2008) suggest long term variability in wind stress forcing seems less perturbed in this way. GECCO has also been used to assess decadal sea level changes (Koehl & Stammer, 2007). Regional changes in sea level were linked predominantly with an intensified sub-tropical gyre circulation and the associated heat redistribution.

In summary, no model can perfectly represent the ocean due to unresolved processes and numerical errors. GECCO and SODA take different approaches to managing these model deficiencies. GECCO, by adjusting the surface fluxes, and SODA by having artifical sources of heat and momentum in the ocean.

2.2.6 BlueLINK Reanalysis

Version 2.1 of the Bluelink ReANalysis (BRAN 2.1) is the latest iteration of the ocean reanalysis from the Australian BLUElink ocean forecasting effort (Oke et al., 2008; Schiller et al., 2008). While BRAN only spans the period 1993-2006, and therefore does not cover the same time period as the other two ocean reanalyses used in this thesis, it is unique in that it focuses on the Australian region at a much

higher spatial resolution than SODA or GECCO. The ocean model is the Ocean Forecasting Australia Model (OFAM) which is based on version 4.0d of the GFDL Modular Ocean Model (Griffies et al., 2004) and is driven by surface fluxes from the ECMWF, including ERA-40, for its duration (until 2001) and operational forecast fields thereafter. The horizontal resolution of OFAM ranges from 1/10° around Australia, to 0.9° across the Indian and Pacific oceans to 2° in the North Atlantic. BRAN will be used in this study for comparisons made during the XBT era.

An advantage of BRAN is that its performance has been comprehensively assessed in the region of interest (Schiller et al., 2008), by comparing the structure and transport of major boundary currents around Australia, providing new insights into the structure and dynamics of the EAC at eddy resolving scales. It was noted by Schiller et al. (2008) that the depth penetration of the EAC was greater than expected, suggesting that the EAC influence may extend through the entire water column.

2.3 Analysis methods and techniques

2.3.1 Use of Ocean Reanalysis Products

Studies of low frequency variability in the ocean circulation are hampered by a lack of long term observations. In the region of interest, Maria provides us with a valuable insight into South Tasman Sea variability and change over the last 60 years, but it is only a single point measurement. Another valuable resource is the expendable bathythermograph (XBT) network, maintained through the Ships of Opportunity Program. Three sections in the Tasman Sea form a closed box, known as the Tasman Box (Roemmich et al., 2005). These lines encompass the main regional currents. They have been operating since around 1991, giving the opportunity to approximately close the heat and mass budgets for the region and

gain insight into the relationships between the main currents, but only for the last 15 years.

Instead of using direct observations to understand ocean variability, an alternative information source are ocean reanalyses. These products provide the only source of estimates of ocean state over multidecadal timescales. Thus, a combination of the GECCO and SODA 50 year ocean reanalyses, Maria, XBT sections and altimeter data are used to explain the role of changes in the South Pacific wind field in causing the decadal variability observed in the EAC system over the last 50 years.

2.3.2 Calculating Transports

Calculating streamfunction and transports from wind fields

Wind stress curl fields were calculated from both NCEP-1 and ERA-40. South Pacific streamfunctions and transports through the Tasman Sea were then calculated using the Island Rule (Godfrey, 1989) for each whole decade, and then compared. The Island Rule is an adaptation of the Sverdrup approximation, which allows for flow around islands. Wind stress curl is integrated in a path from the eastern boundary of the basin, round the back of an island to determine the wind driven flow around that island (Figure 2.6). This gives a transport value to the island, which then allows the streamfunction around the island to be contoured. Consequently, the transport through the Tasman Sea (or net EAC transport) was defined as the difference in Island Rule values for Australia and New Zealand.

Calculating Transport across diagonal sections from gridded Ocean Velocity

Both GECCO and SODA were used to recreate the Tasman Box lines, and calculate transport in to and out of the box so that these could be compared with the in situ data. Figure 2.7 shows a map of the region and the lines which make up the closed

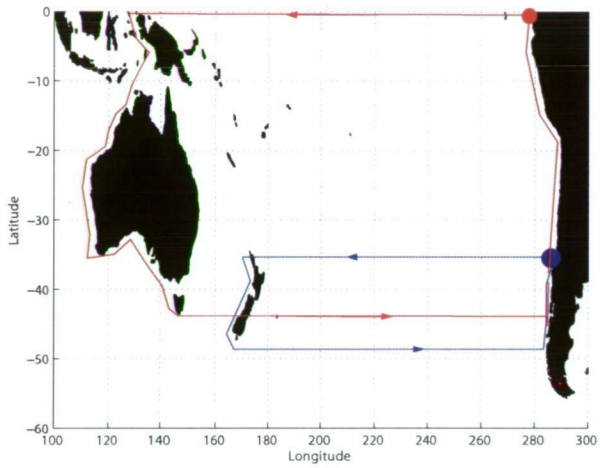

Figure 2.6: A schematic of the Island rule. To calculate the Island rule for a particular island, winds are integrated in a closed path starting in the eastern boundary of the basin at the latitude of the northern limit of the island, across the basin, around the west coast of the island, back across the basin, and back up the eastern boundary of the basin. We define the Island rule transport through the Tasman Sea as the difference between the Island rule value for New Zealand, and the Island rule for Australia.

Tasman Box. As ECCO and SODA use different model grids, different approaches to the calculations were taken. GECCO uses a C grid model which allows a "stair step" approach to be used (see Figure 2.7) without the need for interpolation (Koehl et al., 2006). The sum of transports in to and out of the box balanced to within 10^{-5} Sv, and the net transport through the Tasman Sea averages 5 Sv to the South.

SODA and BRAN use a B-grid model, and in the case of SODA, the results are then remapped, so an approach is used whereby velocity vectors were interpolated to the particular XBT section and then rotated so that they were perpendicular or normal to the section (Oke et al., 2008; Carton & Giese, 2006). Using this approach, the sum of the transports balance to within -0.9 Sv for SODA and -1.6 Sv for BRAN in the mean. While we acknowledge that this approach may introduce some errors, the errors were larger when a stair step method was used (mean inbalance: -4 Sv for BRAN). The largest variations between calculation methods were found on the

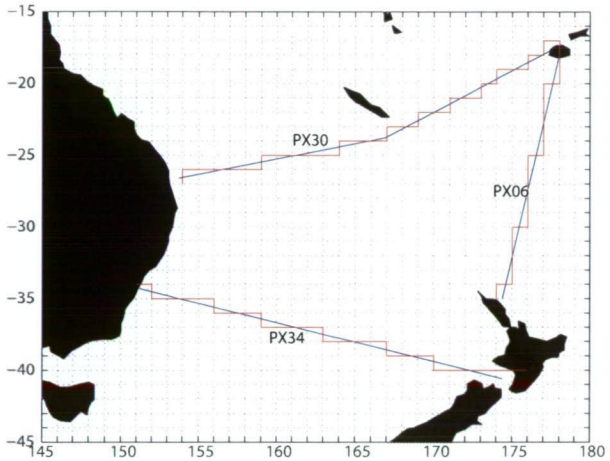

Figure 2.7: A schematic of Tasman box XBT sections and the gridstep approximation used to calculate transports from GECCO.

Sydney to Wellington section which crosses a highly dynamic region of the EAC, close to the separation point (see Figure 2.8). Thus, it was decided to stay true to the XBT section and rotate the velocities. Furthermore, the imbalance appeared as a net offset of 1.6 Sv with an RMS of 1.8 Sv. Therefore while the actual values may be subject to an error, we have confidence in interpreting the patterns of variability. Representation of mesoscale structure and variability along the Sydney to Wellington line maybe the source of this offset. In the case of BRAN, the higher resolution may introduce errors from small temporal scale variability, whose timescales are unresolved in monthly mean. In the case of SODA, the interpolation from the original model grid to the output grid is another source of error.

To plot velocity and temperature sections, GECCO, SODA and BRAN data were interpolated onto the XBT lines. Velocities were rotated to illustrate cross sectional velocity. To illustrate the influence of the position of the SEC on transport across the Auckland to Fiji line, and the extent to which the SEC is partitioned by Fiji, velocity sections were extended north of Fiji towards the equator along 180E.

The Tasman Front transport calculated from the reanalyses was calculated as the

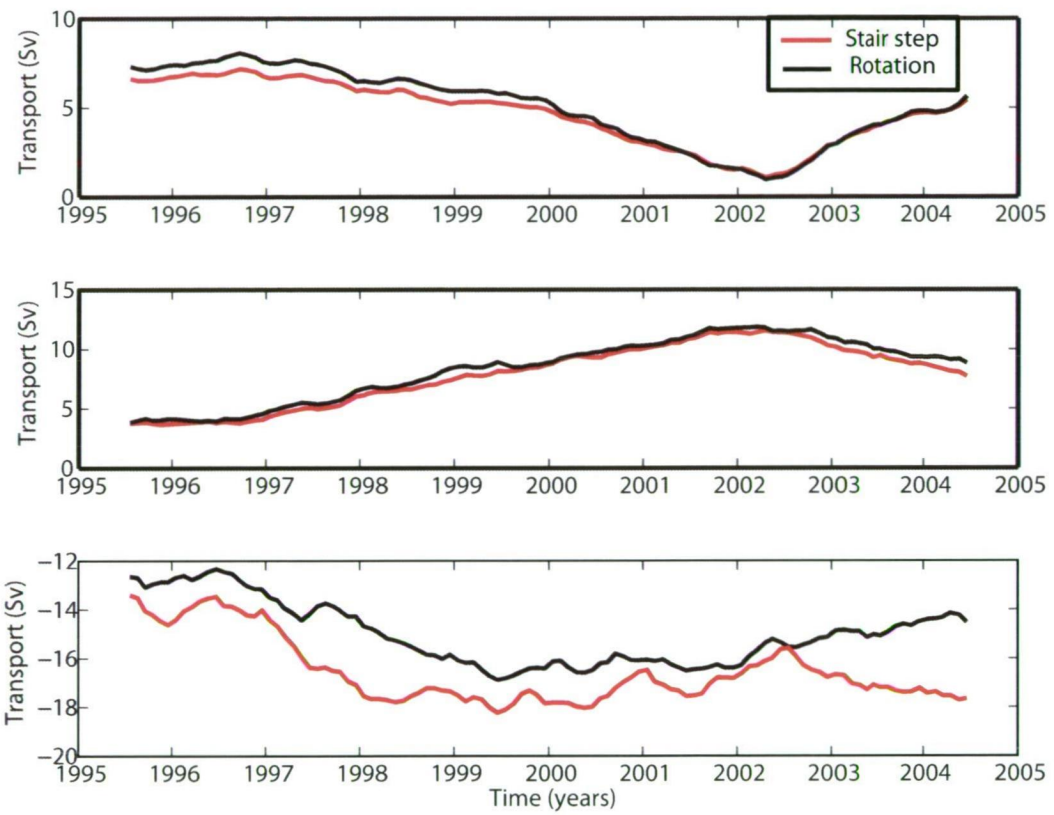

Figure 2.8: Comparing rotation and stairstep methods of calculating transports across diagonal sections PX06 Auckland to Fiji (top), PX30 Brisbane to Fiji (middle) and PX34 Sydney to Wellington (bottom)

sum of transport across the southern section of the Auckland to Fiji line. The northern limit of this analysis was identified in mean rotated velocity sections where there was a coherent transition from eastward to westward velocities. We define this as 32°S for BRAN, 28°S for SODA and 27°S for GECCO (compared to 31°S for the XBT/Altimeter method). A different cut-off latitude was used for GECCO, as features, such as the Tasman Front, are smoother and broader due to the reduced resolution. As the Sydney to Wellington section crosses close to the point where a portion of the EAC separates from the coast to form the Tasman Front, the transport calculations could be contaminated by eddies if the same method was employed. Therefore, the EAC Extension transport was defined as the net southward transport through the Tasman Sea, across the Sydney to Wellington line.

2.3.3 Filtering of Timeseries

To focus on the lower frequency signals in the time series of interest, low pass filtering has been used in the form of a 5 year running mean. This has been used on all time series data to allow us to focus on decadal timescale variability. Figure 2.9 shows the wavelet spectrum for the filtered and the unfiltered Maria time series. The spectrum for the unfiltered time series shows a coherent energy signal on decadal timescales throughout the full time series, in addition to interannual energy which does not seem to fit a consistent timescale throughout the period. The wavelet spectrum of the low pass filtered time series shows that these interannual signals were effectively filtered out, while preserving most of the decadal timescale energy.

2.4 Summary and next steps

In this chapter, the observational data, atmospheric and ocean reanalysis products and their applications have been described. In the following 2 chapters, the results

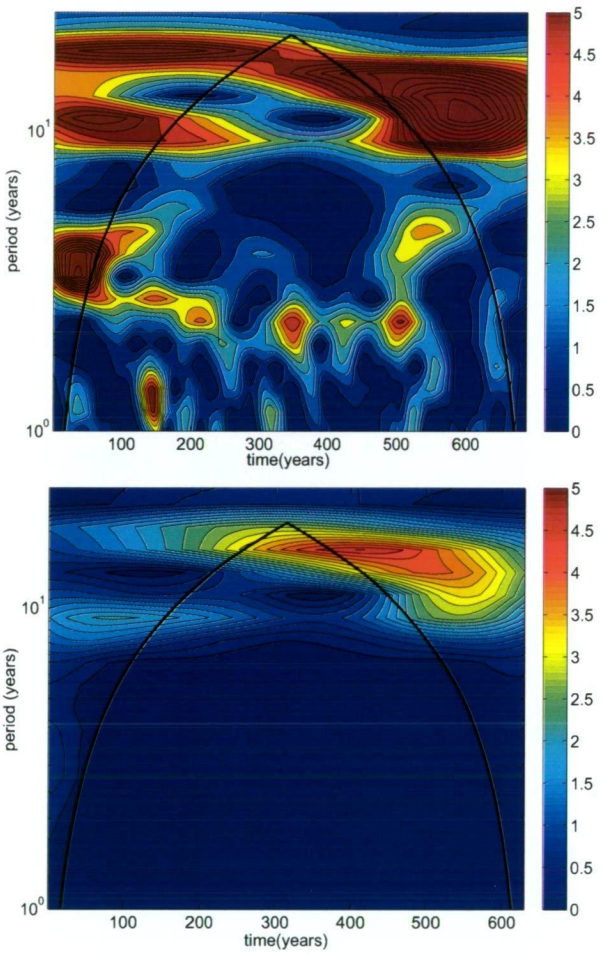

Figure 2.9: Maria Island coast station SST power spectrum for unfiltered (top) and 5 year low pass filtered (bottom) timeseries. Black line indicates the 'cone of influence', outside which, edge effects become important (Torrence & Compo, 1998).

of analyses will be discussed. In chapter 3, the Maria timeseries will be explored, focussing on observed low frequency variability in the timeseries, and compared with wind patterns in the South Pacific from the atmospheric reanalysis. In chapter 4, the 50 year ocean reanalysis products and XBT data will be discussed in the context of gaining further understanding of patterns of low frequency variability in the South Pacific region.

CHAPTER 3

Wind forced variability in the East Australian Current

3.1 Introduction

In this chapter I use Maria Island coast station timeseries, and NCEP and ERA-40 reanalysis winds to make the case that changes in temperature and salinity at Maria are representative of changes in the strength or southward penetration of the EAC. I also present evidence that low frequency variability in the East Australian Current is closely related to low frequency variability in the South Pacific winds. Finally I conclude that the EAC responds to changes in the South Pacific winds faster than is possible by a first mode baroclinic Rossby wave response.

The chapter is set out as follows. First, the observed variability in temperature and salinity from Maria Island coast station time series is described. The relationship between Maria and the EAC is discussed in the context of regional climatology T/S properties in section 3.2.1. The observed changes and variability in the South Pacific wind field are then described in section 3.2.2, and in section 3.2.3, variations in wind driven circulation and net EAC Extension transport are deduced from Island Rule calculations. Section 3.2.4 focuses on the relationship between Maria Island coast station and variations in the South Pacific wind field and section 3.3 is the discussion

for this chapter.

Some of the results in this chapter have been published: Hill, K.L. and S.R. Rintoul and R. Coleman and K. Ridgway (2008) Wind forced low frequency variability in the East Australian Current *Geophysical Research Letters*,35 doi:10.1029/2007GL0391

3.2 Results

3.2.1 Analysis of T/S variability at Maria Island Coast Station

Temperature and salinity timeseries from Maria Island coast station both exhibit a strong positive trend, as well as significant decadal timescale variability (Figure 3.1). The trend in temperature and salinity from 1944-2006 is equivalent to +0.22°C and +0.03psu per decade, respectively. This rate of change is 2-3 times that of the global average ocean temperature trend (Ridgway, 2007; Smith & Reynolds, 2004; Casey & Cornillion, 2001).

On annual timescales, sea surface temperature and salinity (T/S) at Maria Island coast station show significant seasonal variability (see Figures 3.2 and 3.3), with an annual amplitude of 4.2°C and 0.05 psu respectively. This is related to the seasonal variability in the strength of the EAC, which is stronger in austral summer (defined as January to March) than winter (July to September) and brings warm salty water down the east coast of Australia (Cresswell, 2000; Ridgway, 2007). The trend in both temperature and salinity is also stronger in summer (+0.25°C and +0.05 psu per decade) than winter (+0.15°C and +0.02 psu per decade), suggesting this is also related to changes in the strength of the EAC.

Low-frequency changes in temperature and salinity at Maria Island strongly co-vary, with a trend over time from colder and fresher to warmer and saltier waters (Figure 3.4). The co-variation and summer/winter temperature/salinity changes suggest that the observed changes are due to advection. The time evolution of T/S

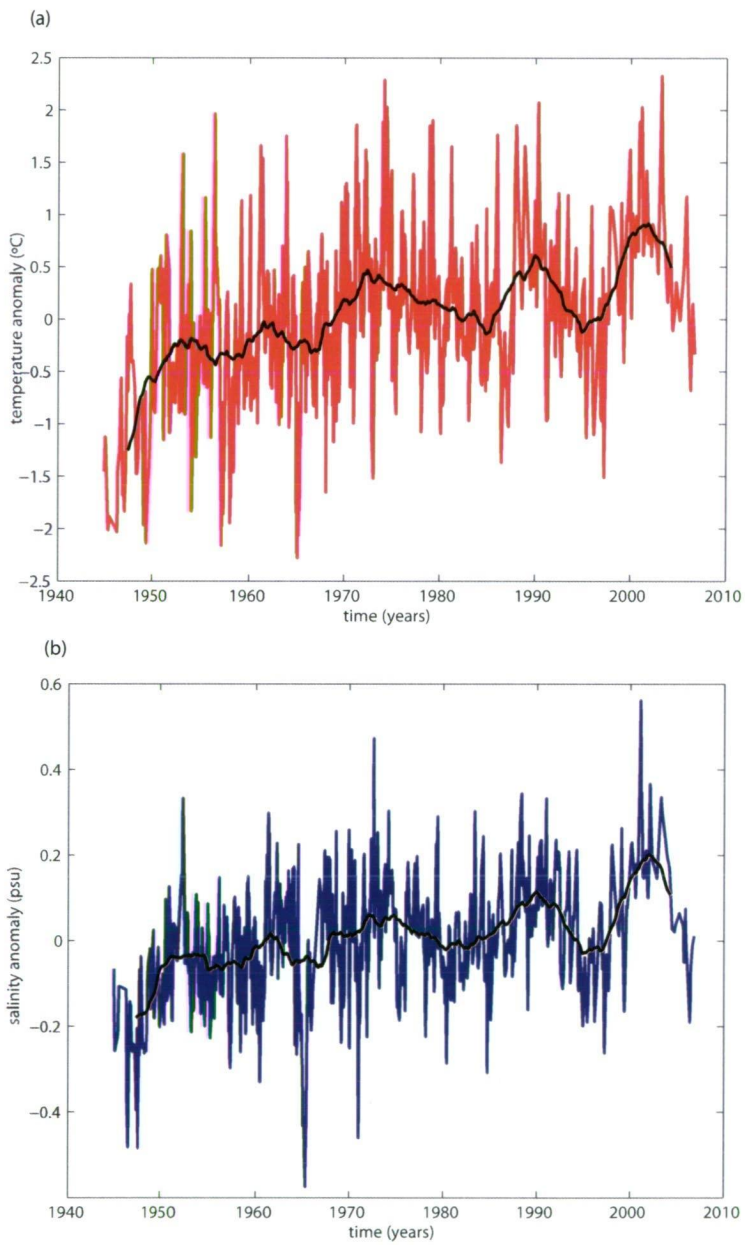

Figure 3.1: (a) Monthly SST anomaly timeseries at Maria Island Coast Station (red) 5 year low pass filtered (black)(b) Monthly surface salinity anomaly at Maria Island coast station (blue) and 5 year low pass filtered (black).

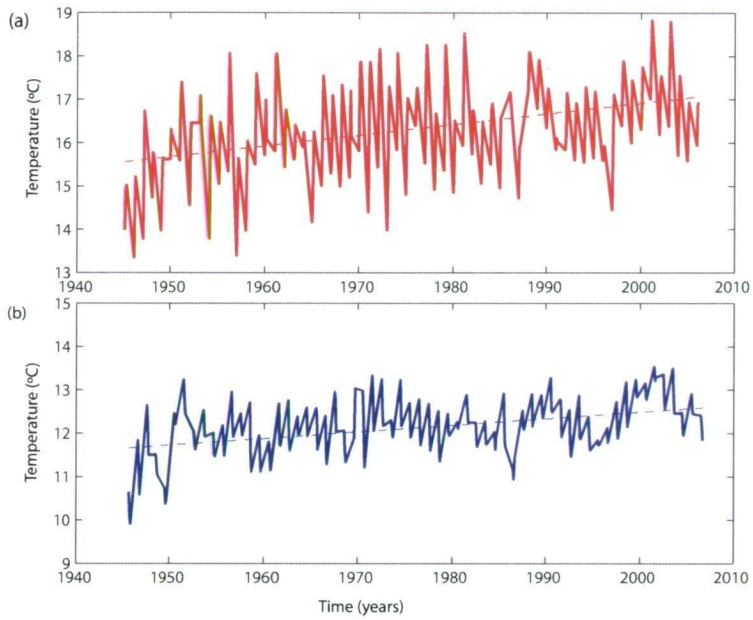

Figure 3.2: Comparing monthly sea surface temperature at Maria during (a) summer (January-March) and (b) winter (July-September)

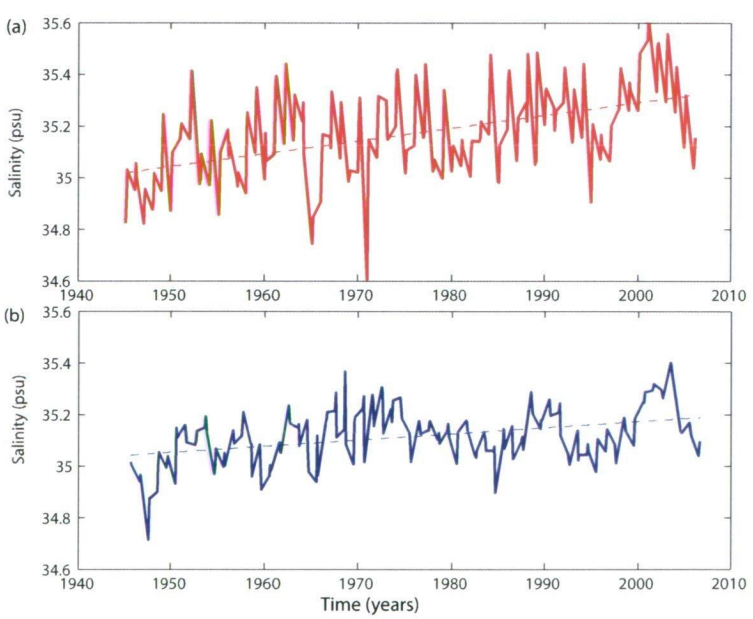

Figure 3.3: Comparing monthly sea surface salinity at Maria during (a) summer (January-March) and (b) winter (July-September)

properties at Maria Island closely follows the CARS climatology T/S relationship along the path of the EAC Extension, and changes in this relationship represent the changes in the influence of cold fresh Southern Ocean waters relative to northern warm salty EAC waters. The influence of the EAC waters relative to Southern Ocean waters has increased markedly over time. The increase in temperature and salinity since 1944 corresponds to a southward shift of the climatological surface temperature and salinity properties by about 2.5 to 3 degrees of latitude (near 44.5°S to 41.5°S as seen in Figure 3.4). The EAC's influence also appears to vary on decadal timescales. As outlined in chapter 1, the EAC forms the western boundary current of the South Pacific wind driven gyre. Hence, it is logical to look to the broader scale wind field to explain the observed changes and variability in the EAC's strength.

3.2.2 Changes in the wind driven circulation of the South Pacific

Changes in the South Pacific wind field

A general positive trend in the strength of the Southern Hemisphere westerly winds south of 50°S is clearly illustrated in the NCEP-1 reanalysis wind stress product (Figure 3.5). The cause of this has been discussed in the literature and outlined in chapter 2. A general weakening of the trade winds can also be seen. However, in terms of driving ocean circulation, it is the wind stress curl field, or gradient of wind stress which is important; predominantly caused by the gradient between the extratropical westerly winds, and the trade winds (Figure 3.6). The maximum curl is at 40-45°S, and a general increase in the curl is found across the South Pacific Basin between the 1950s and 1990s, with maximum changes in the region around southern New Zealand where the wind stress curl has effectively doubled from $0.1*10^{-6}$N/m^3 to $0.2*10^{-6}$N/m^3. The zero curl line marks the boundaries of the gyre. The southern boundary of the gyre does not show a consistent shift north or south. The zero line marking the southern boundary has shifted south by about

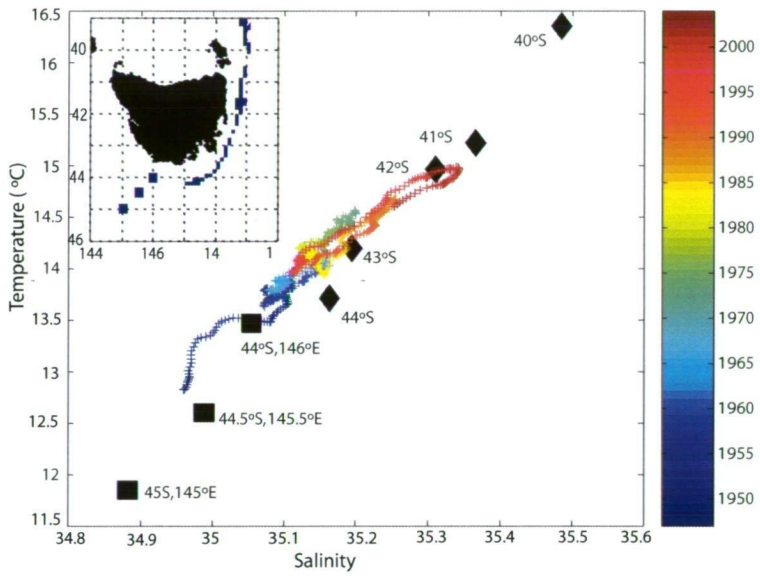

Figure 3.4: The multi-coloured line is the time evolving low pass filtered surface temperature and salinity data from Maria Island coast station (50m isobath). The diamonds represent the mean surface T/S relationship along the continental slope between the 500 and 1500m isobaths from the coastal CARS atlas (blue areas on map), +/-0.5 degrees from specified latitudes. The squares represent the colder/fresher surface climatological temperature and salinity endpoint from the CARS Atlas, at the specified latitudes and longitudes (blue squares on map) south and west of Maria.

5° south of Australia and New Zealand between the 1950s and the 1990s, but has shifted north by a similar amount in the western Pacific and shows very little change in the eastern Pacific

Island rule streamfunction and transport estimates

To determine the influence of the observed changes in winds on the South Pacific circulation, the streamfunction for the South Pacific was calculated using the Island Rule (Godfrey, 1989) and NCEP-1 wind stress (Figure 3.7). There is an increase in the strength of the gyre between the 1950's and 1990's, which manifests in a 5 Sv increase in the EAC transport, as reported by Cai (2006). This increase in gyre circulation is in association with the described increases in wind stress curl. In addition, the gyre appears to be broader both meridionally and zonally in the 1990's. In the 1950s, the bulk of the gyre circulation is confined to 20-30°S, whereas in the 1990's, the gyre appears to occupy the region between 20 and 45°S, with an increase in the recirculation through the Tasman Sea. In both cases, there doesn't appear to be a clear Tasman Front, with no streamlines extending across the Tasman Sea and north of New Zealand.

Limitations and approximations of Island Rule

The Island Rule provides a good approximation of the time mean wind driven circulation, representing the general shape and pattern of the South Pacific Gyre well, including the Western Boundary Current. However, it does have some limitations. Sverdrup approximation and use of the Island Rule assumes the system is linear and in equilibrium which would require an instant adjustment to winds on basin-wide scales. I make this assumption when calculating the time varying Island Rule. Full Rossby wave adjustment can take decades at subtropical latitudes. It should also be questioned whether the linear approximation can hold at western bound-

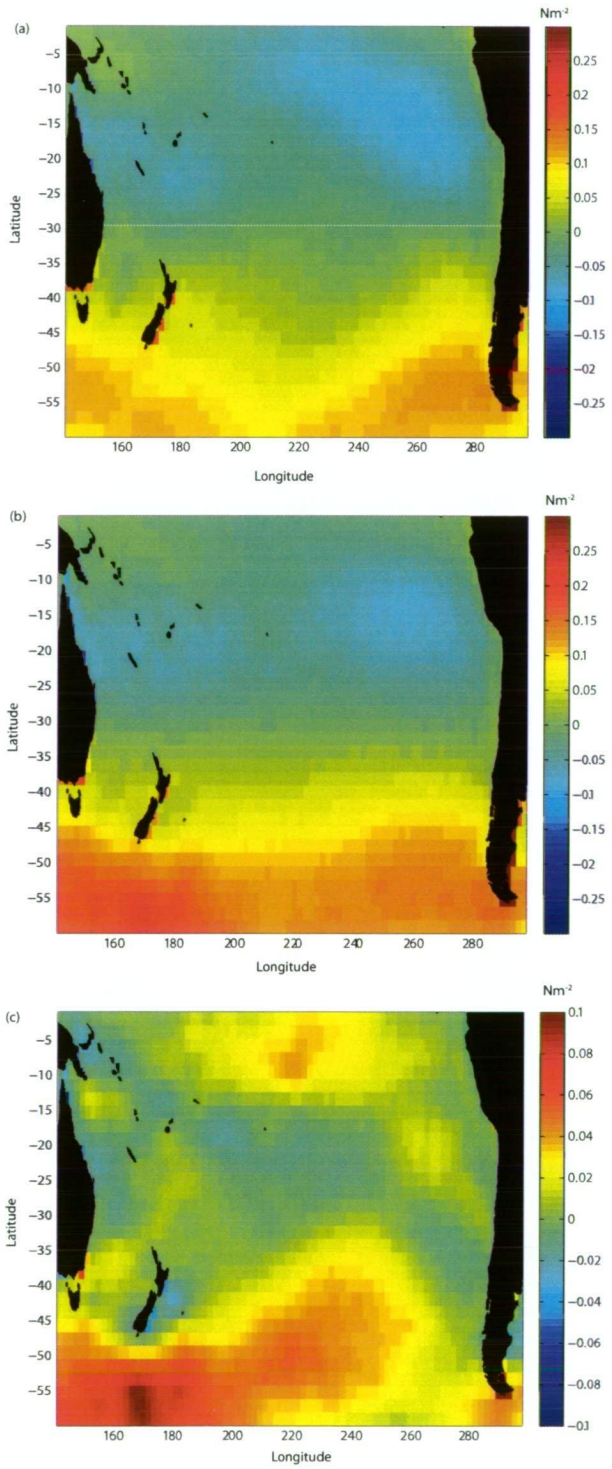

Figure 3.5: NCEP south Pacific zonal wind stress (eastward) for (a)1950s, (b) 1990s, (c) 1990s minus 1950s (N/m^2)

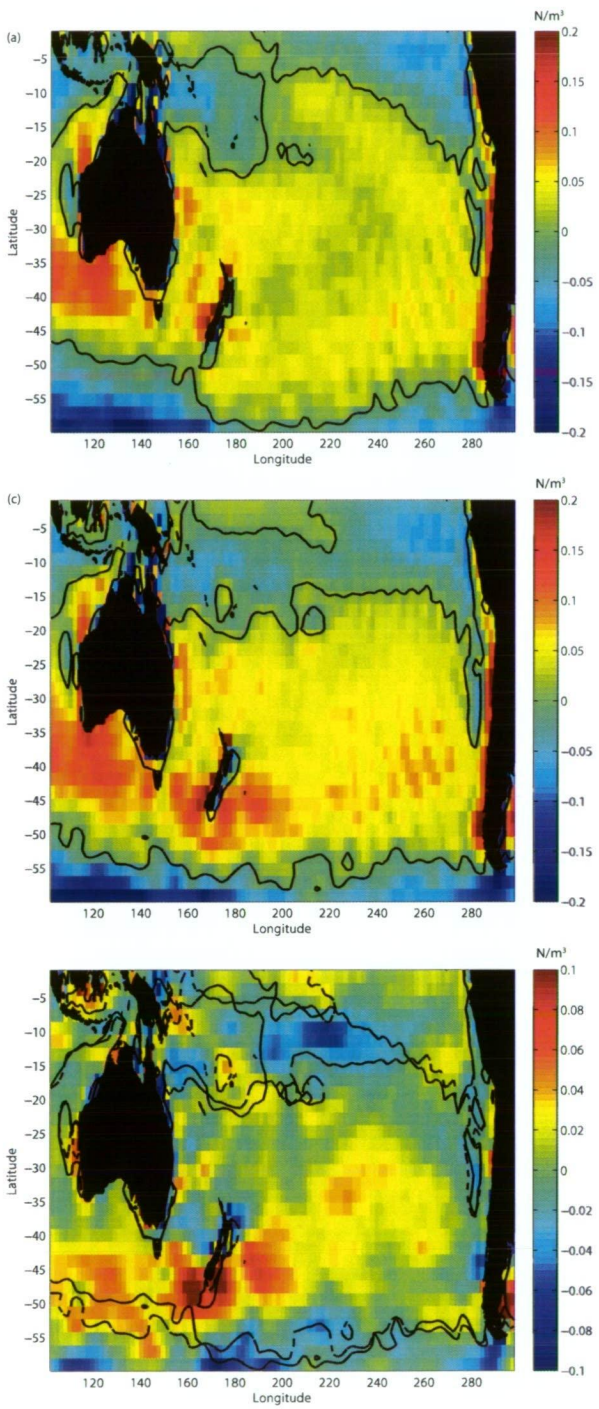

Figure 3.6: NCEP mean wind stress curl for the (a) 1950s (b)1990's (c)1990s minus 1950s (*10^6 N/m^3) in (a) and (b), the black line denotes the zero wind stress curl line. In (c), the solid line is the zero wind stress curl line for 1950s and the dashed line is the zero wind stress curl line for the 1990s

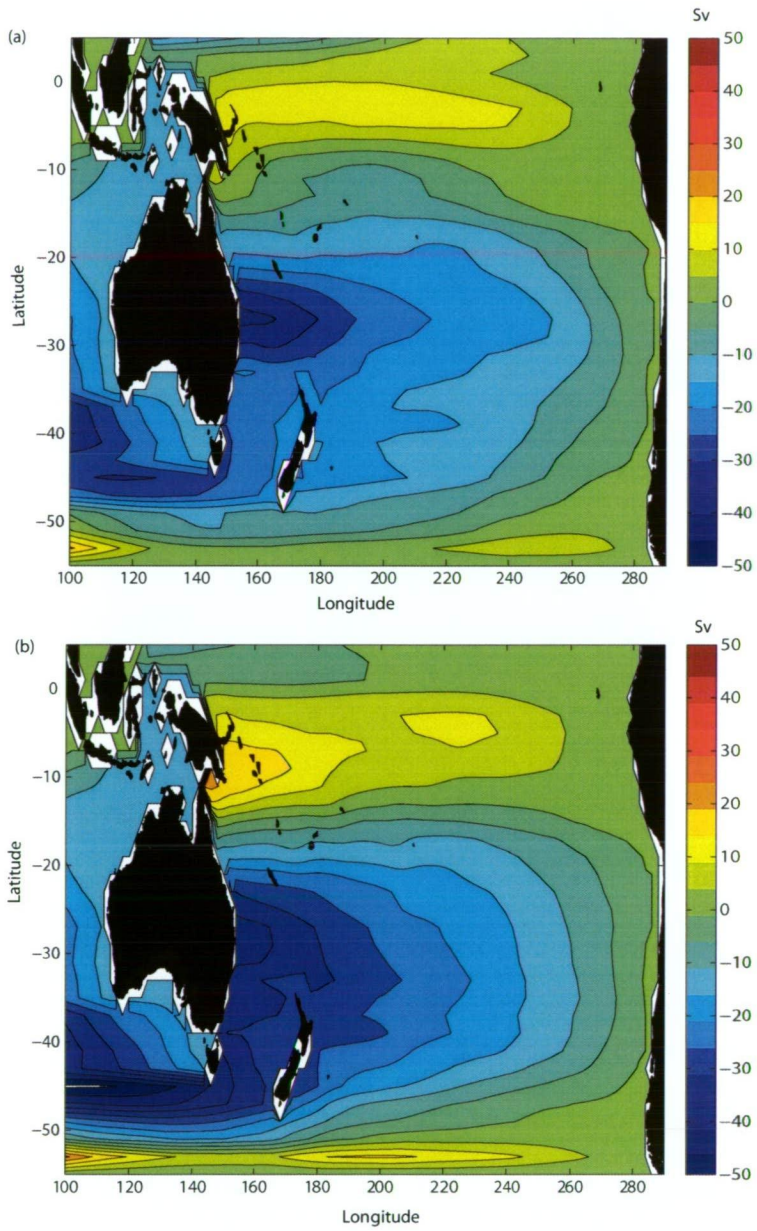

Figure 3.7: The streamfunction in the South Pacific calculated from NCEP-1 wind stress and Island Rule for the a) 1950's and b) 1990's.

aries, which are characterised by non-linear features such as eddies, separations (i.e. the Tasman Front) and retroflection features.

The difference between the Island Rule value for New Zealand and Australia gives us the geostrophic transport through the Tasman Sea, and hence an approximation of the net EAC transport. However the above limitations should be kept in mind. For instance, the Tasman Front is not clearly resolved. This may be, in part, due to the non linear nature of the EAC separation, and the nature of the Tasman Front, which is characterised by a narrow, eddy rich and uncontinuous flow across the basin. The coarse resolution of NCEP-1 wind stress, at 2°, may also mean that these characteristics are not spatially resolved. The lack of a distinct Tasman Front may mean that the estimates of the EAC extension are larger than expected, and the shape of the gyre may not be accurate. The strong jet to the west of Tasmania is also unrealistic. These unrealistic features are likely caused by the assumption that the Gyre is totally governed by linear dynamics. This doesn't hold for the highly energetic regions such as the Southern Ocean and western boundary currents. The Island rule will be compared with models with more complete physics in chapter 4, to quantify the limitations of the Island Rule, and to gain an understanding of the non-linear component of gyre characteristics.

3.2.3 The role of changes in the South Pacific wind field

Comparison of the SST and salinity at Maria, with regional mean wind stress curl in the South Pacific, and transport through the Tasman Sea calculated using Island Rule (Figure 3.8) suggest that changes in Maria SST and salinity can be related to changes in the regional mean wind stress curl over the South Pacific, and hence transport through the Tasman Sea. These time series all exhibit an upward trend, equivalent to +0.22°C, and +0.03psu, $+0.34*10^{-8}$N/m^{-3}, and +2.0 Sv change per decade for temperature, salinity, wind stress curl and transport, respectively. The

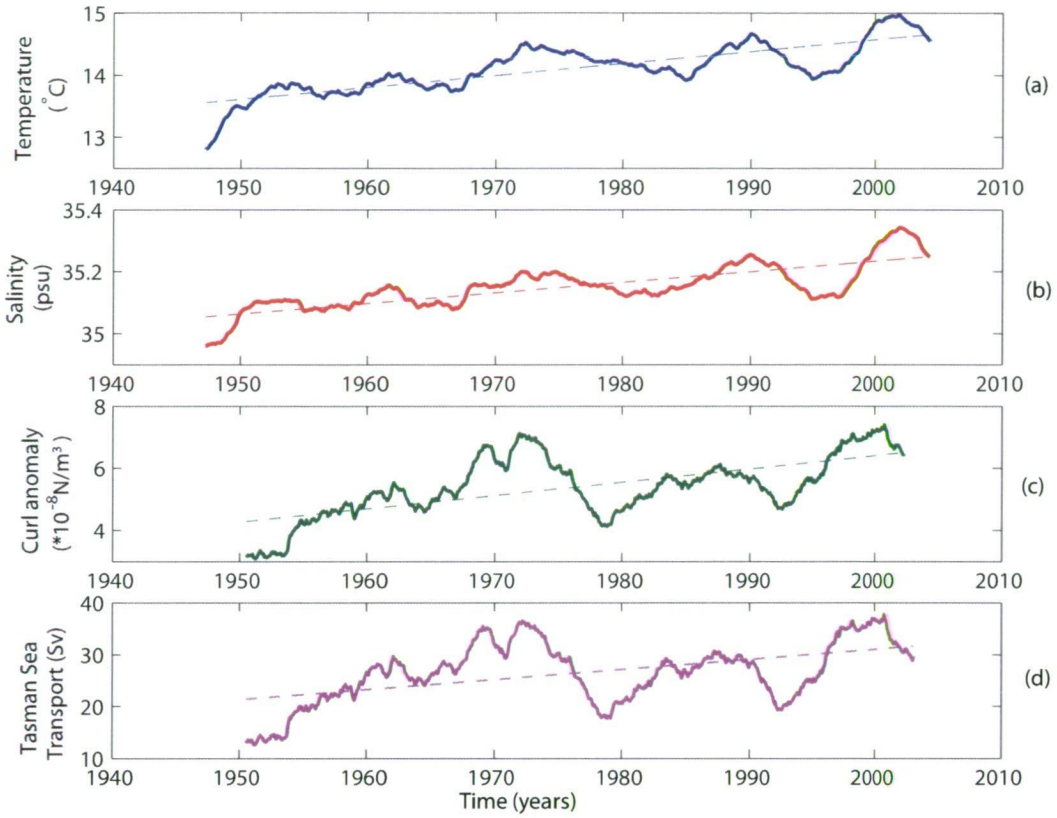

Figure 3.8: Low pass filtered (a) sea surface temperature at Maria (b) surface salinity at Maria (c) South Pacific regional mean wind stress curl (20-50°S, 180-280°E) from NCEP(d)net transport through the Tasman Sea calculated from NCEP and using Island rule.

small difference in temperature and salinity trends between this study and Ridgway (2007) can be accounted for by the longer Maria dataset used here (1944-2006, compared to 1944-2001). Maria temperature and salinity, NCEP wind stress curl and Island Rule transports all exhibit a similar pattern and phase of decadal timescale variability.

Regional mean wind stress curl and transport through the Tasman Sea were also calculated from wind stress ERA-40 fields, and compared with the observations at Maria (Figure 3.9). The trend in the curl is not as large as with NCEP ($0.2*10^{-8}$N/m^3 per decade), and there is a negative trend in the resultant Tasman Sea transport (-1.3

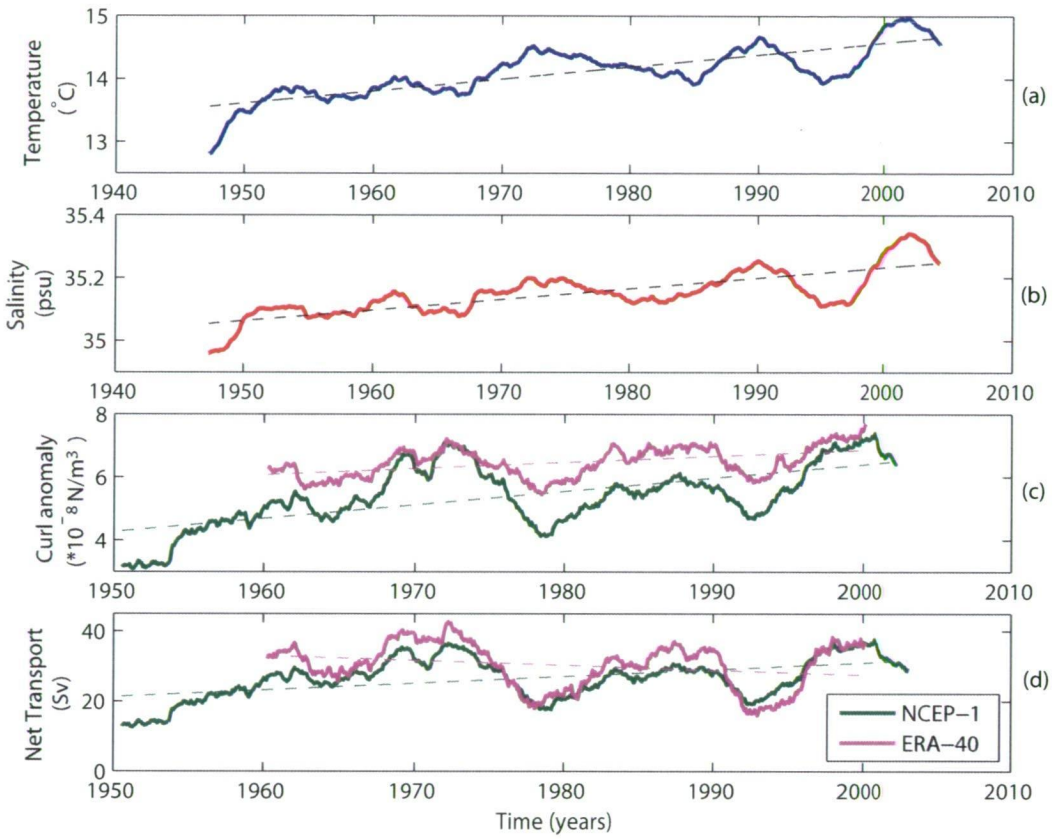

Figure 3.9: Low pass filtered (a) sea surface temperature at Maria (b) surface salinity at Maria (c) South Pacific regional mean wind stress curl (20-50°S, 180-280°E) from NCEP (Green) and ERA-40 (Purple) (d)net transport through the Tasman Sea from NCEP (Green) and ERA-40 (Purple).

Sv per decade). The magnitude of ERA-40 wind stress curl is generally higher, with variability lower in magnitude. However, the pattern and phase of low frequency variability matches NCEP closely (Figure 3.9).

To test the hypothesis that changes in the wind stress curl were the cause of the changes observed in Maria, the lagged cross correlation was calculated between Maria SST and the NCEP-1 reanalysis wind stress curl field in the South Pacific, and SST with transport through the Tasman Sea, calculated from the Island Rule. The maximum cross correlations occur when Maria lags both the wind field and the

Island rule transports by 3 years, with a correlation of r = 0.7 for NCEP winds. The maximum cross correlation between Maria and ERA-40 wind stress curl is seen when Maria is also lagging changes in wind stress curl by around 3 years (r=0.66)and ERA-40 island rule transports by 2 years (r=0.7). The lag between transport and T/S at Maria likely reflects the inadequacies of the Island Rule assumption of an instantaneous response to winds. The observed differences in time lags are likely related to the length of the datasets and the low pass filtering applied (5 years), which means that there are only 3 or 4 realisations of the low frequency signal of interest. However, the visual correspondence of the timeseries, backed up by plausable physical mechanisms of the ocean gyre response to wind forcing adds confidence to the results. For the purposes of this study, I will focus on NCEP-1 winds, as the changes are more consistent with those observed at Maria. NCEP captures both the variability and trend, while ERA-40 appears to only capture the variability.

The spatial pattern of the 3-year lag correlation between Maria SST and winds demonstrates that SST at Maria correlates with wind stress curl basin-wide, with typical r values of 0.4-0.8 (Figure 3.10). The highest correlations are found in the southern part of the basin, east of New Zealand around 210-230°E, and 35-45°S. The black contours show the time taken for the first mode baroclinic Rossby waves to reach the western boundary. It would take 10 years for Rossby waves to transit the South Pacific Basin at 30°S, and 15-20 years at 42.5°S. The areas of high correlation with Maria SST lie well to the east of the line marking the distance from which a first mode baroclinic Rossby wave can reach the western boundary within three years, which is found just to the west of New Zealand.

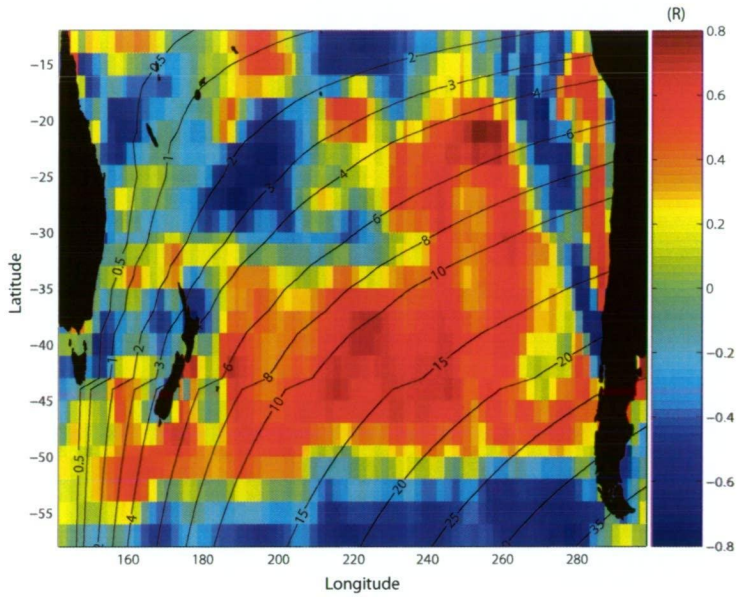

Figure 3.10: Spatial pattern of the 3 year lagged cross correlation between surface temperature at Maria and wind stress curl. Contours are time (years) required for long baroclinic Rossby waves to reach the East coast of Australia.

3.2.4 Modes of variability and the EAC

To determine the relationship between the variability and change in Maria and regional modes of variability, I compare the low pass filtered Maria Island SST with a low pass filtered Southern Oscillation Index (SOI) (Figure 3.11) and the Southern Annular Mode (SAM)(not shown). While both the Maria Island SST and the SAM show a positive trend since 1979, they are uncorrelated because the SAM shows no significant decadal timescale variability. Prior to 1979, estimates of the SAM are less reliable due to the absence of satellite data (Thompson & Solomon, 2002) Maria Island SST and SOI show similar variability on decadal timescales. Both peak in the early 1970s, late 1980s-1990, and around 2002, and the time series are highly correlated (r=0.7 at 12 months lag). This demonstrates a strong relationship between these two time series. However, the time lag doesn't appear to be consistent. Prior to the mid 1970's, peaks in Maria Island SST appear to lead peaks in the SOI,

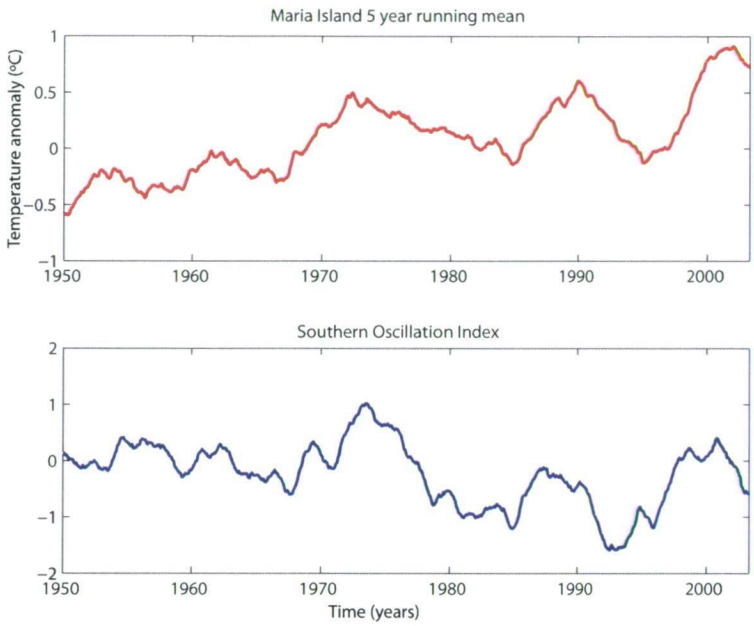

Figure 3.11: Comparing the Maria Island SST anomaly timeseries with the Southern Oscillation Index (SOI). Both timeseries have been low pass filtered with a 5yr running mean

whereas after this date, they seem to lag the SOI. Figure 3.11 shows that the trend in the two timeseries is anticorrelated. This suggests that the trend seen at Maria is related to the Southern Annular mode, but the low frequency variability is related to decadal ENSO variability. Figure 3.12 shows a comparison of the power spectra for both Maria and the SOI. The time evolving decadal variability energy appears to follow a similar pattern with a trend from a period of close to 20 years in 1965, to closer to 10 years in 1995.

3.3 Discussion

The causes of variability and change in the temperature and salinity time series from Maria Island are explored using the CARS climatology data, NCEP atmospheric reanalysis data, and Island Rule theory. Variations in these physical properties at Maria on decadal timescales are shown to reflect the varying influence of EAC waters

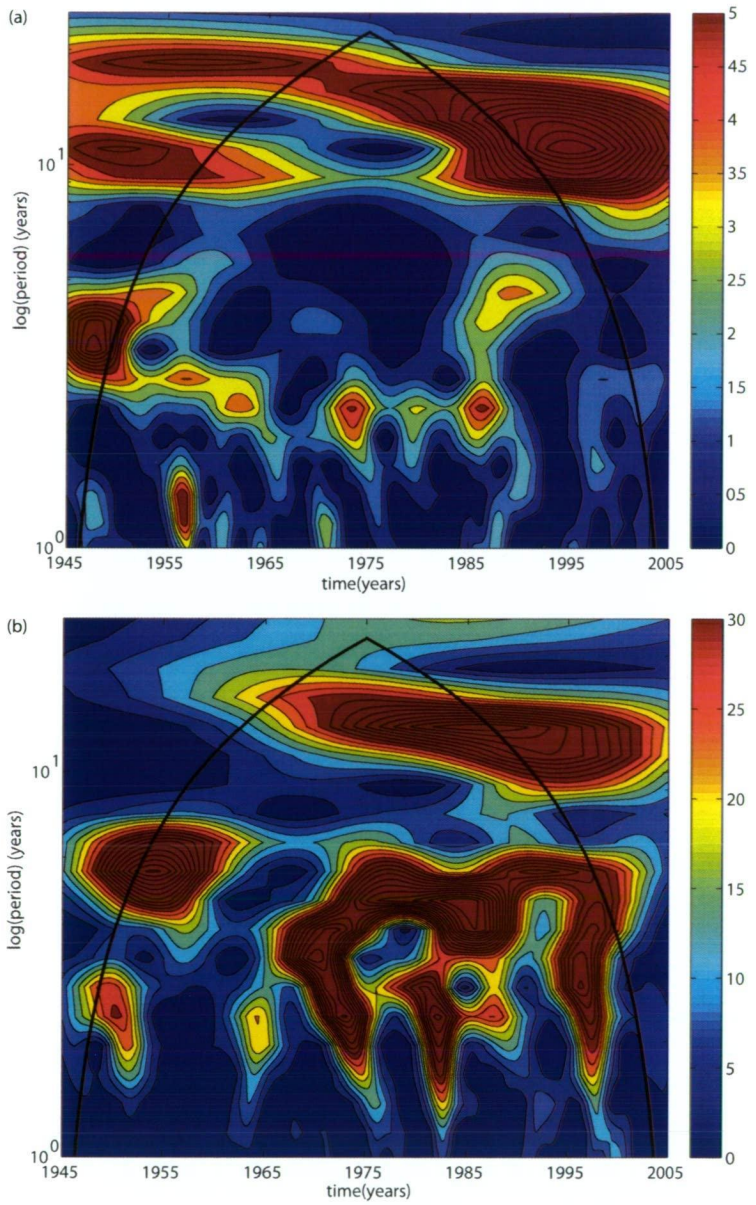

Figure 3.12: Comparing the wavelet spectra of Maria and the SOI. Black line indicates the 'cone of influence' outside which, edge effects become important (Torrence & Compo, 1998)

advecting south. In addition, low frequency variations in the South Pacific winds are strongly correlated with variations in the magnitude of the transport southward through the Tasman Sea, which is dominated by the EAC transport.

Previous work by Ridgway (2007) discussed the 55 year trend in temperature and salinity observed at Maria and related the changes to stronger southward penetration of warm saline EAC waters with time. Cai (2006) used a simple Island Rule model to show that the change in Southern Hemisphere winds over the 55 year period would cause a spin up of the Southern Hemisphere 'super-gyre', consistent with a stronger EAC extension. In section 3.2.2 the link between basin-scale changes in wind forcing and low frequency variability of the EAC is demonstrated, providing a bridge between those earlier studies of the observed trend at Maria, and the trend in the South Pacific winds. Strong decadal variability at Maria is also identified, and the positive relationship between basin - scale wind forcing, transport and temperature and salinity observations at the western boundary is shown to hold on decadal timescales as well.

This study highlights some differences between NCEP-1 and ERA-40 winds. While the utility of these datasets for long term trend analysis has been questioned (Kistler et al., 2001; Bromwich & Fogt, 2004; Hines et al., 2000; Renwick, 2004; Tennant, 2004), the consistency of the decadal variability in both products suggests that they are both useful for analysis of patterns of low frequency signals, which was not possible prior to the advent of these 50 year reanalyses.

The Island Rule solution (Godfrey, 1989) calculated from the NCEP-1 winds suggests that net transport through the Tasman Sea (and hence the EAC) has intensified by almost a factor of two between 1948 and 2001. The low frequency variability of transport is also similar to that of temperature and salinity at Maria. However transports calculated using the Island Rule are large at 10-20 Sv compared

to a mean observed transport of 9.4 Sv from observations (Ridgway & Godfrey, 1994). This could be related to non-linear ocean features such as the separation zone, or bathymetric features not being represented in the Sverdrup approximation. Moreover, the calculated transports through the Tasman Sea lead the observed T/S change by the same time period as the winds. This may reflect the Island Rule's assumption of instantaneous response to changes in wind forcing. The method used in this study is single island rule. More recently, a multiple island rule has been developed (Wajsowicz, 1993; Pratt & Pedlosky, 1998). When calculating the Island rule value for Australia, Multiple Island rule would take a path to the South of New Zealand, whereas single island rule ignores the existence of New Zealand. The Multiple Island rule is something which should be explored in future work. However, for the purposes of this study, the Single Island Rule is a good approximation, for a number of reasons

- A reduction in circulation would be expected due to frictional effects if the barrier is within the western boundary layer (Wajsowicz, 1993; Pratt & Pedlosky, 1998). New Zealand sits outside of Australia's boundary layer, and hence friction along the west coast of New Zealand will have a minimal effect. Pratt & Pedlosky (1998) suggest a maximum over-estimate of 25%

- Helfrich et al. (1999) suggest that an island or ridge to the east of the western boundary would have a shadowing effect for Rossby wave propagation, and hence a reduction in transport of the western boundary current. However, in this study and in Liu et al. (1999), it is demonstrated that Rossby waves are initiated on the west coast of an island, through the interaction of Rossby waves reaching the east coast of an island with a coastal Kelvin wave which propagates around the island, spawning Rossby waves on the west coast. In addition, Helfrich et al. note that the effect of a peninsular is far greater than

that of an island.

- Helfrich et al. (1999) also suggest that a shadowing island enlarges the zone of recirculation. When the Island Rule streamfunction Figure 3.7) is compared with the GECCO streamfunction Figure 4.12), the latitudinal extent of the recirculation is comparable, from 15°S to 48°S.

In general, work by Pratt et al. (1997); Wajsowicz (1993); Helfrich et al. (1999) suggest that single Island Rule may overestimate the transport through the Tasman Sea. This is confirmed when comparing with single Island Rule net transport through the Tasman Sea with estimates from Reanalysis datasets. That said, the single Island Rule over-estimates both the magnitude of transport and amplitude of variability compared to Reanalysis datasets by a factor of 2. However, models are known to underestimate the amplitude of Western boundary currents as 0.5 degree resolution is not sufficient to resolve western boundary processes. That said, single island rule transports accurately represent the pattern and phase of decadal variability in the transport, which is the main focus of this study.

Decadal changes in the strength of the South Pacific Gyre have been discussed by Roemmich et al. (2007) using 12 years of altimeter and hydrography data and Qiu & Chen (2006) using 12 years of altimeter data. Both papers identified a tendency towards a stronger gyre in the 1990s with a reversal of sign in the early 2000's (2003 and 2001 respectively). The phase of this peak fits with the last peak in the time series of Maria which shows increases in temperature and salinity from the mid 1990s before peaking in around 2002-3, wind stress curl (and Island rule transport through the Tasman Sea) increases from 1992-1993 before peaking around 1999-2000. (Figure 3.8). The earlier studies (Roemmich et al., 2007; Qiu & Chen, 2006) relied on the short period of satellite altimeter data and so could not determine the time-scale of variability of the gyre. The 50+ year records analysed here shows clear

evidence of both a trend and significant decadal variability in the strength of the South Pacific Gyre.

Both ENSO and the SAM have been linked to changes and variability in the strength of the South Pacific Gyre and hence the EAC (Sasaki et al., 2008; Roemmich et al., 2007, respectively). Comparisons of Maria Island SST with the SOI and SAM indexes, suggest that both have a role to play, although on different timescales. There is a clear relationship between low frequency variability at Maria and decadal ENSO variability. A positive decadal SOI index is related to La Niña-like conditions, with cooler SST's tropical eastern Pacific and warmer SST's in the South West Pacific and Tasman Sea (Sasaki et al., 2008). This would explain the warmer temperatures seen at Maria Island. However, the trends in Maria SST and the SOI are anticorrelated. It is therefore likely that this long term trend is related to the positive trend in the Southern Annular Mode, which has caused a speed up and shift south of the Southern Hemisphere westerlies, and hence the South Pacific gyre (Roemmich et al., 2007). Sasaki et al. (2008) show a correlation between decadal ENSO and the wind stress curl in the central and eastern South Pacific to the east of New Zealand (200-290°E, 40-50°S). This relates closely to the wind stress curl region which correlates highly with the Maria SST at a 3 year lag (see Figure 3.10). While cross correlations suggest that the Maria SST lags the SOI by 12 months, inconsistency between the timing of the peaks in the SOI and Maria SST suggest that this time lag should be treated with caution. However, Sasaki et al. (2008) also find that the relationship between decadal ENSO and wind stress curl is strongest when the SST lags by 12 months. The precise relationship between the Maria SST, changes in the transport through the Tasman Sea, changes in South Pacific wind forcing and decadal ENSO may be complex, i.e. the ENSO signal could be communicated to Maria through different teleconnection pathways. Caution also needs to be exercised when inter-

pretting time lags when there are only 3 - 4 realisations of the signal. However, cross correlations are useful when discussed in the context of physical processes. Regional and gyre scale responses to wind forcing will be discussed in more detail in chapter 4. Pathways and mechanisms of oceanic response to wind forcing will be discussed in Chapter 6.

Roemmich et al. (2007) and Qiu & Chen (2006) suggested that the changes they observed in the South Pacific gyre reflected changes in the South Pacific winds at 4 and 2 years earlier respectively. Qiu & Chen (2006) conclude that first mode baroclinic physics is sufficient to explain the observed SSH variability in the South Pacific using a 1.5 layer reduced gravity model. However, the model appears to have less skill in the Tasman Sea, and areas of high mesoscale eddy variability such as along the 20-30°S band. The region of maximum SSH trend is also further south and east in the model, at 45-50°S, 190-200°E compared to 40°S,180-190°E in the altimeter SSH field. Qiu & Chen (2006) compared propagation characteristics in weekly altimeter SSH with the linear model using Hövmuller plots. This 1 week temporal resolution is too coarse to be able to identify barotropic propagation, which has been identified in all ocean basins in a 3 day temporal resolution altimeter product (Fu, 2004).

The short observation records that Roemmich et al. (2007) and Qiu & Chen (2006) considered also made it difficult to clearly resolve the time-scale of the lag between wind forcing and ocean response, and the relative importance of propagating baroclinic waves and local Ekman pumping remained unclear. The results in section 3.2.3 show the strongest correlation between the Maria and basin-scale winds occurs at about three years. The areas of strongest correlation (Figure 3.10) are too far east for first mode baroclinic Rossby waves to reach the western boundary within this three year time period. Moreover, it would take around 3 years for 1st mode

baroclinic Rossby waves to propagate from New Zealand across the Tasman Sea to the east coast of Australia. Thus, the relative role of local forcing and propagating waves (baroclinic and barotropic) in determining the response of the subtropical gyre to changes in winds will be further investigated in Chapter 6.

CHAPTER 4

Decadal changes in the South Pacific Western Boundary Current system revealed in observations and ocean state estimates

4.1 Introduction and motivation

The Maria Island coast station time series was discussed in detail in chapter 3, and the value of a 60 year time series is without doubt. However, this station represents a single point measurement in the Tasman Sea. There are three XBT sections which make up the Tasman Box, and they provide another source of information on the regional variability. They have the advantage that they encompass the main currents of the region (the EAC, Tasman Front, the EAC extension, and part of the South Equatorial Current), allowing the changes observed at Maria to be related to variability over a broader region. However, the XBT sections have only been occupied since the early 1990s. I therefore look to two new 50 year ocean reanalysis products and a 15 year reanalysis product focussing on the Australasian region in combination with the above observations, to build a comprehensive picture of low frequency variability in the Tasman Sea and the South Pacific wind driven gyre. For more details of the products and analyses used, see chapter 2.

This chapter is arranged as follows: section 4.2.1 compares the ocean reanalyses with the Maria coastal station, while section 4.2.2 compares the observed relationship between South Pacific winds, transport through the Tasman Sea and changes at Maria (established in section 3.1.3) with the ocean reanalysis products. Section 4.2.3 compares the ocean reanalyses with the Tasman Box XBT sections, and section 4.2.4 explores the velocity structure in the XBT data and ocean reanalyses. In section 4.2.5, the relationship between the EAC Extension and the Tasman Front is discussed, and in section 4.2.6 this relationship is related to broad scale changes in the South Pacific wind field. The summary and conclusions for the chapter are in section 4.3.

4.2 Results

4.2.1 Comparing Reanalyses Products with Maria Island Coastal Station

The time evolving T/S relationship is examined at Maria using data from the in situ observations (Figure 4.1a) and ocean reanalysis products SODA (Figure 4.1b) and GECCO (Figure 4.1c). The observed T-S diagram shows a very clear relationship between changes in temperature and salinity, varying from cooler fresher waters, to warmer saltier waters. This suggests that these changes represent an advected signal, which is related to variations in the strength of the EAC (see section 3.1.1). Both SODA and GECCO show a similar relationship, with properties varying from cold fresh to warm, salty centred on the 1026.3 kg/m^3 density contour. SODA is less able to conserve this T/S relationship in the 1980s when a large drop in salinity (from 35.1 to 34.95 psu) is seen without an associated drop in temperature. Both SODA and GECCO appear to be cooler and fresher than the observations. The slope of the T/S relationship in GECCO and SODA is similar to that found in Maria (+1°C change in temperature = +0.15 psu change in salinity). It is likely

that at least some of the Maria Island timeseries is assimilated into both of these models, as some of the data has been included in the World Ocean Atlas Database. However, the Tasman Sea region is very sparsely sampled; Maria is the only example of a high quality timeseries spanning the length of the Reanalysis time period in the Southern Hemisphere. This coupled with the error bars applied to observations as part of the Assimilation scheme (in part, due to the sparseness of data), means that there is still plenty of scope for large differences between Maria and the reanalysis products. Thus, the comparison of this point measurement with the reanalysis products in the same region is a useful exercise.

To explore the relationship between changes in South Pacific winds and changes in the strength of the EAC Extension in the models, 5-year low-pass filtered time series of SST and surface salinity from observations at Maria Island, and model grid values corresponding to the Maria location from SODA and GECCO are compared. I also compare the wind-stress curl and volume transport from GECCO and SODA (see Figure 4.2).

The RMS difference between the observed and reanalysed SST is 0.43°C for SODA and 0.4°C for GECCO, and for salinity it is 0.08 psu for SODA and 0.13 psu for GECCO. The cross-correlations (r) at zero lag between observed and reanalysed SST are 0.97 for SODA and 0.88 for GECCO (0.91 when Maria leads GECCO by 8 months), and for salinity, SODA is uncorrelated (r= less than 0.2 at zero lag) and r = 0.75 for GECCO. These comparisons demonstrate that the products provide a similar quantitative representation of the ocean at this geographical point with GECCO RMS errors being slightly smaller for temperature and SODA RMS errors being smaller for salinity. However, GECCO arguably offers a much better qualitative representation of the salinity variations, while SODA shows a slightly improved qualitative representation of temperature. Consistent with the compar-

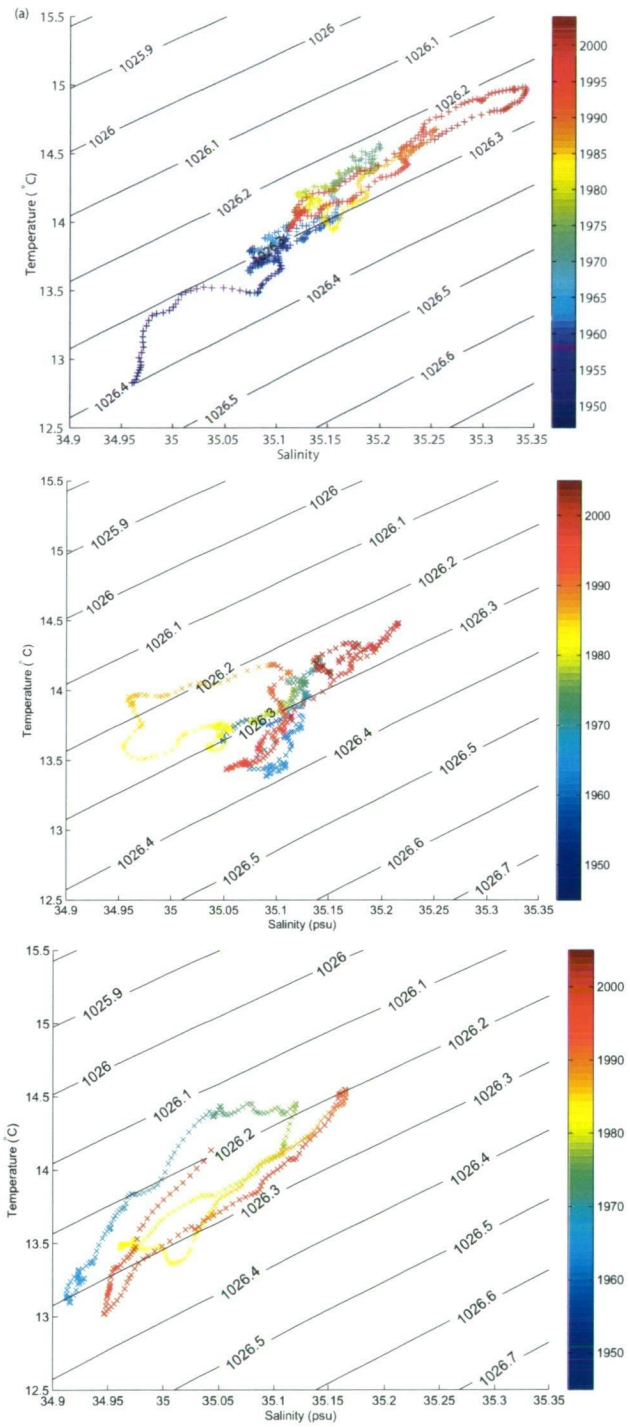

Figure 4.1: Temperature/Salinity plots for (a) Maria (b) SODA at Maria and (c) ECCO at Maria

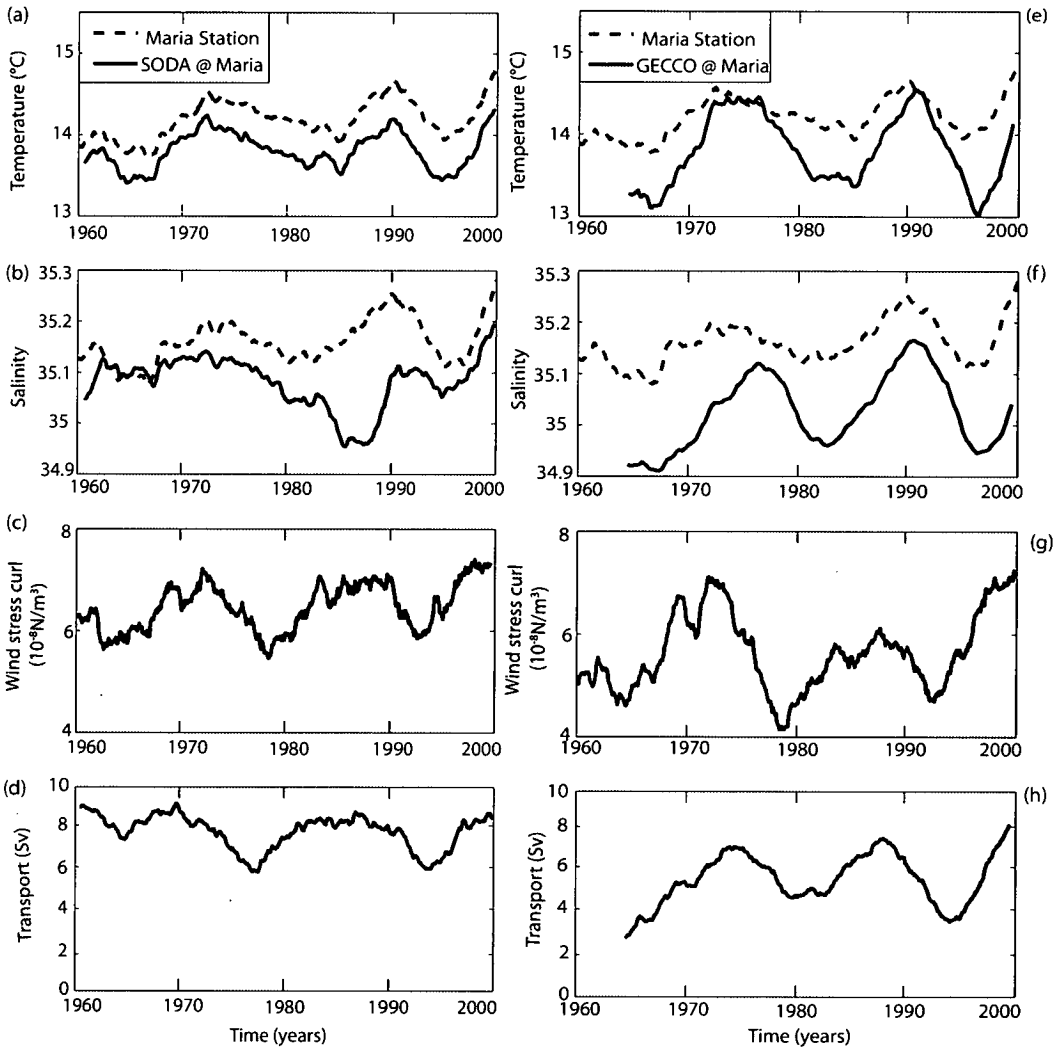

Figure 4.2: Timeseries of (a) SST at the location of Maria, (b) Salinity at location of Maria (c) ERA-40 South Pacific regional mean wind stress curl (180-280°E, 20-50°S) and (d) SODA net southward transport through the Tasman Sea (e) SST at the location of Maria, (f) salinity at location of Maria, (g) GECCO Optimised NCEP South Pacific regional mean wind stress curl (180-280°E, 20-50°S) and (h) GECCO transport through the Tasman Sea.

isons in Figure 4.1, the time evolving relationship between SST and salinity breaks down in SODA, likely due to the relaxation of the model to SST and no restoring to salinity. GECCO, on the other hand, produces T/S variability at Maria consistent with observations, albeit with a significant bias. These characteristics are as we might expect, given the sequential nature of assimilation in SODA and the variational approach used in GECCO. To test this further, the relationship between temperature and salinity at this location will be compared with South Pacific wind stress curl and EAC transport.

4.2.2 Relationship between Maria Island observations, wind and volume transport

It has been demonstrated that the strength of the EAC is closely related to the magnitude of wind stress curl in the South Pacific (see section 3.2). This provides us with the opportunity to test the ability of ocean reanalyses to reproduce this relationship. Figure 4.2d shows the net volume transport through the Tasman Sea, calculated from SODA velocities across 43°S. From the late 1980's to 2000 (one peak to peak cycle), the temperature (Figure 4.2a), wind stress curl (Figure 4.2c) and volume transport (Figure 4.2d) all decrease before increasing again until the end of the 1990's. A minimum in wind stress curl occurs in 1993, whereas the minimum in the volume transport through the Tasman Sea is a year later in 1994 and the minimum in temperature is closer to 1996. This matches the 3 year time lag between changes in winds and changes in temperature at Maria found from observations (section 3.1.3). Prior to the mid 1980's, decadal variability in transport has a similar phase and frequency to that seen in the winds, however the changes in transport appear to be in phase, and sometimes lead the changes in the winds by a couple of years. Furthermore, as discussed in section 4.1.2, variability in SODA salinity appears to de-couple from variability in SODA SST at this location,

and Maria salinity prior to 1990. Lagged cross correlation between SST at the location of Maria, and volume transport through the Tasman Sea (at 43°S) for SODA peak at only r= 0.4 when SST lags transport by 24 months. This suggests a poor correspondence in the model between variations in the volume transport through the Tasman Sea, and variations in SST and salinity at Maria. Changes in SODA volume transport through the Tasman Sea and changes in the regional mean wind stress curl in the South Pacific show correlations (r) of 0.68 at zero lag. The net volume transports are 6-9 Sv compared to observed mean net volume transports of 9.4 Sv (Ridgway & Godfrey, 1994).

The GECCO South Pacific wind stress curl and transports through the Tasman Sea (Figure 4.2g and h) show similar frequency and timing of variability to the GECCO temperature time series, with a strong decadal variability signal. Changes in wind stress curl leads changes in transports by 18 months (r = 0.65), and changes in temperature lag changes in wind stress curl by 36 months (r = 0.65). Even in this model, with more complete physics, changes in transport still leads the temperature response by 20 months (r = 0.8). The magnitude of transport through the Tasman Sea is consistently low compared to observations, with a range of 3-8 Sv compared to a estimated mean of 9.4 Sv from observations (Ridgway & Godfrey, 1994). The robustness of the relationship between temperature and salinity at the location of Maria, winds in the south Pacific, and transport through the Tasman Sea, suggests that the dynamical response of the GECCO model to changes in winds, is consistent with observations (section 3.2).

4.2.3 Comparing Ocean Reanalyses with Tasman Box XBT lines

Although the Tasman Box XBT lines only span a 15-year period, they have the advantage that we are able to study the ocean variability across three sections which encompass the northern Tasman Sea region. The currents captured in the Tasman

Box include part of the South Equatorial Current (SEC) that cuts across the northern part of the Auckland to Fiji and Brisbane to Fiji lines (the remainder flows to the north of Fiji); the Tasman Front that crosses the southern section of the Auckland to Fiji line; and the EAC/EAC Extension that crosses the southern/western part of the Brisbane to Fiji section and the western part of the Sydney to Wellington section (Figure 2.2).

Temperature sections from XBTs, BRAN, SODA and GECCO for 1993-2001 (Figure 4.3) all show the warm core of the EAC in the western portion of the section. The model representation of the mesoscale structure along this section is related to the model resolution. For instance, the zonal extent of the 20°C isotherm at the surface increases with decreasing spatial resolution.The XBT data, BRAN and SODA show a secondary warm core to the east of the main EAC, although this is further east in BRAN and SODA at 159°E and 161°E respectively. GECCO has a warm core confined to the top 200 metres at around 164°E. Below the surface, the sloping isotherms of the EAC penetrate to at least 900m in the XBT section (the limit of the XBT observations). In the reanalysis datasets, both BRAN and SODA still exhibit an EAC signature and an offshore counter-current in the form of sloping isotherms at 1000m, while GECCO's isotherms flatten out at around 500m, and do not reproduce the complex frontal structure across the Tasman Sea, which are likely associated with meanders in the Tasman Front. Apart from the smoothing related to the horizontal resolution discussed above, the reanalysis fields and XBT data all show generally consistent vertical temperature distribution with temperatures of around 10°C at 500m.

To understand the time evolving variability in this region and the performance of the models, volume transport time series across the sections occupied by the XBT lines are calculated from GECCO, SODA, BRAN and the combined XBT/Altimeter

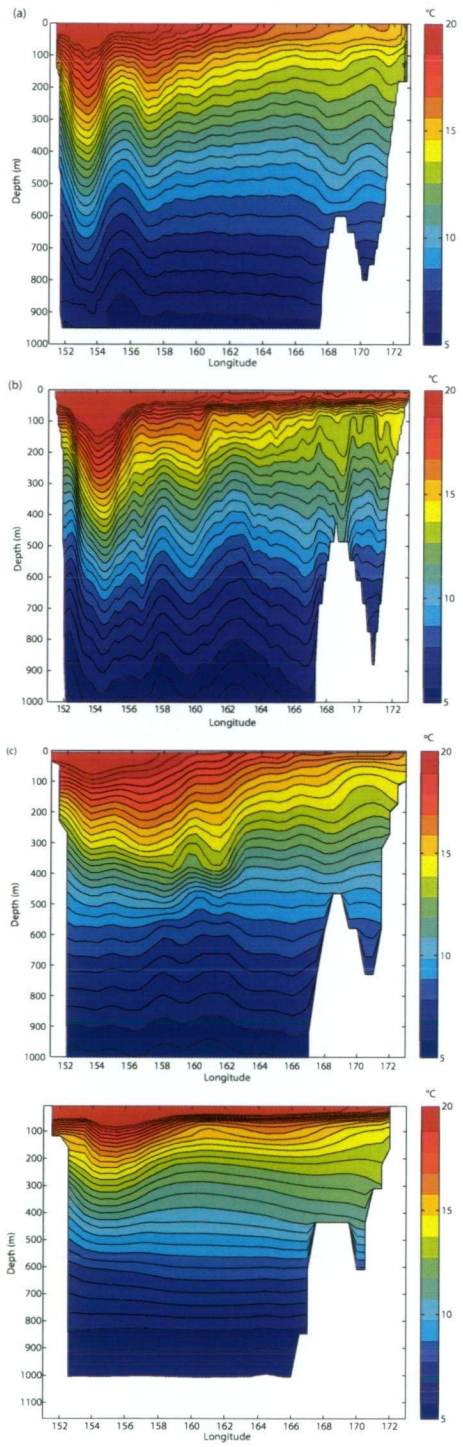

Figure 4.3: Temperature along PX34 from (a)XBT data, (b) BRAN (c) SODA and (d) GECCO for overlapping years (1993-2001). Models are sampled during months when the XBT section was occupied.

method with Ekman transport incorporated (Figure 4.4)(see section 2.3.2 and Ridgway (2008) for details of the method). Transports are calculated relative to 2000m for XBT data and the reanalyses. Full depth transports (to model bottom) are also calculated for the reanalyses, which provides an assesment of the validity of assuming a 2000m depth of no motion (Ridgway, 2008). There is a clear relationship between the resolution of the reanalysis, and depth penetration of currents. For GECCO, a 2000m reference level appears to almost completely capture the transport across each section, whereas BRAN, with the highest spatial resolution, shows the largest disparity between the transports relative to 2000m and full depth transports, which are even opposing signs in the case of the Brisbane to Fiji (PX30) line. If we focus on all transports relative to 2000m, GECCO shows the opposite sign to SODA, BRAN and XBT/Altimeter for the Auckland to Fiji (PX06) (Figure 4.4a). Similarly, for the Brisbane to Fiji (PX30) line, GECCO and BRAN show a net inflow, while SODA and XBT/Altimeter transport show a net outflow. All estimates show a net outflow along the Sydney to Wellington line (PX34), except BRAN for the pre 1998 period.

Net transports across the Sydney to Wellington line for GECCO and SODA (Figure 4.4c) both show decadal timescale variability with transports of comparable magnitude from around 5-10 Sv, and this variability appears to be in phase. While the XBT data suggest a stronger transport of 8-13 Sv, the XBT data and both models show increasing southward transport between 1995 and 2000. During this period, XBT transport increases outflow by 5 Sv and SODA and GECCO increase by 5 Sv, and 4 Sv respectively. The BRAN transports successfully recreate the phase and magnitude of variability seen in the XBT sections across this line. But while SODA and GECCO underestimate net transports, BRAN transports relative to 2000m are much smaller ranging from 2 Sv inflow to 7 Sv outflow. Full depth transports of

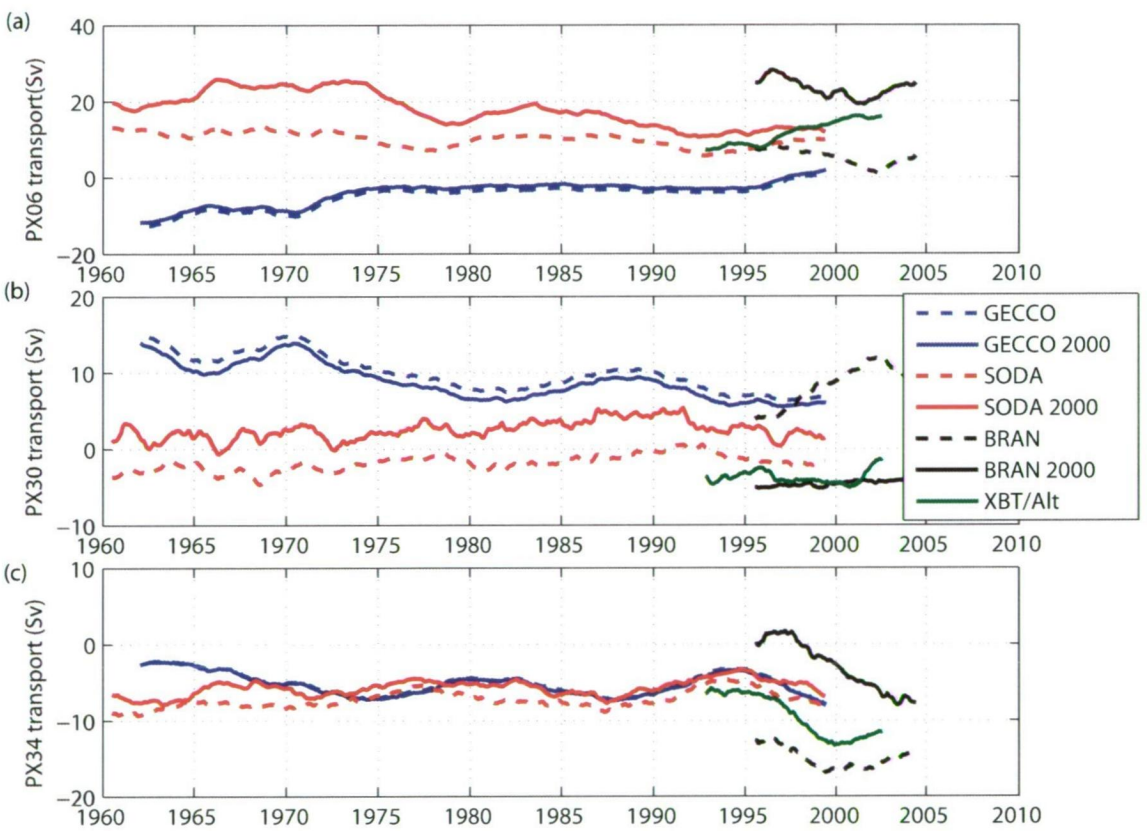

Figure 4.4: Transports into the Tasman box from reanalysis data (a) PX06 Auckland to Fiji (b) PX30 Brisbane to Fiji (c) PX34 Sydney to Wellington (positive = into the box).

BRAN are much larger than the XBT/Altimeter method and the other reanalyses, ranging from 12-17 Sv.

Schiller et al. (2008) note the deep current structure which would lead to this disparity, citing the surprisingly strong, deep currents as the cause, stating that "the EAC sometimes extends to the bottom" in the vicinity of PX34. The depth penetration of the EAC from full depth CTD observations was discussed by Ridgway (2008) in assessing the use of the 2000m reference level for XBT/Altimeter transport calculations. While it was acknowledged that the EAC extended far deeper than the 2000m level, the currents were relatively weak at this depth. The shallow bathymetry in the eastern part of the section also precluded a deeper reference level. It is noteworthy, that the phase and pattern of variability for BRAN full depth transports and XBT/altimeter is similar, with a minimum in transport around year 2000, while the magnitude is slightly larger for the XBT method (6 Sv, compared to 4.6 Sv for BRAN).

4.2.4 Velocity structure

The volume transports across the Auckland to Fiji line (PX06) and the Brisbane to Fiji line (PX30) for the 3 reanalyses and XBT data are very different (see Figure 4.4 a and b). Figure 2.2 shows the regional currents which intersect these sections, and the velocity section from Auckland to Fiji (Figure 4.5) indicates why the net transports across these sections vary so much in the different models. The Tasman Front in the south (blue) and a branch of the SEC to the north (red) can be identified in all three plots. In GECCO (Figure 4.5a), the Tasman Front is strong and broad, compared to the component of the SEC flowing south of Fiji, causing there to be a net outflow across the Auckland to Fiji section, and inflow across the Brisbane to Fiji section. In SODA (Figure 4.5b), the component of the SEC that flows to the south of Fiji is large enough to offset the strength of the Tasman Front, resulting

in a net inflow into the Tasman Box across the Auckland to Fiji section, and a net outflow across the Brisbane to Fiji section. In BRAN (Figure 4.5c), the westward counter-current north of the Tasman Front, and the multiple cores of the SEC more than compensate for the eastward flow in the Tasman Front.

These sections also highlight the impact of increasing the spatial resolution in models on the horizontal and vertical structure of these currents. With lower resolution models, currents appear to be broader and shallower than in higher resolution models. The Tasman Front in GECCO is a broader shallower feature than in SODA or BRAN, only penetrating to 500m depth and extending across 8 degrees of latitude. Also, the SEC is a smoother feature with an absence of the characteristic multiple jets. SODA shows the Tasman Front as a narrow (3° of latitude) deep feature that penetrates to 2000m, and the SEC has more structure, with two main cores that tend to shift further south with depth as observed (Kessler & Taft, 1987). BRAN as expected, has higher spatial definition with a strong narrow Tasman Front that has velocities of 0.04 m/s at 2000m, compared to the same velocity at 1000m in SODA. BRAN has a strong counter current to the north of the Tasman Front and the SEC is seen as multiple cores that tend to be farther south with depth, in a similar way to SODA.

Depth integrated transport profiles for the period 1993-2001 provide a more quantitative method for understanding the balance of flows across the Auckland to Fiji line and the benefits of increased resolution for the accurate measurement of transports become apparent. Mean eastward cumulative transport is calculated for XBT/Altimeter, BRAN, SODA and GECCO from south - north along the Auckland to Fiji line, and then a section north of Fiji along 180°E for BRAN, SODA and GECCO (Figure 4.6). This illustrates the balance between the westward flowing SEC and the eastward flowing Tasman Front. Starting in the south, the Tasman

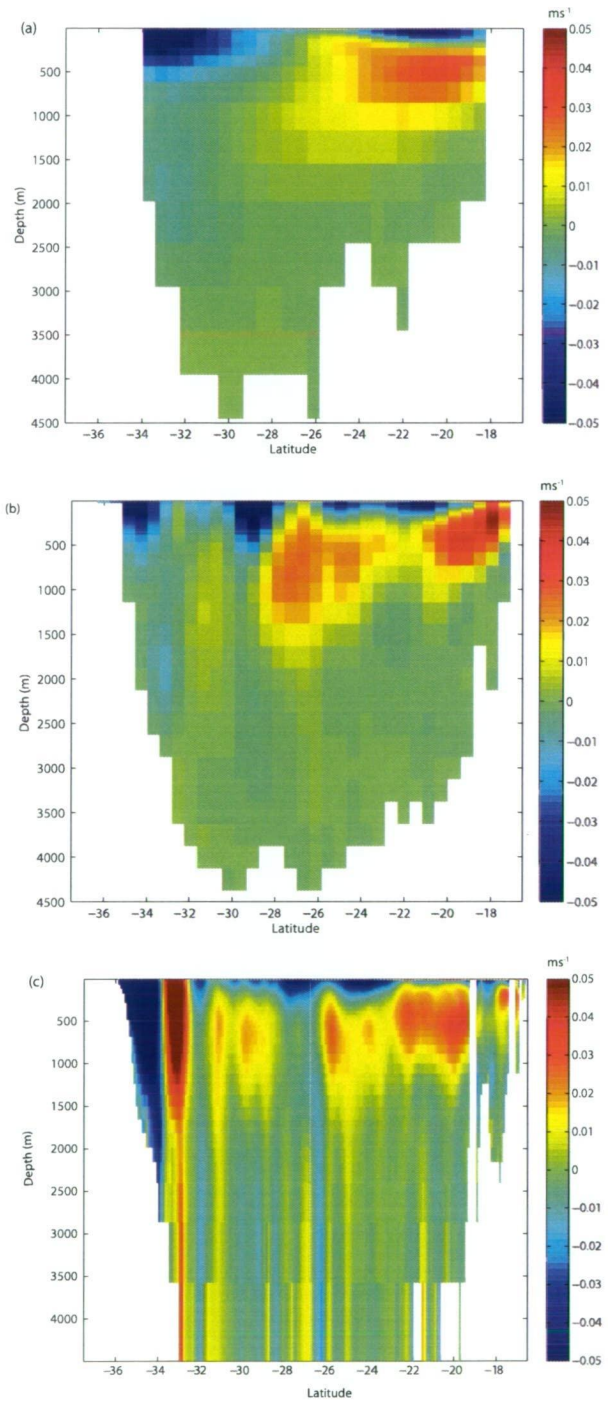

Figure 4.5: Mean velocity across PX06 1993-2001 for (a) GECCO (b) SODA (c) BRAN. Positive values represent flow into the Tasman Box (westward)

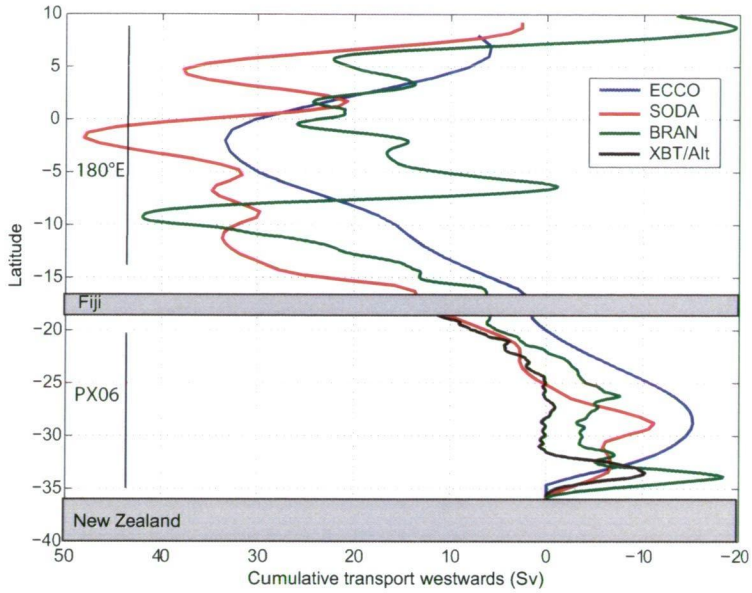

Figure 4.6: Cumulative westward transport across PX06 and north of PX06 across 180°E for GECCO, SODA, BRAN and combined XBT/Altimeter 1993-2001.

Front is much stronger and wider in GECCO than SODA (transports of -15 Sv and -12 Sv respectively) and BRAN has an even stronger and narrower Tasman Front, reaching -18 Sv. All three models show a stronger Tasman Front transport than XBT/Altimeter (10 Sv), which assumes a depth of no motion of 2000m. This is balanced by the westward flowing SEC component to the south of Fiji, which is stronger in SODA and BRAN (22 Sv and 24 Sv respectively) than in GECCO (17 Sv). SODA and XBT/Altimeter therefore show a net inflow into the Tasman Box of around 10 Sv, while BRAN and GECCO shows a smaller net inflow of 6 Sv and 2 Sv respectively. North of Fiji, the mean SEC transport is comparable for BRAN GECCO and SODA (32 Sv, 30 Sv and 36 Sv respectively). All three models show that the bulk of the SEC flows to the north of Fiji. Changes in the net transport across the Auckland to Fiji line by changes in the strength of the Tasman Front, changes in the strength of the SEC, or changes partitioning of SEC flow around Fiji.

The balance between the SEC and the Tasman Front can also be seen for the years

of minimum and maximum eastward transports for GECCO and SODA (Figures 4.7a and b). In SODA, it is mainly the Tasman Front transport which seems to dictate the variability in net transport across the section. The distribution of the SEC north/south of Fiji doesn't appear to vary much, but a stronger SEC is related to a weaker Tasman Front. The Tasman Front is weaker (-12 Sv) when net inflow across the section is at a maximum, and increases in strength when the inflow is at a minimum (-15 Sv). The Tasman Front also appears to be broader in meridional extent, with maximum cumulative transports reached at 28°S compared to 33°S for the minimum case. This is balanced by the component of the SEC to the south of Fiji (27 Sv for maximum and 23 Sv for minimum), giving a net balance of 15 Sv and 8 Sv respectively. When the net transport into the Tasman Box across the Auckland to Fiji line is at a maximum (i.e., the southern component of the SEC is strong relative to the Tasman Front); to the north of Fiji, SEC transport is also stronger (38 Sv compared to 33 Sv). This suggests that the variations in the net transport across the Auckland to Fiji line is not related to North-South meanderings of the SEC changing the proportion of the current flowing to the south of Fiji; rather, changes in the strength of the SEC both north and south of Fiji.

In GECCO, again, the balance of flow across this line appears more related to the strength of the Tasman Front than the SEC transport south of Fiji. When net inflow across the Auckland to Fiji line is at a minimum in GECCO, Tasman Front transport is double the strength it is when net transport is at a maximum (-20 and -10 Sv respectively), whereas there is only a small change in the strength of the SEC (12 to 15 Sv). North of Fiji, the SEC transport reaches 42 Sv when the transport across the Auckland to Fiji line is at a minimum and 30 Sv when it is at a maximum.

In both GECCO and SODA, the net transport appears to be related to the strength of the Tasman Front, rather than the proportion of the SEC that flows to the south

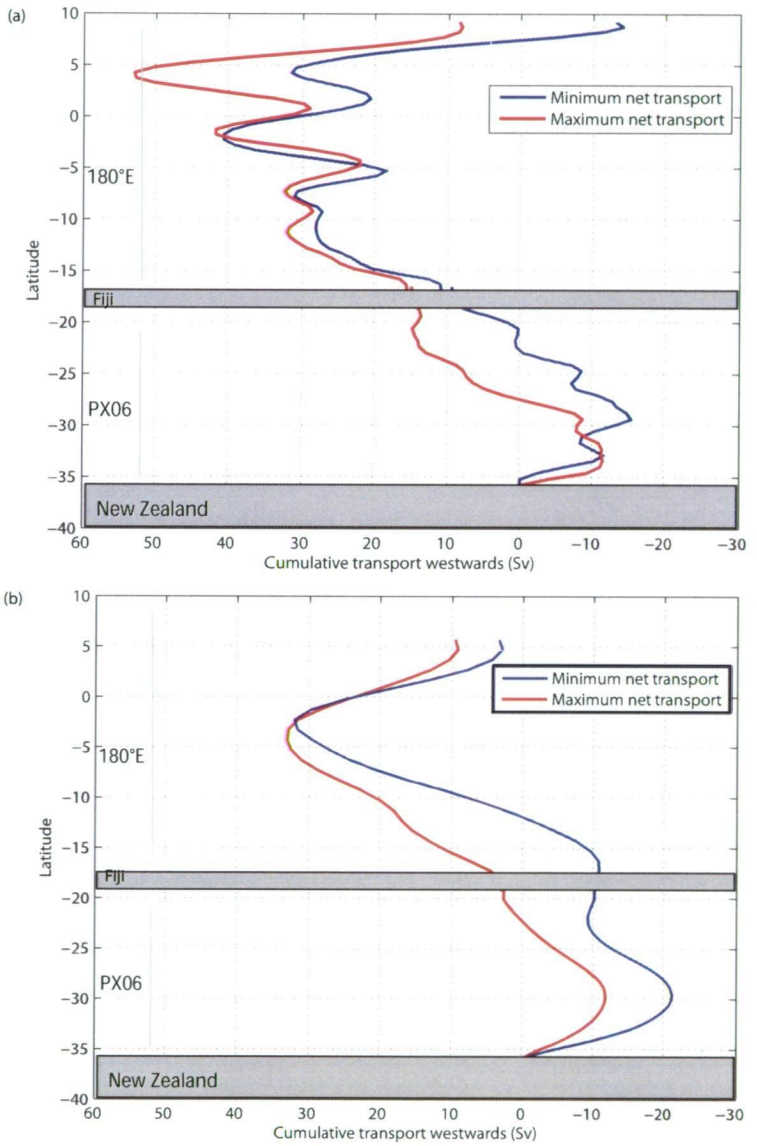

Figure 4.7: Cumulative westward transport profiles (a)minimum (1994) and maximum (1962) years of transport across PX06 for SODA and (b) minimum (1962) and maximum (2000) years of transport across PX06 for GECCO.

of Fiji. However, a stronger Tasman Front is related to a stronger SEC in GECCO, and a weaker SEC, and hence a weaker gyre circulation in SODA. We therefore cannot draw any conclusions about the relationship between the strength of the SEC and the strength of the Tasman Front without further investigation.

4.2.5 EAC Extension and Tasman Front

Following on from discussions of the relationship between the SEC and the Tasman Front, we look at the relationship between the transport of the Tasman Front and the EAC. The Tasman Front is defined as the maximum eastward transport (at each depth) across the southern section of PX06, and the EAC extension as the net transport through the Tasman Sea. The transports calculated for the Tasman Front and the EAC Extension from the combined Altimeter/XBT method (Ridgway, 2008) show an inverse relationship between the strength of the EAC Extension and the Tasman Front (Figure 4.8). These transports are found to be strongly anti-correlated, with r values of -0.96 at zero lag. At the point of separation, water can either separate and flow east into the the Tasman Front, or continues south down the coast to in the EAC Extension. These results suggest that one or the other of these pathways is favoured on decadal timescales.

The relative strengths of the EAC Extension and the Tasman Front from BRAN show a similar relationship, with a peak in the EAC Extension and trough in the Tasman Front around year 2000 (Figure 4.9). While the Tasman Front is significantly stronger in BRAN than in the XBT/Altimeter data, this was expected from the analysis of the depth integrated transport profiles which showed mean Tasman Front transports of around 18 Sv for BRAN and 10 Sv from XBT data. The detrended timeseries of transports are anti correlated (r=-0.7 at zero lag). While the robustness of the relationship between the EAC Extension and the Tasman Front in both the XBT's and BRAN is encouraging, there is only one realisation of the

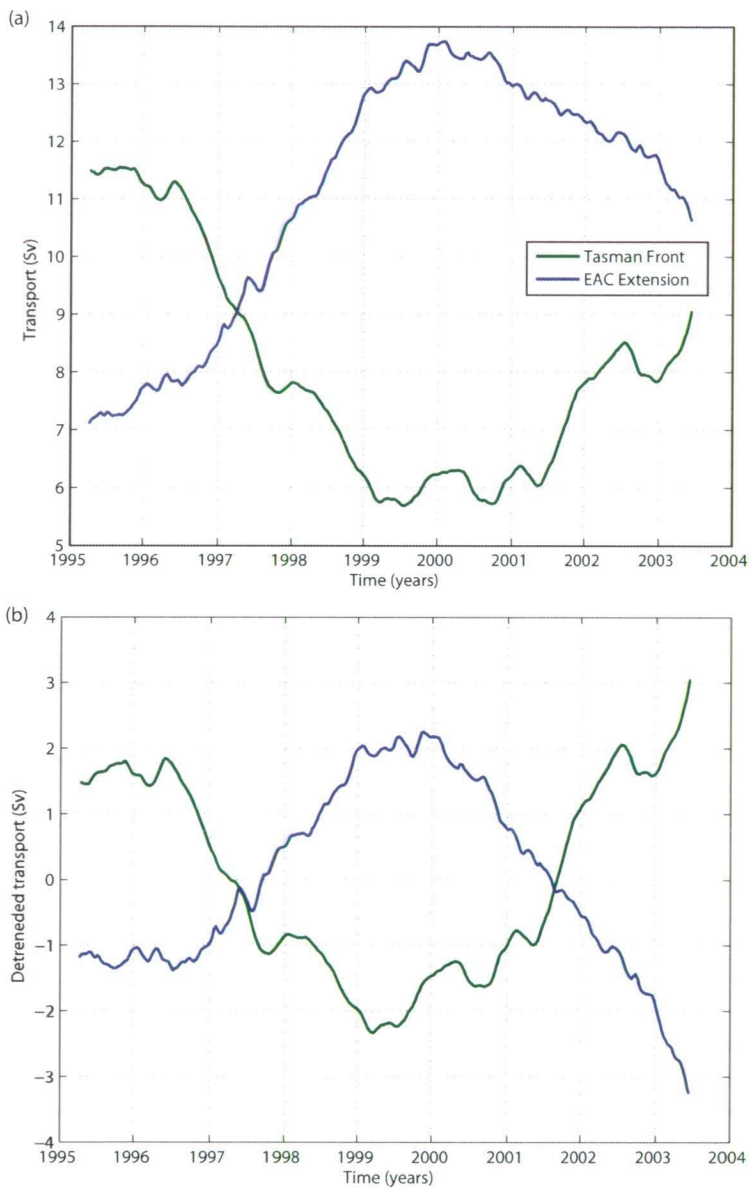

Figure 4.8: (a) Transports for the Tasman Front and EAC Extension calculated using a combined altimeter/XBT method (b) detrended.

cycle and so the correlation is not statistically significant.

The relationship between these two currents is explored in GECCO and SODA (Figures 4.10 and 4.11), to see if the same relationship could be established over a much longer time frame. Figure 4.10a shows the strength of the EAC Extension plotted against the Tasman Front transport for SODA. As with BRAN, the Tasman Front is much stronger (13-20 Sv) compared to the EAC Extension (5-10 Sv). The relationship is clearer in the detrended timeseries, where a stronger out of phase relationship is apparent from the early 1980's and the time series show a clear anti-correlation (r=-0.62 at 0 lag) (Figure 4.10b). GECCO shows that the Tasman Front gets gradually weaker with time, and the EAC extension to trend towards getting stronger (Figure 4.11a). In 1965, Tasman Front transport is 24 Sv, and the EAC Extension is 3 Sv. The EAC Extension reaches 8 Sv by 1999, when the Tasman Front carries 16 Sv. Again, when these time series are de-trended (Figure 4.11b) a clear anti-correlation between the Tasman Front and the EAC Extension is evident, with r values of -0.8 at zero lag. Both GECCO and SODA also appear to agree with the XBT/altimeter between 1995 and 2000, with all timseries showing a transition from a minimum in EAC Extension and a maximum in the Tasman Front transport in 1995, to a maximum in the EAC and a minimum in the Tasman Front in 2000.

While the differences in these products have been highlighted, the fact that all three products consistently produce the anti-correlation between the EAC Extension and the Tasman Front suggests that this is a robust result. This suggests that on decadal timescales, one of two pathways is favoured at the separation point: the flow either separates to form the Tasman Front and flow north of New Zealand, or continues down the coast to Tasmania as the EAC Extension. It also suggests that when looking at large scale dynamical relationships, GECCO and SODA provide a useful and credible estimate of the state of the ocean and its variability.

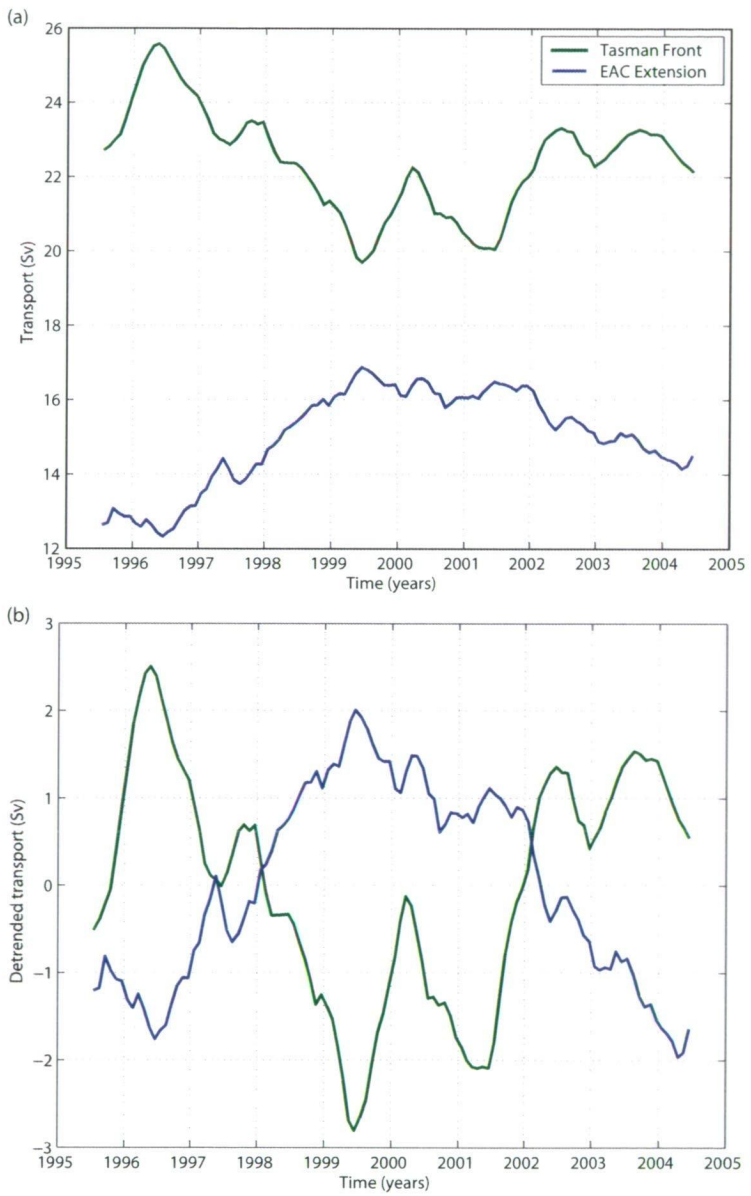

Figure 4.9: (a) Transports for the Tasman Front and EAC Extension calculated from BRAN (b) detrended transports.

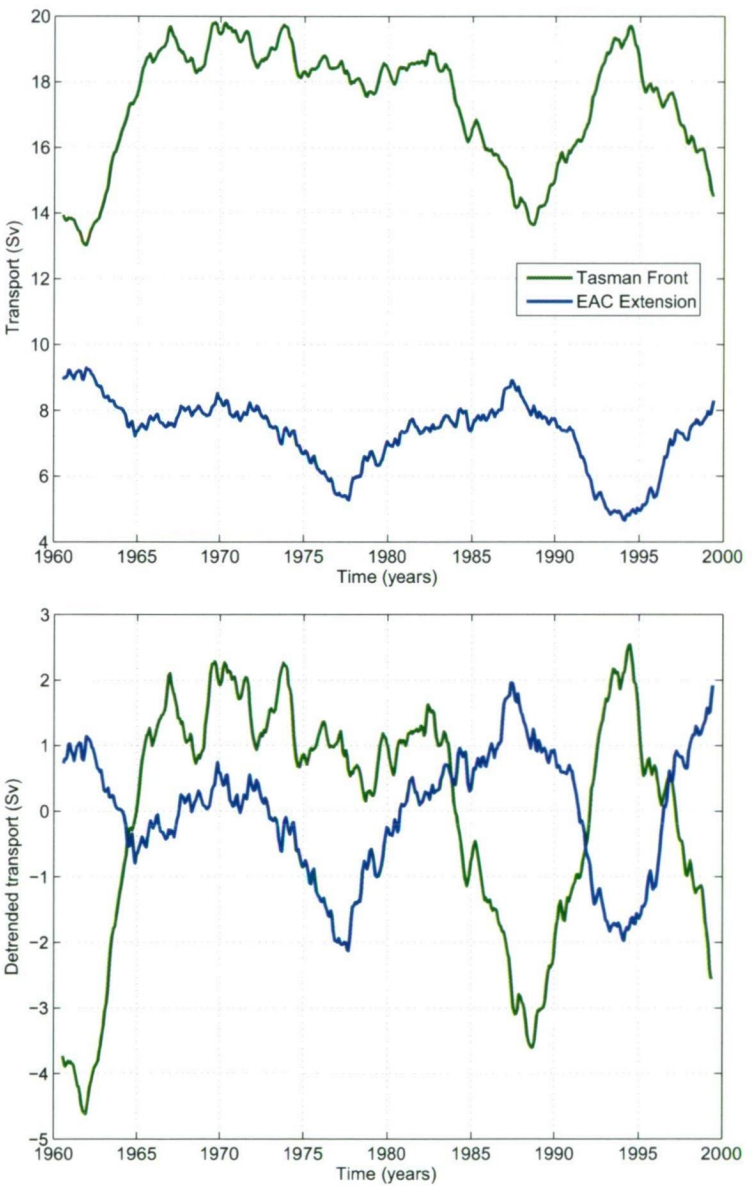

Figure 4.10: Transports for the Tasman Front and the EAC Extension calculated from (a)SODA, (b) SODA detrended

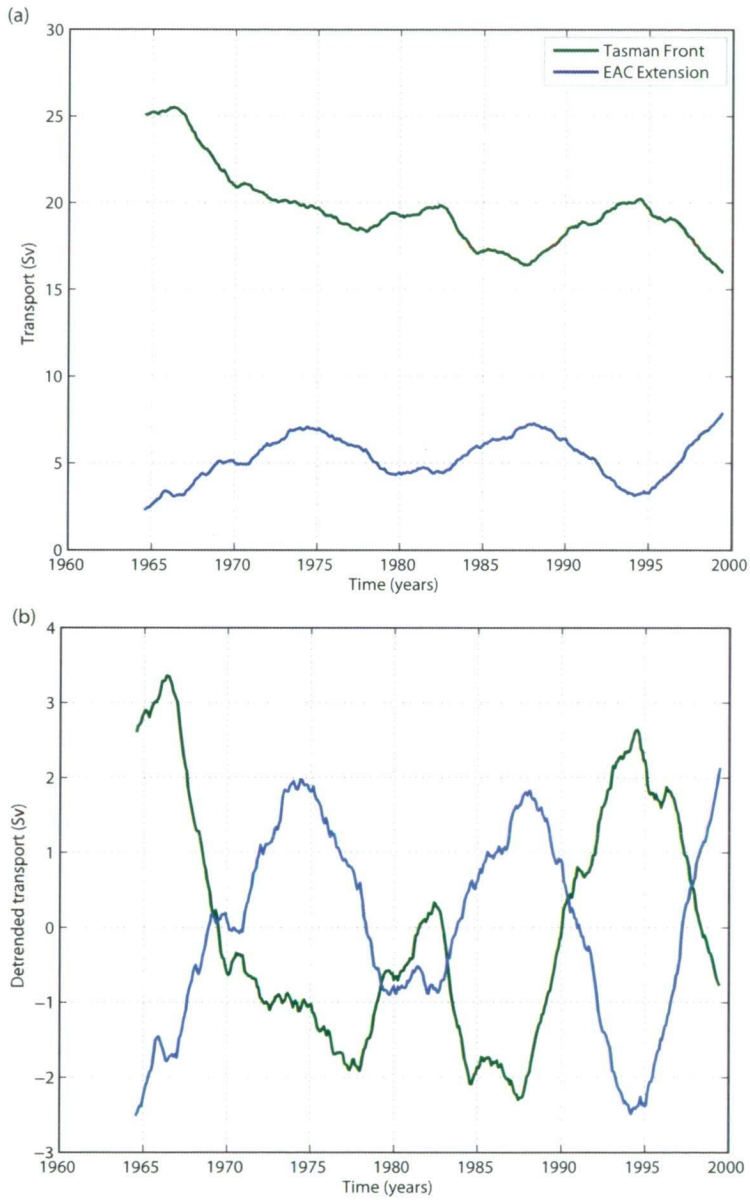

Figure 4.11: Transports for the Tasman Front and the EAC Extension calculated from (a) GECCO and (b) GECCO detrended

The differences in the gyre for the the Tasman Front-favoured and EAC Extension-favoured states can be seen by looking at the GECCO South Pacific depth integrated stream functions (Figure 4.12). Two distinct gyre structures are apparent with a stronger southern limb of the gyre when the EAC extension is favoured. In 1994, when the Tasman Front is favoured, the South Pacific circulation has a single gyre structure, with the bulk of the gyre recirculating to the north of New Zealand. In 1988 when the EAC extension is favoured, stronger transport through the Tasman Sea is evident, and the South Pacific circulation has a double gyre structure, with a second gyre centred to the east of New Zealand between 35 and 50°S and extending east to 120°W. The impact on the EAC and Tasman Front is evident from the streamlines. In 1988 (Figure 4.12a), when the EAC extension is favoured, there is a 5 Sv increase in transport through the Tasman Sea, so New Zealand sits within the gyre. In 1994, when the Tasman Front is favoured (Figure 4.12b), tighter streamlines are seen across the Tasman Sea and to the north of New Zealand, which appears to sit outside the bulk of the South Pacific Gyre. In 1988, there are only 3 streamlines (15 Sv) across the Tasman Sea to the north of New Zealand, and in 1994, there are 4 (20 Sv). These two gyre structures are also found for the other realisations of two states (not shown), which suggests that the two states (EAC Extension favoured and Tasman Front favoured) reflect robust gyre scale changes throughout the 50 years of GECCO.

4.2.6 Role of changes in winds in determining the strength of the EAC extension and Tasman Front

The close relationship between South Pacific wind stress curl, the strength of the South Pacific gyre and the strength of the EAC has previously been demonstrated in chapter 3 (see also Cai, 2006; Roemmich et al., 2007). We therefore explore the relationship between the EAC and Tasman Front transports and the South Pacific

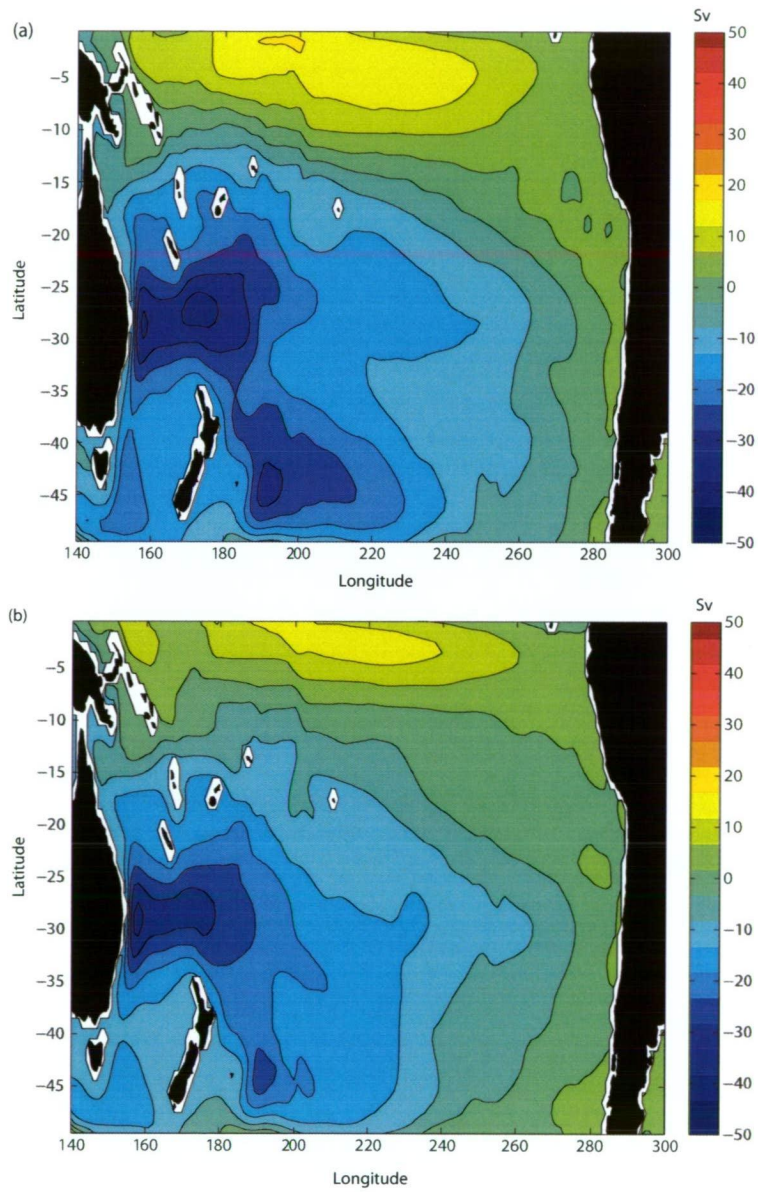

Figure 4.12: GECCO annual mean streamfunctions for (a) 1988 (Stronger EAC Extension, weaker Tasman Front) (b) 1994 (Weaker EAC Extension, stronger Tasman Front). Contours every 5Sv.

wind stress curl in the context of gyre scale processes.

The low frequency variability in South Pacific wind stress curl can be clearly demonstrated in a latitude-time plot of zonal mean wind stress curl from GECCO (Figure 4.13a). The region of maximum wind stress curl sits between 45 and 50°S. However, this region broadens north periodically, by 5 degrees to 40°S, and the maximum wind stress curl increases from $10\text{x}10^{-8}$ to $12\text{x}10^{-8}\text{N/m}^3$. The wind stress curl maximum is always centred around 48°S, and the line of zero wind stress curl consistently sits at 52-53°S. Three periods of stronger wind stress curl can be identified. These can each be associated with maxima in the transport of the EAC Extension, and minima in Tasman Front transport a few years later (Figure 4.13b). Similarly, a few years after a minimum in the wind stress curl, Tasman Front transport peaks and EAC Extension transport reaches a minimum.

In terms of gyre scale processes, a stronger wind stress curl maximum appears to favour a broader gyre structure at the latitude range of New Zealand, where New Zealand is in the middle of the gyre, a larger amount of water recirculates through the Tasman Sea, and there is a stronger double gyre structure with a second circulation east of New Zealand (Figure 4.12). A weaker wind stress curl maximum appears to favour a state where New Zealand sits outside of the gyre, with the bulk of the transport recirculating north of New Zealand as the Tasman Front. I do not find a consistent strengthening or weakening of the South Pacific gyre, but changes in the shape of the gyre that are related to variability in the curl, causing one of 2 gyre scale patterns to be favoured.

4.3 Summary and Conclusions

This chapter builds a picture of low frequency variability in the Tasman Sea, and how it relates to South Pacific gyre-scale processes using a combination of two new

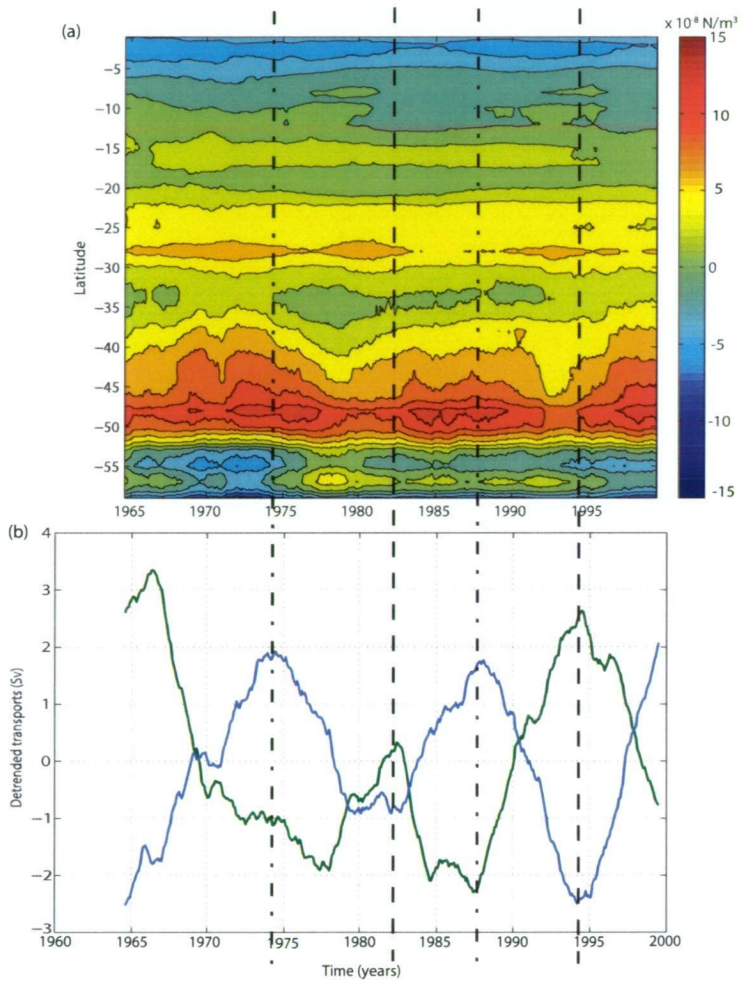

Figure 4.13: GECCO (a) South Pacific zonal mean wind stress curl (180-280°E) (b) EAC Extension and Tasman Front transport

50 year ocean reanalyses, 1 high resolution 15 year reanalysis, 3 XBT timeseries, and a coastal station timeseries. Despite differences between the models in terms of set up, forcing, and resolution, all reanalyses and observations consistently show that the EAC extension and the Tasman Front are anti-correlated on decadal timescales. The switching between two gyre scale pathways, is related to decadal variations in wind stress curl in the South Pacific. Enhanced positive wind stress curl east of New Zealand causes the circulation patterns to favour the EAC Extension over the Tasman Front. The consistency of these findings across all the ocean reanalyses and data suggests that this is a robust result.

This study highlights the importance of long time series for separating decadal variability from long term trends. Attention in the literature has focussed on the spin up of the South Pacific gyre in the 1990's, observed in in-situ observations and satellite altimeter data (Qiu & Chen, 2006; Roemmich et al., 2007; Sutton et al., 2005), which has been related to the positive trend in the Southern Annular Mode (Roemmich et al., 2007). Analysis of Sverdrup/Island Rule streamfunction calculated from NCEP-1 atmospheric reanalysis, has also pointed to a gradual spin up of the South Pacific gyre over 50 years due to strengthened subtropical westerly winds caused by the trend in the Southern Annular mode (Cai, 2006; Godfrey, 1989), although questions have been raised about the magnitude of the trend in the NCEP reanalysis winds. This strengthening is also predicted to continue according to a climate change model run (Cai et al., 2005). However, further analysis over longer timescales (50 years) suggests that the spin up observed in the 1990's is predominantly related to decadal timescale variability (Sasaki et al., 2008), although this variability appears to be superimposed on a long term trend, as discussed in chapter 3.

As discussed in section 1.3, the southward range expansion of marine species across

a range of taxa down the coast of southeast Australia has been related to the strengthenning of the EAC Extension (Lyne et al., 2005; Ling et al., 2008; Ling, 2008). Furthermore, southeast Australia has been highlighted as a region most at risk from climate change, related to the predicted continued strengthenning of the EAC. The increased transport facilitates the southward advection of larvae, and the increased water temperatures increases the range of species close to the lower limit of their temperature tolerance. Long (multidecadal) high quality ecological time series are a rarity, making it difficult to deduce decadal variations in species distribution. Distributions of Salmon in the North Pacific has been related to the Pacific Decadal Oscillation (Mantua et al., 1997; Hare et al., 1999). The observed decadal variability between two circulation patterns in the Tasman Sea could have similar consequences for species distribution within the Tasman Sea.

Sasaki et al. (2008) described low frequency variability observed in an eddy resolving global ocean hindcast model (OFES), driven by NCEP-1 reanalysis winds, and attributed South Pacific and Tasman Sea sea level variability to decadal ENSO variability. In Figure 4.14, the first EOF of OFES sea level anomaly (SLA), is compared with the OFES Tasman Sea SLA, and GECCO transport through the Tasman Sea. The positive phase of the EOF is associated with higher sea levels, north and east of New Zealand and hence a stronger gyre circulation. Sasaki et al. (2008) relate this decadal variability in Sea level and hence gyre strength to decadal ENSO variability. The OFES Tasman Sea SLA and the GECCO transport through the Tasman Sea (the strength of the EAC Extension) both show peaks in the mid 1970s and late 1980s and minima in 1980 and 1995 which is followed by a sharp increase up to year 2000. This is further evidence that the variability observed in the EAC extension and Tasman Front are related to decadal ENSO variability (see section 3.2.4).

GECCO shows a close relationship between the changes in the wind stress curl east

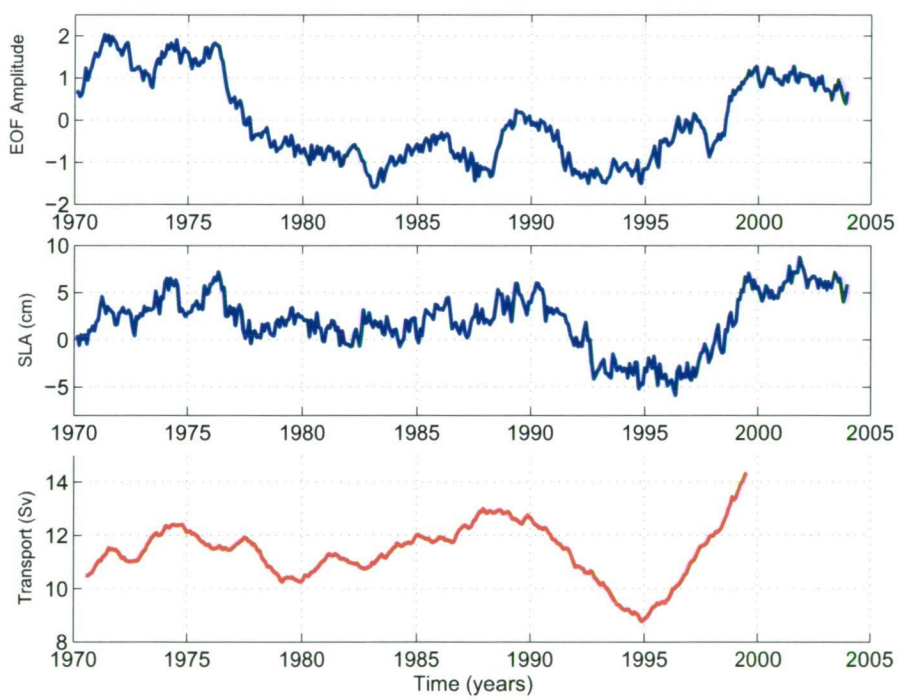

Figure 4.14: OFES Sea level anomaly in the Tasman Sea averaged over 38.5-45°S, 150-170°E (redrawn from Sasaki et al., 2008) (upper pannel) and Net southward transport through the Tasman Sea from GECCO (lower panel)

of New Zealand (20-50°S, 180-280°E) and the relative strengths of the EAC extension and Tasman Front transports. GECCO wind stress exhibits decadal variability in the magnitude of wind stress curl in the region 40-50°S, 180-280°E, and such decadal variability in the winds is not seen elsewhere in the South Pacific region. This is the same region which Sasaki et al. (2008) identified as having the strongest correlation between wind stress curl and decadal ENSO in the South Pacific. Sasaki et al. (2008) show a strong correlation between wind stress curl east of New Zealand and the 1st EOF of OFES SLA, and they associated this region with the Pacific South American Mode, which is the South Pacific atmospheric response to ENSO (Garreaud & Battisti, 1999; Mo, 2000). Therefore, this suggests that decadal variations in the EAC extension and Tasman Front transports are related to the decadal ENSO variability, via the imprint of the Pacific-South American Mode on the subtropical South Pacific. SAM impacts on the same region (see Qiu & Chen, 2006; Roemmich et al., 2007), but there is no evidence of decadal timescale variability in the SAM itself, which mainly varies on weather timescales, superimposed on a long term trend (Thompson & Solomon, 2002). This suggests that SAM is responsible for long term trend in South Pacific wind stress curl, but decadal ENSO responsible for low frequency variability, further corroborating findings in section 3.2.4.

Sasaki et al. (2008) also relate positive SLA's in the South Pacific with weaker eastward currents in the Tasman Front, and a decrease in eddy activities north of the front. This study takes this relationship a step further and relates variability in the South Pacific winds to decadal variability in the patterns of circulation in the South Pacific gyre; in particular, enhanced wind stress curl in the South Pacific favours the EAC extension pathway over the Tasman Front. In other words, decadal El Niño- like warming (La Niña-like cooling) in the tropical Pacific is associated with a weaker (stronger) South Pacific wind stress curl maximum, a weaker (stronger)

EAC Extension, and a stronger (weaker) Tasman Front.

Decadal changes in gyre strength cannot be determined conclusively from variability in transport patterns seen in SODA and GECCO; rather a change in the shape of the gyre, driven by changes in wind stress curl, which causes either the Tasman Front state, or the EAC Extension state to be favoured. This is at odds with the results of Sasaki et al. (2008) who relate a stronger gyre with a weaker Tasman front and Roemmich et al. (2007) also relate the increasing South Pacific Sea level during the latter half of the 1990's to a stronger gyre.

The close relationship between central South Pacific wind stress curl and transport through the Tasman Sea is demonstrated in section 4.2.6 and in chapter 3. Sasaki et al. (2008) attribute OFES SLA variability in the Tasman Sea (Figure 4.14b) to a combination of incoming Rossby waves interacting with New Zealand (52.6%) (see Liu et al., 1999) and Ekman convergence along New Zealand (33.7%), with only a very small amount being attributed to local wind stress curl over the Tasman Sea (2.4%). In addition, Sasaki et al. (2008) and Qiu & Chen (2006) suggest that South Pacific wind forcing first mode baroclinic physics is sufficient explain most of the variability in the South Pacific Gyre, with Sasaki et al also suggesting that wave propagation around New Zealand is important. In chapter 3, I conclude that 1st mode baroclinic physics is not sufficient to explain the observed 3 year time lag between changes in the winds and changes in temperature and salinity at Maria. In this chapter, results from GECCO and SODA, reanalysis models with more complete physics, confirm that there is a 3 year lag between changes in the winds, and changes seen in the physical properties in the South Tasman Sea.

The range of time lags discussed in chapters 3 and 4 is something that requires further investigation. Sasaki et al. (2008) suggest that changes in the first EOF of OFES SLA lags changes in the wind stress curl east of New Zealand by 12 months,

while Qiu & Chen (2006) suggest that this lag is 2 years. Furthermore, Roemmich et al. (2007) suggests that the lag between changes in winds and changes in in the gyre strength is 4 to 5 years. These differences could be related to to the length of datasets, with the conclusions of both Roemmich et al. (2007) and Qiu & Chen (2006) based on only 1 realisation of a decadal signal. However, changes in GECCO transport through the Tasman Sea lag changes in wind stress curl by 18 months, whereas changes in SST at the location of Maria lag changes in wind stress curl by 3 years. This suggests that there is a lag between a strengthening of the gyre and hence stronger transports through the Tasman Sea, and a change in the physical properties in the region. It also suggests that there may be a physical explaination for the range of time lags discussed between changes in wind stress curl and the ocean response. Never the less, it would still take 10-15 years for 1st mode baroclinic Rossby waves to cross from the central South Pacific (the region of strongest correlation), which is much slower than the range of time lags (1-5 years) discussed here.

This study demonstrates how a combination of observations and reanalysis data can be successfully used to build a picture of decadal ocean variability. The observations were used to pinpoint specific features and processes such as the low frequency variability in the EAC, and the relationship between regional currents, which were then explored in the ocean state estimates. Strengths and weaknesses of the different approaches to ocean state estimates were identified. Nevertheless, the inverse relationship between the EAC Extension and the Tasman Front was remarkably robust in the XBT data, and all three reanalysis analysed. This work builds on Sasaki et al. (2008), Roemmich et al. (2007) and Qiu & Chen (2006) to relate the broad scale patterns of variability observed in the South Pacific Gyre to regional current variability in the south west Pacific and EAC System. This demonstrates

the utility of ocean state estimation for understanding decadal ocean variability, when the technique is still in its infancy, and despite the challenges of incorporating an ever evolving and expanding ocean observing system.

The precise relationship between changes in the wind stress curl, the strength of the South Pacific gyre and processes governing the gating between the EAC Extension and the Tasman Front at the separation remains unclear. This relationship is explored further in a global ocean model and idealised wind perturbation experiments in the following chapters. Chapter 5 details the model and design of the experiments, and the results are discussed in chapter 6.

CHAPTER 5

Models and Forcing Experiments

5.1 Motivation for model forcing experiments

In previous chapters, the available observations and reanalysis are used to describe the relationship between the EAC western boundary current system and the South Pacific winds. Questions are also raised which cannot be tackled through analysis of observations alone.

In chapter 3, it is shown that the EAC responds to changes in basin scale forcing with a lag of 3 years. This is too fast for first mode baroclinic adjustment, which would take at least 10 years from the middle of the South Pacific at mid latitudes (Figure 3.10) and too slow for barotropic adjustment, which would take only a matter of days. Therefore it is hypothesised that there is a fast mechanism by which changes in the South Pacific winds can be communicated to the western boundary.

In chapter 4, it is demonstrated that the EAC Extension and Tasman Front are anticorrelated on decadal timescales, and that this is related to a "'gating"' effect at the separation point of the EAC (32°S), where either the EAC Extension or the Tasman Front is favoured. This reflects variations in the shape and location of the wind driven gyre, which switches between two distinct states. However, precisely what aspect of the wind variability was causing such a mode switching was not

pinpointed .

In Figure 3.10, it shows it would take 3 years for Rossby waves to reach the EAC from New Zealand. Tanaka & Ikeda (2004) suggest that ridges can provide a mechanism for effective conversion of barotropic wave energy into baroclinic wave energy. Liu et al. (1999) demonstrate baroclinic Rossby wave interaction with the east coast of an island, setting up a coastal Kelvin wave, spawning baroclinic Rossby waves to the west of the island. In the case of the South Pacific, changes in the winds in the South Pacific could be communicated near instantaneously as barotropic waves as far as New Zealand and the ridges which fan out to the north of New Zealand . Tanaka & Ikeda (2004) suggested that barotropic wave energy can be scattered on ridges, to form baroclinic modes. If a combination of these mechanisms were applied to the South Pacific with barotropic propagation across the South Pacific and baroclinic propagation across the Tasman Sea, it would take around 3 years for the EAC system to respond to changes in the South Pacific winds.

This theory is tested the model forcing experiments which are described in this chapter. The results are presented in chapter 6. Figure 4.13 suggests that it is variations in the strength of the wind stress curl maximum which cause the anticorrelation between the EAC Extension and the Tasman Front. To perturb the wind stress curl, the zonal wind is enhanced in a region designed to increase the wind stress curl maximum (discussed further in section 5.3.1). This allows us to also test whether we can recreate the observed relationship between the EAC Extension and the Tasman Front

In summary, a global ocean model and idealised forcing experiments are used to test two hypotheses:

1) The observed time lags between variations in the South Pacific winds and the EAC system can be explained by a fast mechanism of propagation involving baroclinic

Rossby waves, spawned in the interaction of barotropic waves with topography.

2) The observed anti-correlation between the EAC and the Tasman Front is caused primarily by variations in the strength of the South Pacific wind stress curl maximum.

This chapter is organised as follows; Section 5.1 describes the model used for the experiments, and how it was spun up. Section 5.2 describes the design of the forcing experiments including the development of the forcing anomaly characteristics, and tests performed to determine model sensitivity to friction and dissipation, as well as the magnitude, zonal extent and temporal extent of the forcing anomaly. In section 5.3, I outline the data analysis methods used. The results of these experiments are described in chapter 6.

5.2 CSIRO Ocean Model

I used the CSIRO Mk3.5 ocean model, which is based on version 4 of the Geophysical Fluid Dynamics Laboratory Modular Ocean Model (MOM4) code (Griffies et al., 2004). To test the above hypotheses, a model with complete physics (barotropic and baroclinic) and hence realistic stratification is needed. It also requires realistic bathymetry, and a free surface, so that the SSH response could be examined. The use of a global model also means that no artifical boundary affects the results. The model grid spacing is 1.875° degrees zonally, 0.94° meridionally, and 31 levels in the vertical with vertical grid spacing ranging from 10 metres at the surface to 400m at depth. The model uses Bryan-Lewis vertical diffusivity which ranges from $1*10^{-5}m^2/s$ at the surface to $1*10^{-4}m^2/s$ at depth in the tropics and $3*10^{-5}m^2/s$ at the surface to $1*10^{-4}m^2/s$ at depth at higher latitudes (Bryan & Lewis, 1979). Neutral mixing and Laplacian friction are used, and the model restores to climatology surface temperature and salinity. Bathymetry is based on Smith and Sandwell

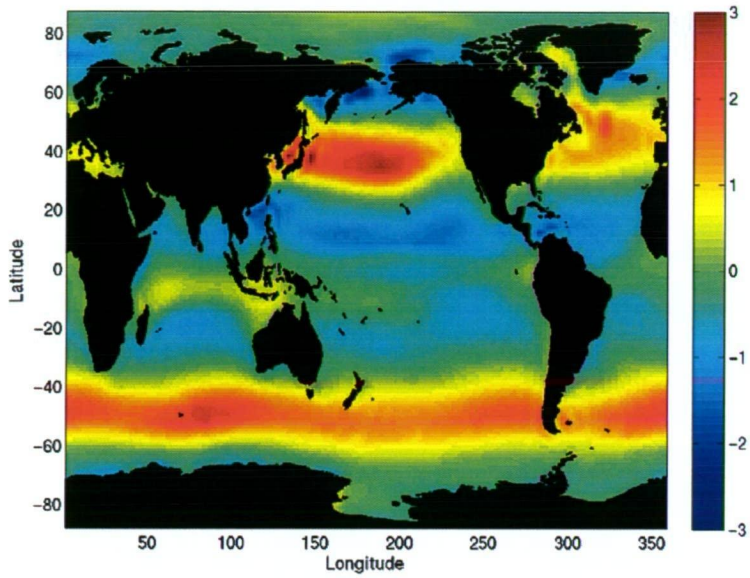

Figure 5.1: ERA-40 mean January zonal wind stress (N/m^2).

(Smith & Sandwell, 1997). While this grid spacing is fairly coarse for resolving mesoscale features such as fronts, such models are routinely used to study large scale ocean processes (Oke & England, 2004; Lu & Stammer, 2004).

The model is spun up for 200 years with a cyclic mean annual cycle calculated from ERA-40 winds (see section 2.2.1). The mean January zonal wind stress is shown in Figure 5.1. The Southern Hemisphere is dominated by the subtropical westerly winds, which completely encircle the globe between 40°S and 60°S. The easterly trade winds can be seen between 10 and 30°S. The wind stress curl pattern (Figure 5.2) is predominantly determined by the gradient set up between the trade winds and the subtropical westerly winds. The maximum wind stress curl in the South Pacific is found between 38 and 45°S.

The representation of the bathymetry at model grid spacing is shown in Figure 5.3 a and b. The East Pacific Rise is clearly visible; rising to 3000m, comparable to depths recorded on hydrographic charts. The Campbell Plateau to the south of New Zealand and the complex ridge structure to the north is also represented. This

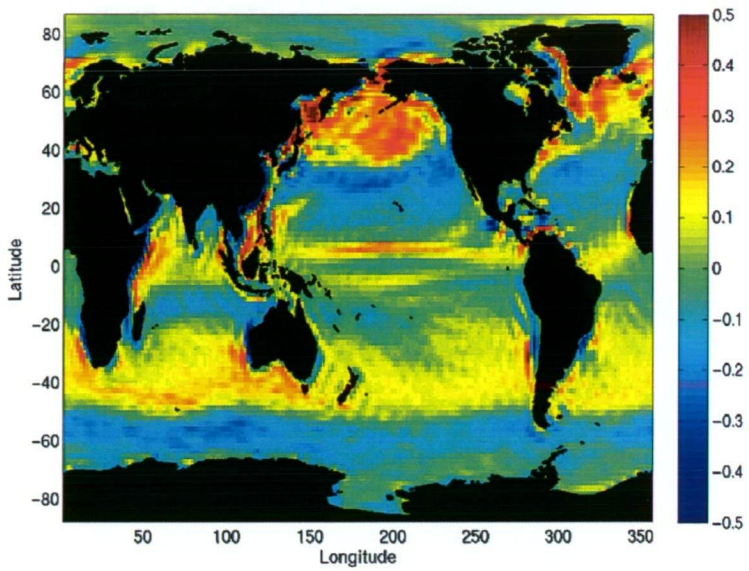

Figure 5.2: ERA-40 mean January wind stress curl (N/m^3).

complex topography allows the role of ridges as well as islands on the propagation of Rossby waves across the South Pacific to be explored (Liu et al., 1999; Tanaka & Ikeda, 2004).

The depth structure of the model can be assessed by comparing the model temperature at zonal and meridional sections across the South Pacific with CARS climatology temperature. Figure 5.4 compares the model with climatology at zonal sections 25,30 and 35°S. In all the sections, there is good agreement between the model and climatology below 500m with the 6°C isotherm sitting just above 1000m in the west, sloping upwards across the basin in all three sections. The general features of the South Pacific Gyre can be identified in the isotherm structure of both the model and the climatology sections. The deepening of isotherms to the east, associated with the southward EAC, is matched by a shoaling just offshore, associated with the offshore counter current. The broad bowl structure across the rest of the South Pacific, with isotherms gradually deepenning toward the centre of the basin and shoaling toward the west is associated with the broad gyre structure of the South

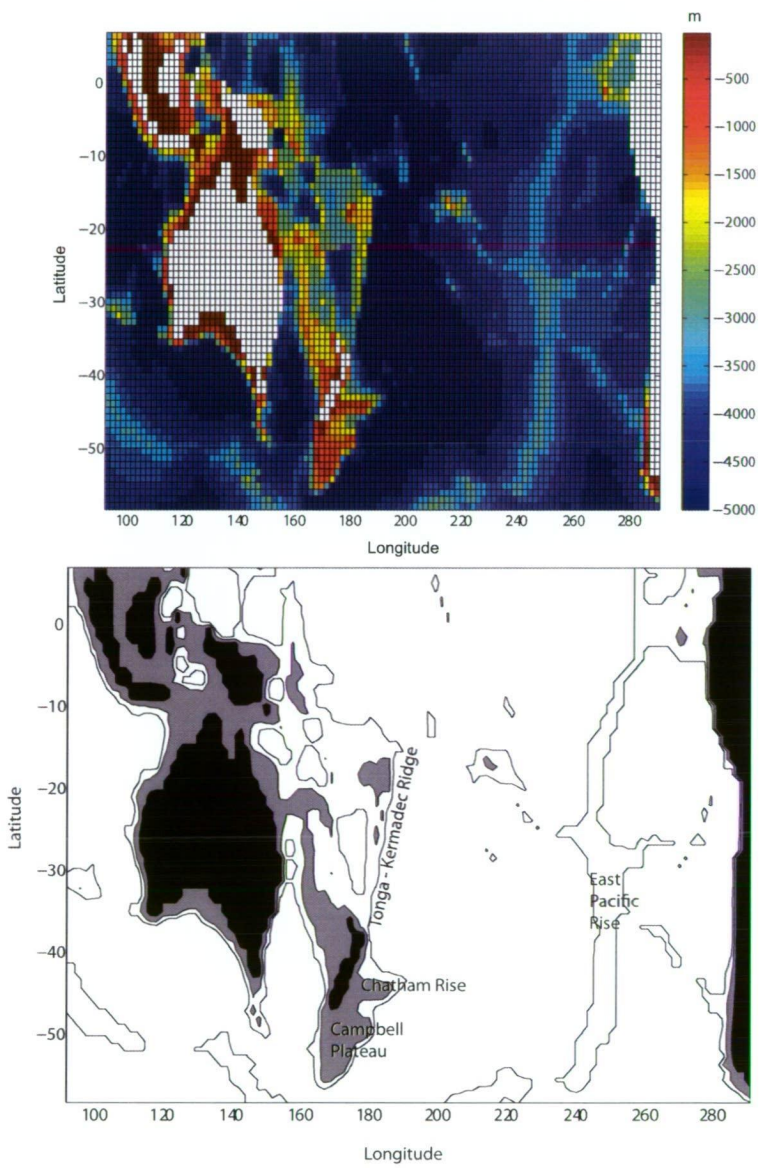

Figure 5.3: Bathymetry of the South Pacific (a) at model (1.875° longitude x 0.94° latitude) grid spacing. Depths in metres. (b)with major bathymetric features labeled. Black shaded area is above sea level,grey shaded area is above 2000m, and grey line marks the 3500m depth contour.

Pacific. In the 25°S section, there is good agreement in the top 500m also, although the shoaling of the isotherms around 170-180°E followed by a deepening between 180 and 200°E is slightly more exaggerated in the model. This pattern of an enhanced shoaling followed by a deepenning of isotherms in surface waters is more apparent in the 30°S model section, with a strong shoaling at 190-200°E followed by a deepenning around 210-220°E. The 35°S sections clearly show the southward EAC and Tasman Front with deepenning isotherms. However, a familiar pattern of shoaling in the central Pacific, further east than the more northerly sections at around 200-230°E, followed by a deepening west of 240°E.

Figure 5.5 shows the meridional sections through the South Pacific at 190,220 and 260°E. North of 40°S, all model sections provide a similar representation of the depth structure of temperature as the climatology. In particular, the shoaling of the isotherms toward the north associated with the SEC in the 260°E section is reproduced well in the model. South of 40°S, some differences in the latitude at which isotherms shoal is seen, and the 2°C and 4°C isotherms shoal slightly further north in the model than in the climatology, especially in sections 190°E and 260°E. Overall, the general temperature structure of the South Pacific is reproduced reasonably well in the model. For the purposes of the perturbation experiments carried out, the differences discussed at not likely to make a significant difference to the propagation speed of Rossby waves, which is what is important here (Owen et al., 2005).

The ocean streamfunction for the South Pacific (see figure 5.6) shows a broad scale South Pacific gyre structure similar to that seen in GECCO in chapter 4. Maximum streamfunction values reach 50 Sv. The mean transport through the Tasman Sea at 37°S is 3 Sv northward, compared to 9.5 Sv southward seen in observations (Ridgway & Godfrey, 1994), suggesting that the EAC Extension is too weak. The streamfunction pattern suggests strong recirculation within the Tasman Sea. The

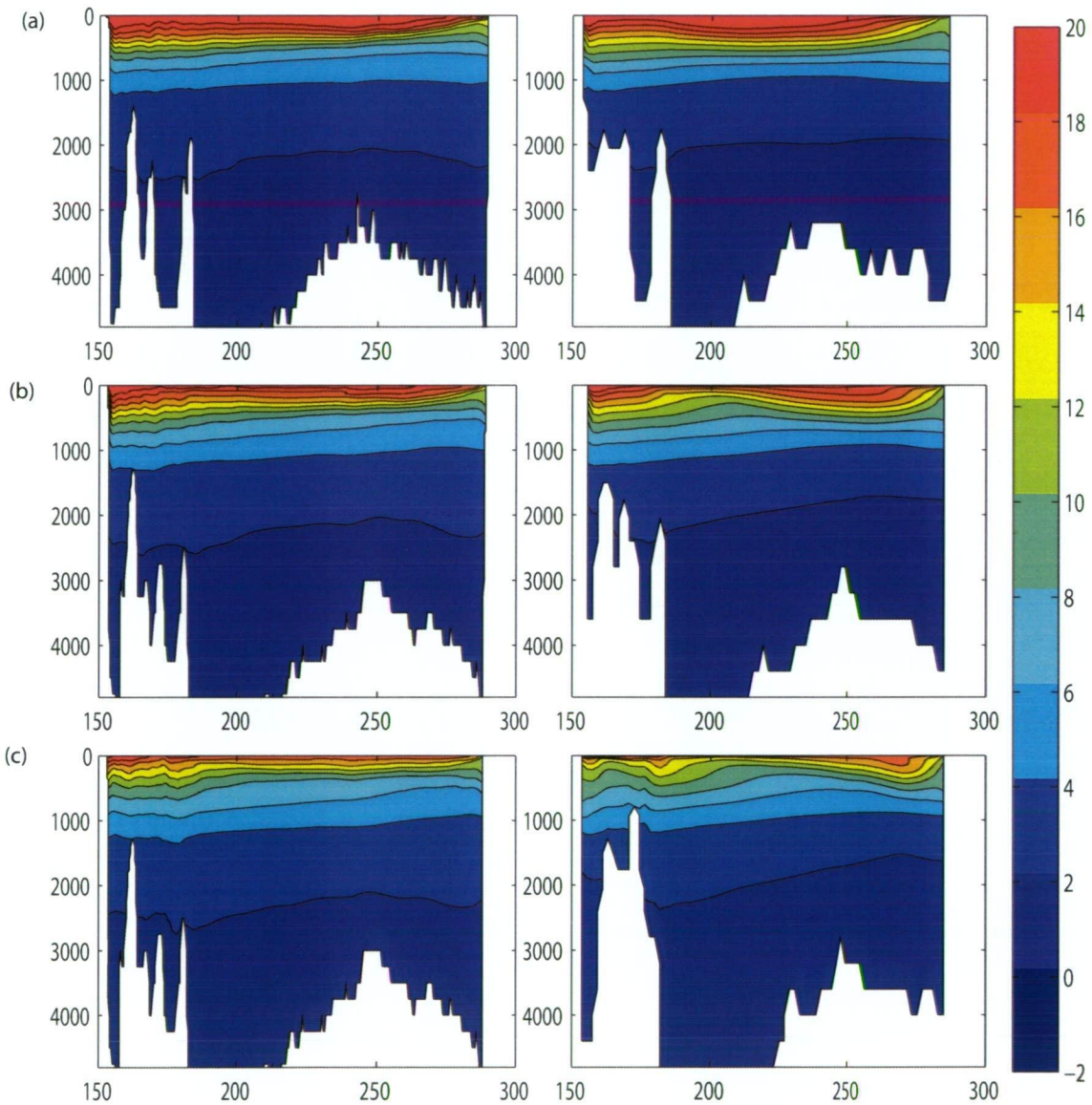

Figure 5.4: Temperature section across the Pacific at (a) 25°S (b) 30°S (c) 35°S for the CARS climatology (left) and model (right) in °C

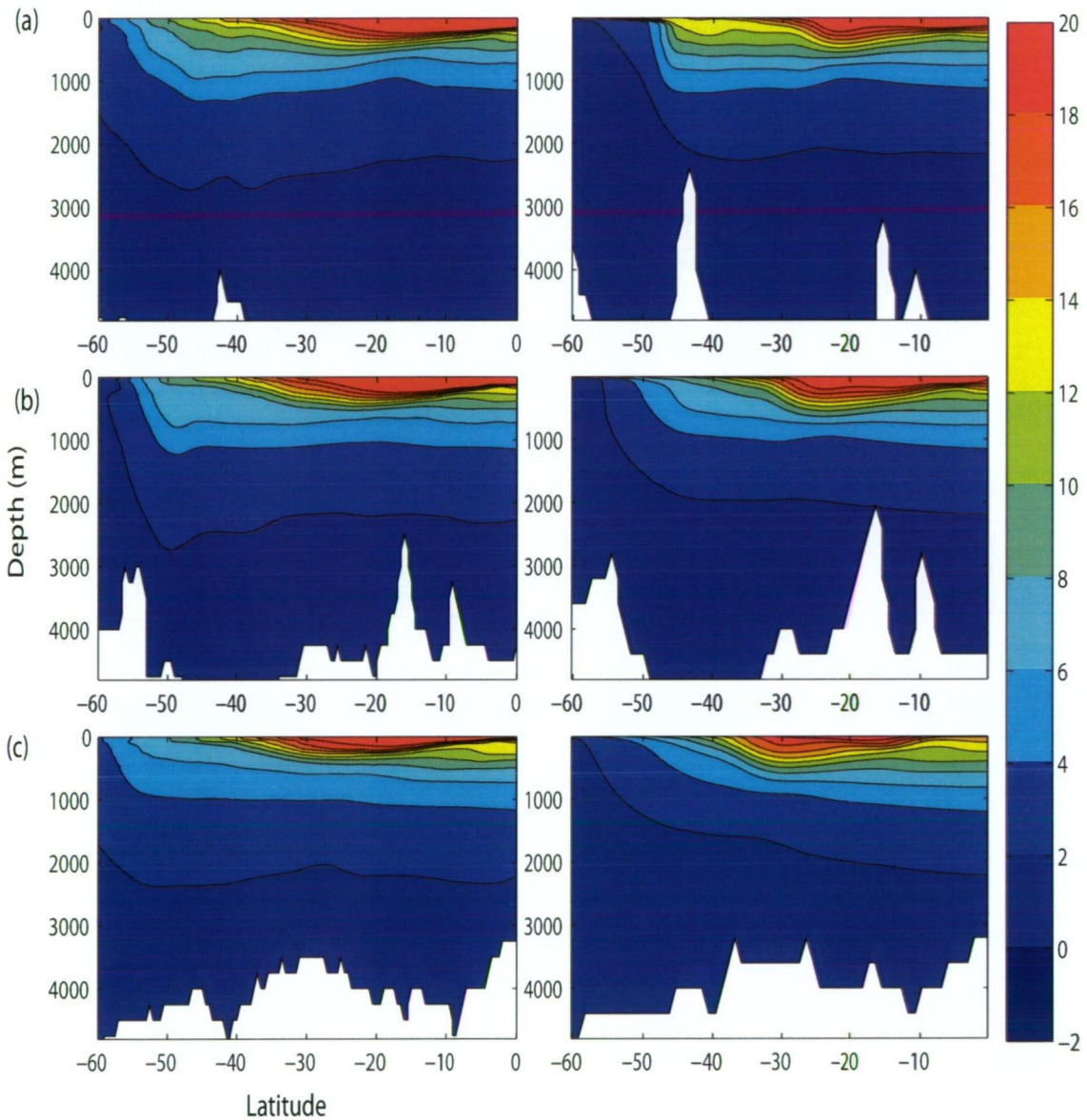

Figure 5.5: Temperature section across the Pacific at (a) 190°E (b) 220°E (c) 260°E for the CARS climatology (left) and model (right) in °C

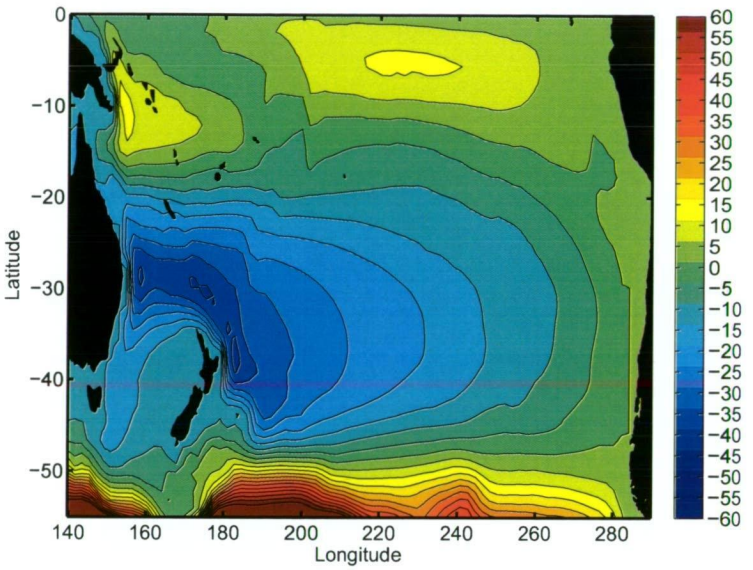

Figure 5.6: Mean South Pacific streamfunction in Sverdrups from control run (Sv)

annual cycle of the transport through the Tasman Sea varies in phase with observations (Figure 5.7 shows a maximum net southward transport of 3.8 Sv in March and a net northward transport of 7.6 Sv in August, giving a large seasonal amplitude of 11Sv, compared to 6Sv seen in observations (Ridgway & Godfrey, 1994). The Tasman Front is weakest in March, with a transport of 23Sv, and strongest in September, when the transport increases to 32 Sv (Figure 5.8). The mean transport is 28 Sv. Direct observations of the seasonal cycle of the Tasman Front have not been found, but from the XBT results in section 4.2.4 suggest a mean Tasman Front transport of 8 Sv; much smaller than found in this model. This suggests that the Tasman Front pathway is generally favoured over the EAC extension pathway in this model.

Model output fields are all saved as monthly means, except for sea surface height which is saved daily so that features related to barotropic processes can be identified.

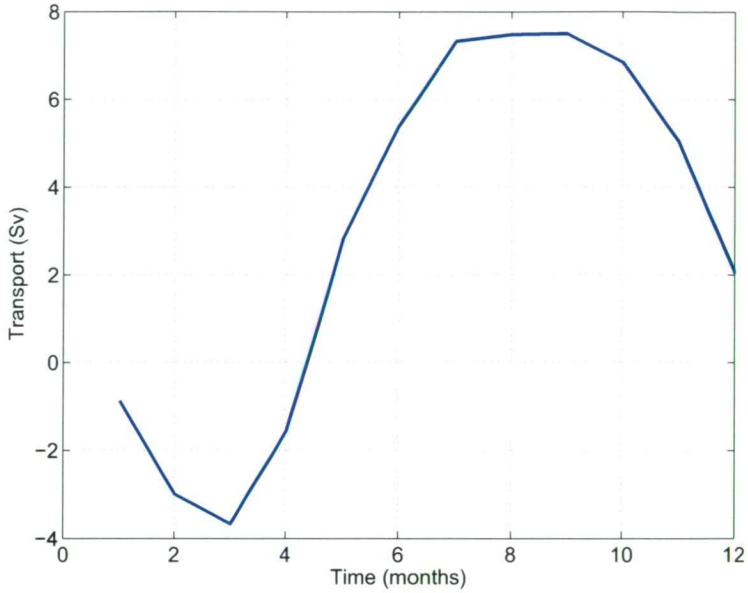

Figure 5.7: Mean annual cycle of net northward transport through the Tasman Sea in Sverdrups.

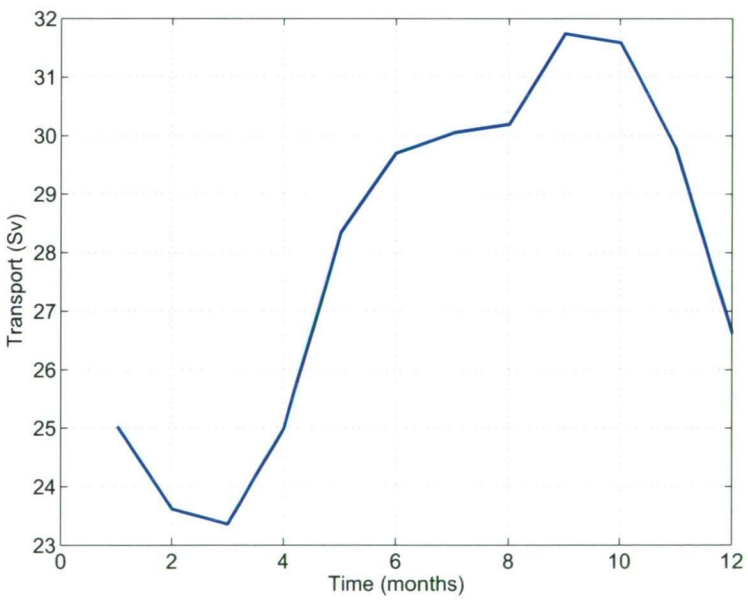

Figure 5.8: Mean annual cycle of Tasman Front transport (westward) in Sverdrups.

5.3 Details of Forcing experiments

We test the hypothesis that the observed time lag between South Pacific wind forcing and changes in the EAC can be achieved through a fast barotropic response across the South Pacific, converted to baroclinic energy in the form of coastal Kelvin wave propagation round New Zealand, spawning baroclinic Rossby waves on the west coast of New Zealand. To do this, the wind stress curl is modified by applying a zonal wind anomaly to different regions of the South Pacific. The anomaly is centred in the subtropical westerly winds to change the magnitude of the resultant wind stress curl maximum as this is the dominant low frequency variability observed in reanalysis winds (Figure 4.13b). We apply the anomaly to different longitudinal zones, to observe differences in the time it takes for the signal to reach the coast of Australia.

5.3.1 Designing forcing anomaly

The anomaly is produced by multiplying the monthly mean climatology with a mask (Figure 5.9). The mask is valued 1 everywhere, except in the region of the forcing anomaly. Zonally, the forcing anomaly is 5x observed over 10° longitude, and then reduces to 1x by 5° either side of this. In total, the anomaly is 20 degrees wide. Meridionally, the forcing anomaly is centred on 42°S and increases from 1x at 35°S to 5x at 50°S to increase the gradient of zonal wind stress (Figure 5.10) and hence wind stress curl (Figure 5.11) and stays at this level to the coast of Antarctica. While this affects the wind stress curl to the south of the region of interest, this is unavoidable. If the mask value south of 50°S was reduced back down to 1, the wind stress curl would be increased further. The effect of this is an enhanced region of negative wind stress curl.

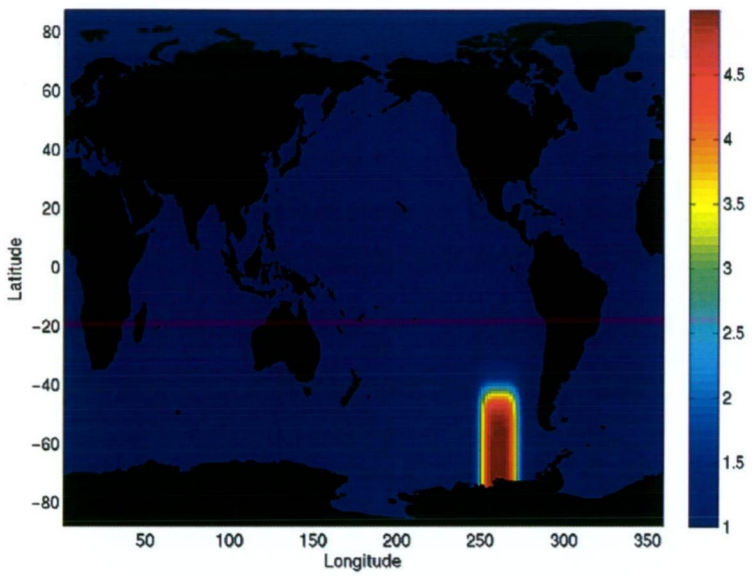

Figure 5.9: Mask multipled with first year of zonal wind stress in eastern perturbation run.

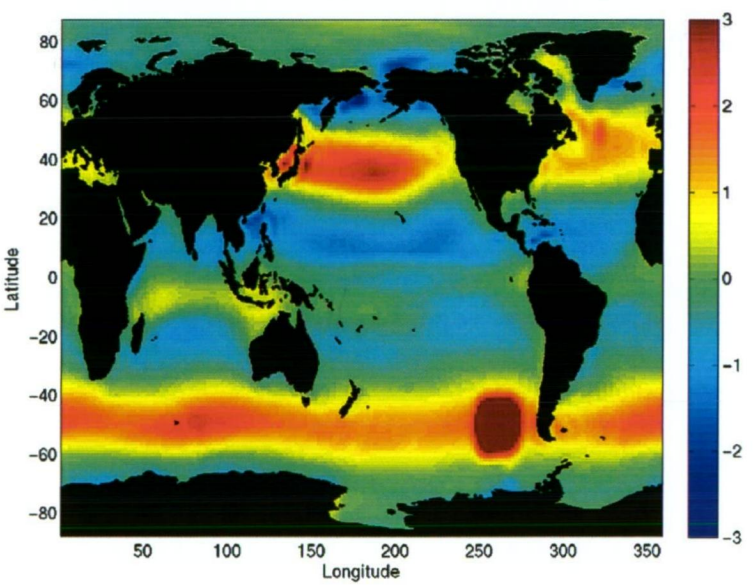

Figure 5.10: ERA-40 mean January zonal wind stress with eastern perturbation applied (N/m^2).

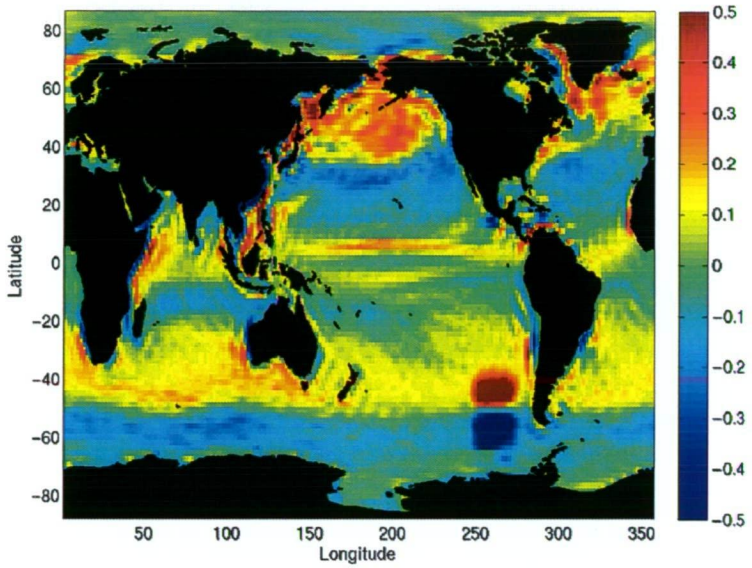

Figure 5.11: ERA-40 mean January zonal wind stress curl with eastern perturbation applied (N/m^3).

5.3.2 Sensitivity experiments

Changing friction and dissipation

As this is quite a coarse model, friction and dissipation constants are used to dampen numerical noise. As I am interested in propagation features, there is a delicate balance between setting friction and dissipations schemes low enough so that propagating features do not dissipate too quickly, and high enough that the model remains stable. Laplacian friction and dissipation was used and on assessing the effect of a range of dissipation and friction constants, were set to $3x10^4 m^2/s^{-1}$ and 100 respectively. Hence, the wind anomaly needs to be larger than those observed to produce a clear observable response in the sea surface height.

Spatial and temporal scales of anomaly

Initial forcing experiments were performed with a 1 month (20x background) zonal wind anomaly. Barotropic and baroclinic waves were apparent in the South Pacific,

but the signal doesn't reach the Tasman Sea. This could be due to a) the integrating effect of Rossby waves on the ocean is not considered, the anomaly is not broad enough or b) As we are looking at the low frequency variability, 1 month of forcing is not long enough. The period of baroclinic Rossby waves is a function of Latitude (Gill, 1982). At 20°S, the minimum baroclinic wave period is 100 days. Whereas at 45°S, the period is closer to 300 days, and in excess of 500 days south of 50S. This may explain why sustained forcing is needed for a minimum of a year centred on 42°S before barotropic wave energy is converted to baroclinic Rossby waves at the coast of New Zealand.

A run was tried with a forcing anomaly across the full width of the South Pacific basin. However, it is difficult to isolate the Rossby wave response in this case, as they are initiated across the full width of the South Pacific basin causing the propagating signature in SSH to be blurred. I conclude that forcing the model with a 1 year anomaly in a 20 degree longitude band produced a clear signal in the Tasman Sea, and also allowed us to explore the effects of forcing the ocean with an anomaly in different longitude regions across the South Pacific.

If the dominant mechanism of response was baroclinic, then the EAC would respond to wind forcing in different regions with very different timescales of response. If the mechanism involved the conversion of barotropic to baroclinic energy by New Zealand, and the ridges to the north, the near instantaneous barotropic adjustment across the South Pacific to New Zealand would mean that the position of New Zealand dictated the timescale of response, not the position of the forcing.

Magnitude of anomaly

The model is forced with a zonal wind anomaly of 1.5, 3, 5 and 20x ERA-40 mean seasonal cycle wind stress over a 20 degree longitude band, as described above.

From observations , a 1.5 wind stress curl anomaly should produce a 1°C change in temperature at Maria Island coast station (see Figure 3.8). However, this is a coarse model, and therefore relatively diffuse (see discussion on changing friction and dissipation, above), so a range of wind stress anomalies are tested. The primary aim is also to identify patterns of basin scale propagation, not reproduce realistic variability.

Runs with 5 and 20x zonal wind stress anomalies demonstrated clear propagation features. While the 1.5x and 3x runs show some response across the basin and into the Tasman Sea, the nature of the response is not coherent. I therefore focus on the 5x runs.

Regional forcing anomalies were applied in the east and centre of the basin, with the 20° wide anomaly centred on latitude 42°S, with centres at longitudes of 260°E (E5) and 225°E (C5) respectively. The anomaly is applied for the first year, and then the model was run for a further 19 years. This helps isolate the features formed as a result of the anomaly.

A full summary of all of the model runs performed is listed in Table 5.1.

5.4 Analysis of model results

Propagation of features were observed in SSH anomalies. These were calculated by subtracting the control run from the forced run, to produce daily timestep movies, and longitude/time (Hovmöller) diagrams. EAC Extension and Tasman Front transports were calculated, and Hovmöller diagrams across the current at a specific latitude were used to define the offshore edge of the current. The model EAC Extension transport was calculated across 37°S and is defined as the net transport through the Tasman Sea, the position of the separation zone and strong recirculation within the Tasman Sea mean that this is the most accurate representation of the EAC

Name	Position	Magnitude	Duration
—W1.5	190°E+/-5	1.5 x mean ERA-40 winds for January	1 month
—C1.5	225°E+/-5	1.5 x mean ERA-40 winds for January	1 month
—E1.5	260°E+/-5	1.5 x mean ERA-40 winds for January	1 month
—W3	190°E+/-5	3 x mean ERA-40 winds for January	1 month
—C3	225°E+/-5	3 x mean ERA-40 winds for January	1 month
—E3	260°E+/-5	3 x mean ERA-40 winds for January	1 month
—W5	190°E+/-5	5 x mean ERA-40 winds for January	1 month
—C5	225°E+/-5	5 x mean ERA-40 winds for January	1 month
—E5	260°E+/-5	5 x mean ERA-40 winds for January	1 month
—F5	225°E+/-20	5 x mean ERA-40 winds for January	1 month
—W20	190°E+/-5	20 x mean ERA-40 winds for January	1 month
—C20	225°E+/-5	20 x mean ERA-40 winds for January	1 month
—E20	260°E+/-5	20 x mean ERA-40 winds for January	1 month
—C5 year	225°E+/-5	5 x monthly mean ERA-40 climatology winds	1 year
—E5 year	260°E+/-5	5 x monthly mean ERA-40 climatology winds	1 year

Table 5.1: Summary of Model Runs. Magnitude refers to the multiples of the seasonal cycle wind stress applied, position denotes the location of the centre of the forcing anomaly +/- the range of this anomaly (sloping down to 1 another 5° either side of this range), and duration is the period of time which the anomaly was applied, after which the model is forced by mean seasonal cyle wind stress to produce a total run length of 20 years.

Extension transport. Net Tasman Sea transport was also used to define the EAC Extension in chapter 4. The model Tasman front transport was calculated across 178°E and the offshore limit was defined as 30.5°S. Due to the relatively coarse grid spacing of the model, there is little variability in the zonal extent of this current.

The velocity of propagating features were estimated from Hovmöller diagrams of SSH, measuring the time it took to travel 20 degrees of longitude, and using this to determine propagation speed in cm/s.

The results of these model experiments are discussed further in chapter 6.

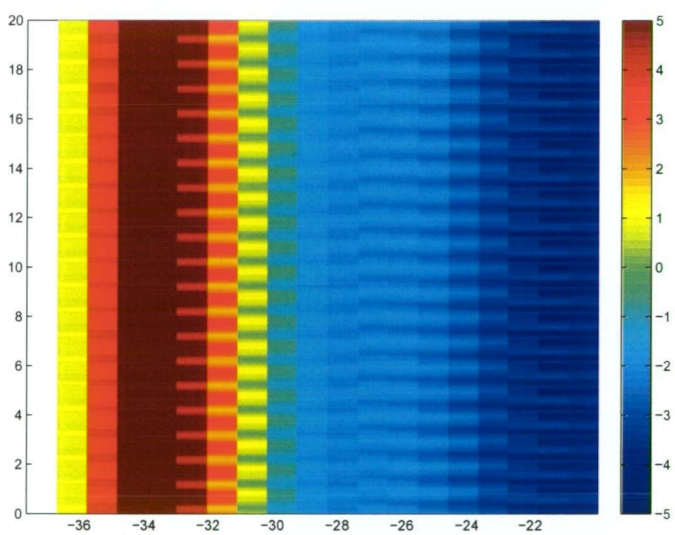

Figure 5.12: Latitude/time plot of depth integrated transport across 178E (eastward transport north of New Zealand)in Sverdrups. This was used to define the northern boundary of the Tasman Front as 30.5°S.

CHAPTER 6

Mechanisms and response timescales

6.1 Introduction and Motivation

While analysis of in situ ocean observations and reanalysis can be used to describe patterns and relationships, it is sometimes difficult to gain a full dynamical understanding without performing model runs, which allow us to isolate the processes we are interested in. We used a coarse resolution ocean model, forced by monthly mean climatology winds and perturbed the model with idealised regional wind anomalies designed to increase the wind stress curl magnitude in the region of maximum curl at different locations across the South Pacific. In chapter 5, I describe the motivation for the experiments, the model used, and design of the forcing experiments. In this chapter, I describe the results and discuss these in the context of observational findings set out in chapters 3 and 4.

In 5.1, the range of model runs performed are described. In this chapter, I will focus on 2 runs - the C5_year and E5_year runs (from now on, these will be referred to as C5 and E5 respectively). For these runs, a regional anomaly of 20° longitude width centred along 42.5°S, (the latitude range of the wind stress curl maximum), and 5x ERA-40 zonal wind stress monthly climatology is applied for 1 year, centred on 225°E (C5) and 260°E (E5) (see Figures 5.9 and 5.10).

This chapter is set out as follows: In section 6.2.1, the response of the ocean to a change in wind forcing in the central Pacific is discussed in terms of SSH response, and changes in the Tasman Sea regional current transports. Section 6.2.2 focuses on the response of the ocean to forcing in the eastern sector of the South Pacific, and in particular the interaction between propagating features and bathymetry. The model results are discussed in the context of recent literature in section 6.3.

6.2 Results

6.2.1 Response of the South Pacific to enhanced forcing in the centre of the basin (C5 year run)

Sea Surface Height (SSH) response

The wind stress maximum was enhanced in the centre of the basin at 225°E (C5 year run) for model year 1, and the response is shown in daily sea surface height (SSH) anomaly fields (Figure 6.1). On day 1, a positive SSH anomaly of 1cm appears in the centre of the basin (directly below the forcing anomaly). By day 2, a 5cm SSH anomaly is apparent, with evidence of westward propagation. A positive SSH anomaly has reached the Tonga-Kermadec Ridge north of New Zealand (NZ) by day 3. Such a fast propagation is too fast even for barotropic propagation, which, travelling at 2m/s, would take up to 3 weeks to cross to the Tonga-Kermadec ridge from the central Pacific (Pedlosky, 1996). At a calculated speed of 14m/s, this feature is likely to be gravity wave propagation (Pond & Pickard, 1983). The propagation is strongly constrained by deep topography, represented by the 3500m depth contour. From day 3 to day 6, a positive SSH anomaly develops along the Tonga-Kermadec ridge, and then the scattering and westward propagation of an SSH anomaly across the ridge is seen from day 7, but dissipates before reaching Australia. At around 42°S, the SSH anomaly propagates westward until it reaches Chatham Rise, and this feature appears to prevent further propagation westwards.

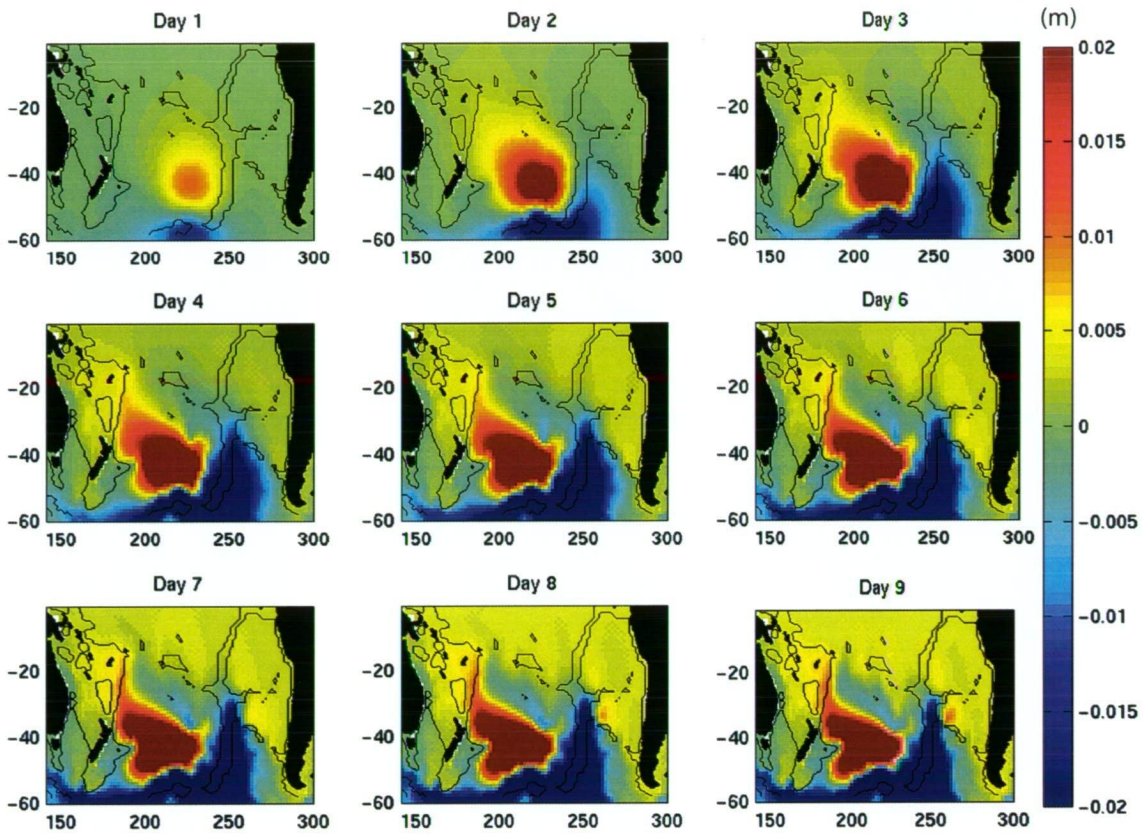

Figure 6.1: Snapshots of SSH anomaly (in metres) for the C5 run from 1-9 days after the initiation of enhanced wind forcing in the central South Pacific. Black line represents the 3500m bathymetric contour.

South of 42°S, the positive SSH anomaly has not yet propagated to the shelf off NZ. South of 50°S a negative SSH anomaly develops from day 1, which is related to the negative wind stress curl anomaly south of the positive anomaly in the forced winds. This negative anomaly appears to move east and north along the East Pacific Rise (EPR) as a topographic wave. However, it doesn't seem to influence the westward propagation of the positive anomaly.

A series of SSH anomaly maps over a period of 15 years gives a picture of how these propagating features evolve over a longer time frame, interacting with NZ and the regional topography (see Figure 6.2). The 12 maps show the SSH anomaly

in the South Pacific at different periods after the beginning of the initial 1 year forcing perturbation. As discussed above, on reaching the Tonga-Kermadec Ridge, the barotropic energy in the form of a 1.2 cm SSH anomaly propagates north along the ridge as a topographically trapped mode, before propagating across the Tasman Sea to the north of NZ between 1 week and 6 months after the beginning of the forcing period as a 0.5-1 cm SSH anomaly. The conversion on the ridge, situated at about 180°E, is seen in Figure 6.3 where fast (barotropic) westward propagation suddenly slows. It is difficult to identify a precise speed for the feature which is propagating from 180°E to Australia (150°E), due to the scattering of energy at the ridge, producing multiple propagation modes. In the first 2 months, features propagating rapidly appear to disperse prior to arriving at the Australian coast. Between month 3 and 4, a 1.5 cm anomaly reaches the Australian coast. A defined and slower anomaly moves west of 180°E at around 5 cm/s, which is at the upper limits of Killworth theory for 1st mode baroclinic Rossby waves suggesting a range of 3-5 cm/s at 28°S (Killworth et al., 1997). This fits well with work by Moore & Wilkin (1998) who identified the Tonga-Kermadec Ridge as a source of enhanced Rossby wave energy for the Tasman Sea. A positive SSH anomaly persists off the coast of Australia (around 30-32°S) between 7 months and a year after the initiation of forcing, which is the latitude of the separation point of the EAC. During the 1st year, a negative anomaly forms in the centre of the South Pacific, just south of the positive anomaly.

South of 40°S, it takes 3 weeks for the positive SSH anomaly to reach the shelf east of NZ. This is the equivalent of a propagation speed of 2 m/s, consistent with barotropic Rossby wave propagation (Pedlosky, 1996). The anomaly stalls at Campbell Plateau and does not cross the shelf for 6 months, when a positive anomaly is seen crossing the shelf towards NZ. A positive anomaly also begins to propagate around to the

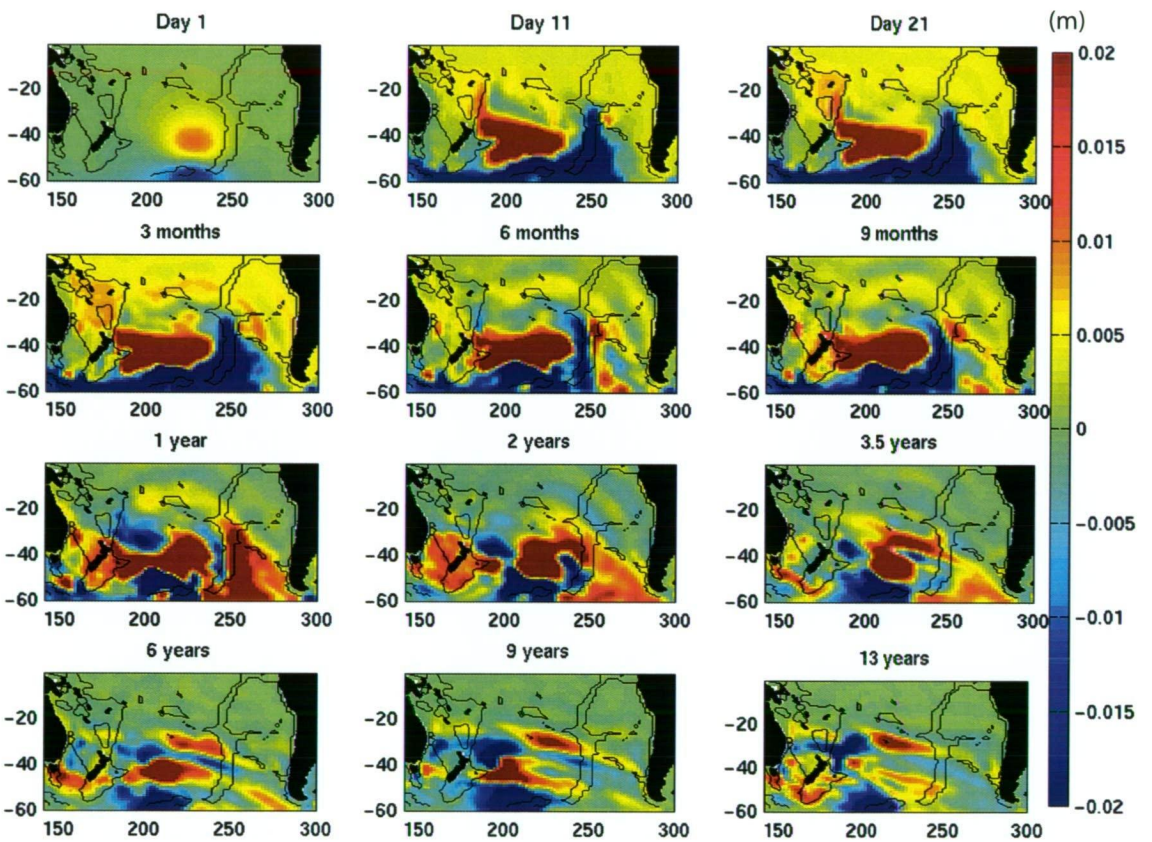

Figure 6.2: Snapshots of SSH anomaly from the C5 year run (metres) at periods after the initiation of enhanced wind forcing in the central South Pacific. Black line represents the 3500m bathymetric contour.

north of NZ, which takes 10 days to propagate around to the west coast of NZ, when a SSH anomaly begins to establish itself along the west coast of NZ. This is equivalent to a propagation speed of roughly 1.5 m/s and is likely to be a coastal Kelvin wave; although compared to observations of 2.7 m/s (Li & Clarke, 2004), it is slightly slower than expected. An SSH anomaly builds up along the east coast of NZ between 9 months and 1 year. It takes 2-3 years after the initial forcing for the anomaly established along the east coast of NZ to propagate across the Tasman Sea. A positive SSH anomaly then persists in the South Pacific around years 5-7. Meanwhile, at the end of year 1, a positive SSH anomaly has built up along the East Pacific Rise (EPR), perhaps as a topographically trapped mode (Fu, 2004; Weijer & Gille, 2005). This EPR anomaly moves eastward between 2 and 3.5 years after the start of the run, which then follows the gyre streamlines (see 5.6), and propagates towards the Australian coast at 25°S. The SSH anomaly propagates to NZ in 12 years, consistent with Killworth et al. (1997) modified theory for first mode baroclinic Rossby waves, which suggests it would take 15 years to reach the Australian coast, and 12 years to reach the NZ coast from the centre of the South Pacific (see Figure 3.10).

The rapid initial response to enhanced wind forcing is seen in a Hovmöller diagram across 40°S for the first 2 years of the run (see Figure 6.4). There is an initial fast westward propagation response which crosses the basin to NZ immediately (within 1 day) as discussed above. This is faster than barotropic Rossby wave theory speeds of 2m/s, which would take about 3 weeks to get from the central South Pacific to the coast of NZ (Pedlosky, 1996). While there is some reduction in the size of the SSH signal, an SSH anomaly of 5cm reaches the east coast of NZ. There is no evidence of barotropic energy produced on the west side of NZ as a result of the coastal Kelvin wave propagation identified in 6.2. Instead, a slower response is apparent.

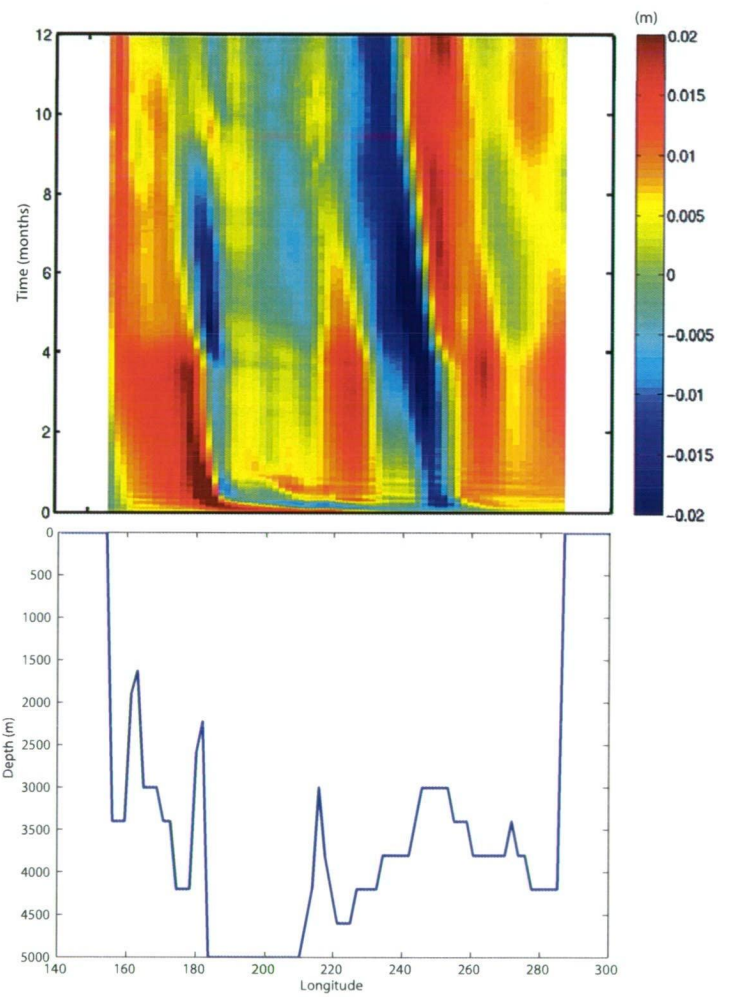

Figure 6.3: A longitude/time plot of SSH anomaly (metres) for C5 year forcing experiment along 28°S (above) and bathymetry along 28°S

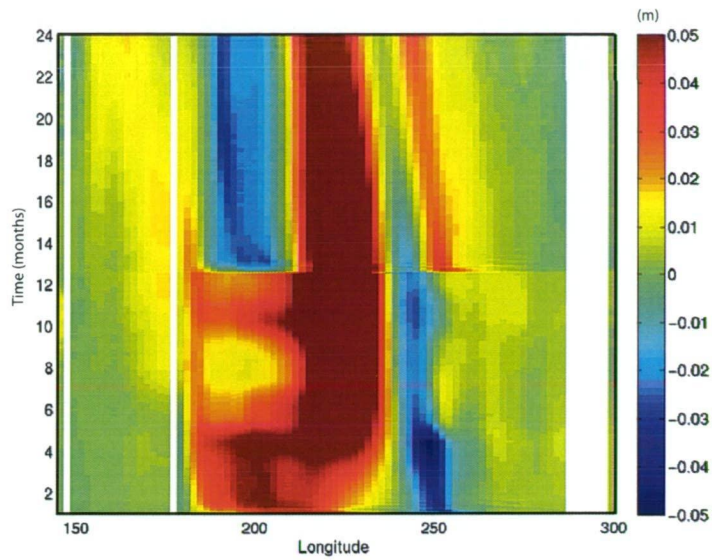

Figure 6.4: A longitude/time plot of SSH anomaly (metres) for C5 year forcing experiment along 40°S

This slower propagation can be seen in a Hovmöller diagram covering 20 years (see Figure 6.5), which shows an SSH anomaly of 2cm propagating from NZ at around 2.7cm/s westwards, reaching the east coast of Australia within 3 years. These are slightly faster speeds than predicted by Killworth modified theory for 1st mode baroclinic Rossby waves, which suggests speeds of 1-2 cm/s would be expected in this region at 40°S (Killworth et al., 1997). This barotropic/baroclinic propagation pathway via a coastal Kelvin wave around NZ reaches the east coast of Australia at the same time lag as that identified in Chapter 3 between changes in winds and the oceanic response at Maria.

Figure 6.6 provides a summary of this proposed mechanism. Enhanced wind stress in the central South Pacific initiates fast barotropic Rossby waves. On reaching NZ, barotropic energy is converted to baroclinic energy via the NZ coastal Kelvin wave which propagates around the northern part of NZ, forming a sea level anomaly on the west coast of NZ. This anomaly then spawns baroclinic Rossby waves which subsequently take a few years to cross the Tasman Sea.

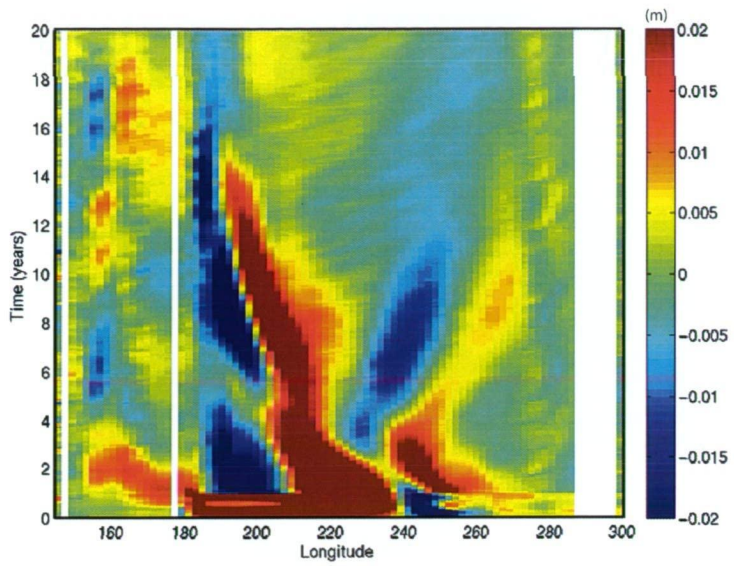

Figure 6.5: A longitude/time plot of SSH anomaly (metres) for C5 year forcing experiment across 40°S

Energy is lost on conversion from barotropic to baroclinic waves on reaching NZ. A 4 cm SSH response reaches the east coast of NZ, but the SSH signal that travels around the north of NZ and reaches the west coast of NZ in the Tasman Sea is only 2cm. This west coast NZ SSH anomaly begins to build up after 6 months. The delay between the barotropic signal hitting the east coast of NZ, and the build up of the SSH anomaly on the west coast appears to be related to two factors. First, the SSH anomaly stalls for 6 months before it is converted from barotropic to baroclinic energy and begins to propagate around the north coast. Secondly, the propagation of the Kelvin wave appears to be slower than observations at roughly 1.5 m/s when speeds of around 2.7 m/s have been observed off the south coast of Australia (Li & Clarke, 2004). The slightly slower propagation of the Kelvin wave could be related to the coarse resolution of the model (Hsei et al., 1983). However, the bulk of the delay in communicating the SSH signal around NZ is related to the conversion of barotropic Rossby wave energy into the baroclinic Kelvin wave. A delay of 3-6 months is found in all cases where such a conversion takes place.

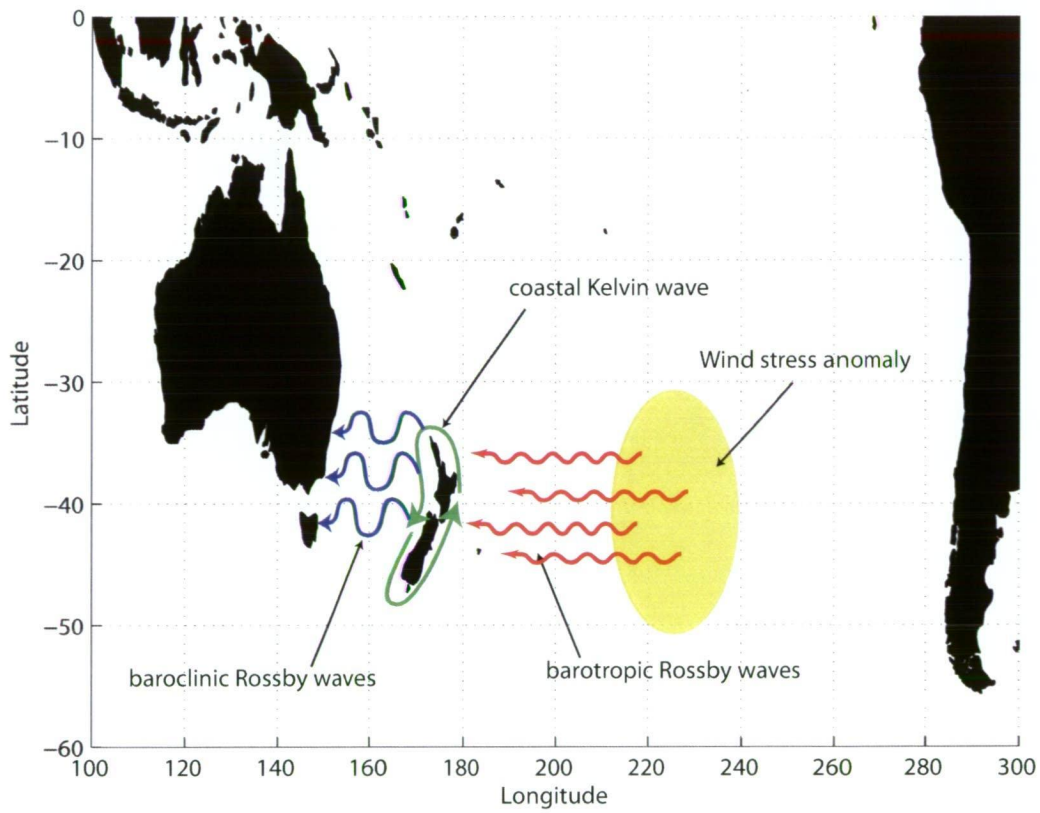

Figure 6.6: A schematic of the rapid mechanism by which changes in the winds in the South Pacific can be communicated to the East Australia Current.

In addition to the fast response discussed above, a slower feature is spawned directly at the region of forcing in the central Pacific, with an SSH anomaly of 3cm reaching the coast of NZ after 12-14 years (see Figure 6.5). This slower feature propagates at 0.6 cm/s, which is 2-3 times slower than speeds predicted by Killworth modified theory for 1st mode baroclinic waves (1-2 cm/s) (Killworth et al., 1997). This feature also manages to make it into the Tasman Sea, albeit much weakened, as an SSH anomaly of 0.7 cm.

Variations in transports

Net northward transport through the Tasman Sea for the control run and the C5 run can be compared in Figure 6.7 (the more negative the transport, the stronger the EAC Extension). The transports have been smoothed with a 1 year low pass filter to smooth the annual cycle. While some low frequency variability is apparent in the control run, the magnitude is small (less than 0.5 Sv). Periods of lower net northward transport can be interpreted as periods of strengthened southward transport through the Tasman Sea. However, as the SSH anomalies have been calculated by subtracting the control run from the forced run, it is more accurate to relate these anomalies to transport anomalies (forced minus control run). This also allows me to isolate the impact of the enhanced forcing from the intrinsic ocean variability.

The transport anomalies for the EAC Extension and Tasman Front are shown in Figure 6.8 (positive anomaly = stronger transport of the EAC Extension south and Tasman Front front), showing that the first peak in the EAC Extension (+2.3 Sv) and trough in the Tasman Front (-2.3 Sv) appears after 6 months. If this is compared with Figure 6.5, it matches up well with the time that it takes the barotropic response to travel across to the east coast of NZ, and a topographic wave to travel up the Tonga-Kermadec Ridge, spawning baroclinic Rossby waves to the

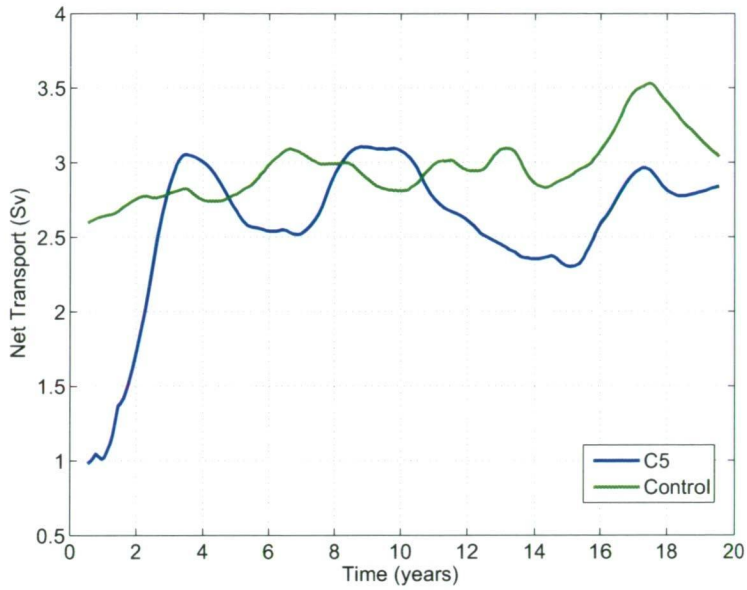

Figure 6.7: Net northward transport through the Tasman Sea for Control run and C5 run (Sv)

west of the ridge, that propagate across the Tasman Sea (Figure 6.2) which takes 1-7 months. As baroclinic waves reach the western boundary, they are reflected into short wavelength waves, which are quickly dissipated, releasing energy into the system and hence enhancing the western boundary current transport (Pedlosky, 1979).

A second minimum in the Tasman Front is seen after 1 year (-4.4 Sv) and 1-2 years in EAC Extension (1.3 Sv) (Figure 6.8). This appears to be associated with the build up of the SSH anomaly around the north of NZ as a coastal Kelvin wave, and the propagation of the positive anomaly across the Tasman Sea, which would act to weaken the Tasman Front, and hence indirectly strengthen the EAC Extension.

A third minimum in the Tasman Front (-1 Sv) and peak in the EAC Extension (0.5 Sv) is seen after 6-7 years in Figure 6.8. While it is not clear what mechanism causes this, it is associated with a positive SSH anomaly in the South Tasman Sea. When compared with the Hovmöller diagram of SSH anomaly at 40°S, it

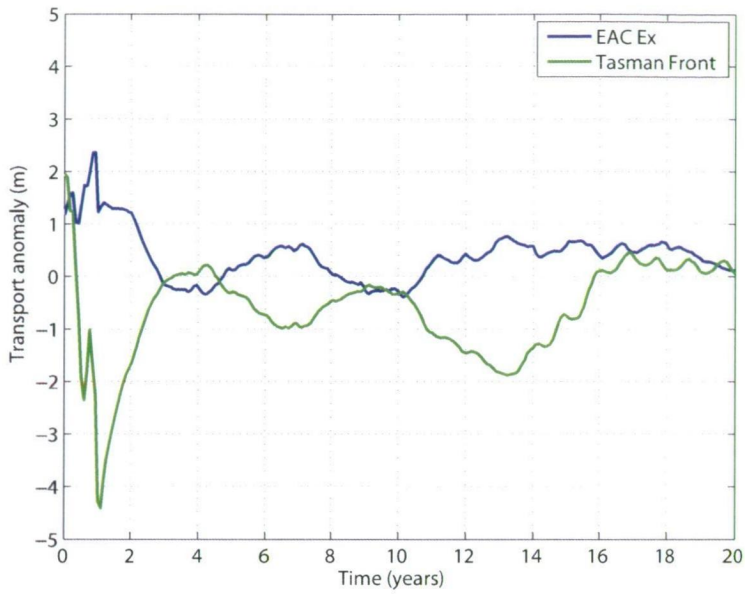

Figure 6.8: Transport anomaly (C5 run minus control run) for EAC Extension and Tasman Front (Sv)

might be expected that a positive anomaly would be seen after 2-3 years, when the first baroclinic Rossby wave (formed via the barotropic/coastal Kelvin wave pathway) reaches the coast of Australia (Figure 6.5). However, as noted in section 5.2, the mean net transport through the Tasman Sea is northward, caused by strong recirculation within the Tasman Sea. This water then joins the Tasman Front, which means that the Tasman Front is stronger in the model than in observations, and similarly the EAC extension is much weaker than in observations with a weak net southward flow only found in summer. When just the southward component of the flow is considered (i.e. east of 158°E), the magnitude of the transport anomalies are similar to those seen when considering the net flow through the Tasman Sea. The EAC Extension is dominated by eddies, and the separation dynamics are also inherently non linear, and these processes are not resolved at the grid spacing of the model. This may in part explain the weak transport response in the EAC system to a large perturbation to the winds. The dispersive nature of a coarse model also

may have a role to play.

After 12-14 years, a 4th minimum in the Tasman Front(-1.8 Sv) and peak in the EAC Extension (0.7 Sv) is seen (Figure 6.8), which is related to the 1st mode baroclinic Rossby wave reaching NZ causing an increase of SSH around the north of NZ, hence weakening the Tasman Front. This suggests a direct negative (or damping) affect of this anomaly on the strength of the Tasman Front. If this is considered in terms of mass balance, if the water doesn't exit the Tasman Sea in the Tasman Front, then it must continue south. Hence a reduction in the strength of the Tasman Front enhances the strength of the EAC Extension. There is no evidence of an immediate transition of this anomaly to the Tasman Sea, for it to have a direct effect on the strength of EAC Extension. A weaker high sea level feature is seen propagating to the middle of the Tasman Sea after year 14.

It is interesting to see that with a single pulse of perturbation to the winds, the model is able to create a low frequency variability in the strength of the EAC Extension and Tasman Front. The strength of these two currents are also anti-correlated (r = -0.54), as seen in Chapter 4.

Mechanisms and Pathways

In summary, three propagation pathways can be identified. The first and fastest method involves barotropic wave propagation, forming a topographic wave along the Tonga-Kermadec Ridge, which then spawns baroclinic waves which cross the Tasman Sea. As the baroclinic waves are propagating at a lower latitude, and hence propagate more quickly, they impact the EAC system within a year. The second mode involves barotropic waves, hitting NZ, converting to a coastal Kelvin wave which propagates around the coast of NZ spawning baroclinic waves on the west coast. The transit time for this pathway is 2-4 years. Lastly, there is the baroclinic

only pathway, which also includes propagation around the coast of NZ, takes 12-14 years to propagate from the region of forcing to the Australian coast.

Analysis of model results also suggests that there are two ways in which propagating features influence the EAC Extension and Tasman Front. This can be described in terms of changes to the SSH gradient or slope across the currents. First, the Tasman Front is associated with an increase in SSH away from the north coast of NZ. The build up of SSH around the north of NZ due to the propagation of the coastal Kelvin wave will reduce the gradient of SSH across the current, and hence the strength of the Tasman Front. This will consequently send more water down the EAC Extension pathway. Pedlosky (1979) describes the role of Rossby waves in western boundary current intensification in terms of energy dissipation, but perhaps it can also be described in terms of SSH gradients. The EAC Extension is also associated with a positive slope in SSH between the coast of Australia and offshore. The baroclinic Rossby waves propagate across the Tasman sea to the shelf edge, enhancing the offshore SSH, strengthening the EAC Extension and drawing more water down the coast, and thus reducing the transport in the Tasman Front.

The size of the transport anomaly appears to depend on which of the two pathways is being forced directly by the propagating SSH anomalies. These SSH anomalies reflect changes in the depth integrated streamfunction. However, as transport variations in the EAC Extension and Tasman Front are only 1-2 Sv in a gyre which has transports of 60 Sv, it is difficult to deduce any gyre scale changes. I have therefore not included these in this study. While variations in the strength of the EAC produces temperature variations as demonstrated in chapter 3, the weak ocean transport response to wind forcing means that no clear change in temperature is seen. This will be discussed further in section 6.3.

6.2.2 Response of the South Pacific to enhanced forcing in the east of the basin (E5 year run)

Sea Surface Height (SSH) response

A second forcing experiment was carried out in the eastern part of the South Pacific basin, with the anomaly centred further east at 260°E (E5). Figure 6.9 shows the response of the ocean SSH to the wind perturbation for days 1-9. When Figure 6.9 is compared to the centrally forced run in Figure 6.1, the most obvious difference is the absence of a strong immediate barotropic response across the South Pacific basin to NZ. The relationship between the development of the SSH anomaly and the East Pacific Rise (EPR - represented by the 3500m bathymetry contour) is very clear. The EPR seems to act as a very effective barrier to westward propagation. In addition, the negative SSH anomaly appears to propagate north up the ridge from day two. Again,this is perhaps a topographically trapped barotropic mode (Fu, 2004; Weijer & Gille, 2005).

The Hovmöller diagram of SSH anomaly (Figure 6.10a) also shows the absence of a clear immediate westward propagating response. The position of the forcing anomaly sits right to the east of the East Pacific Rise, as demonstrated with the cross section of bathymety for this latitude (Figure 6.10b). The initial SSH response is in the form of a 20cm anomaly. The first mode baroclinic response dominates the plot, with an SSH anomaly of 10cm propagating across the EPR. This anomaly propagates across the entire width of the South Pacific Basin at 1.5 to 2.5 cm/s, but has decreased to a 3cm SSH anomaly by the time it reaches the coast of NZ. More interestingly, there is also evidence of a feature which moves across the Pacific basin faster, resulting in an SSH anomaly of 0.6-0.8cm in the Tasman Sea after 4 years. While the SSH response across the South Pacific is patchy at this latitude, the propagation appears to be a barotropic response which crosses the South Pacific

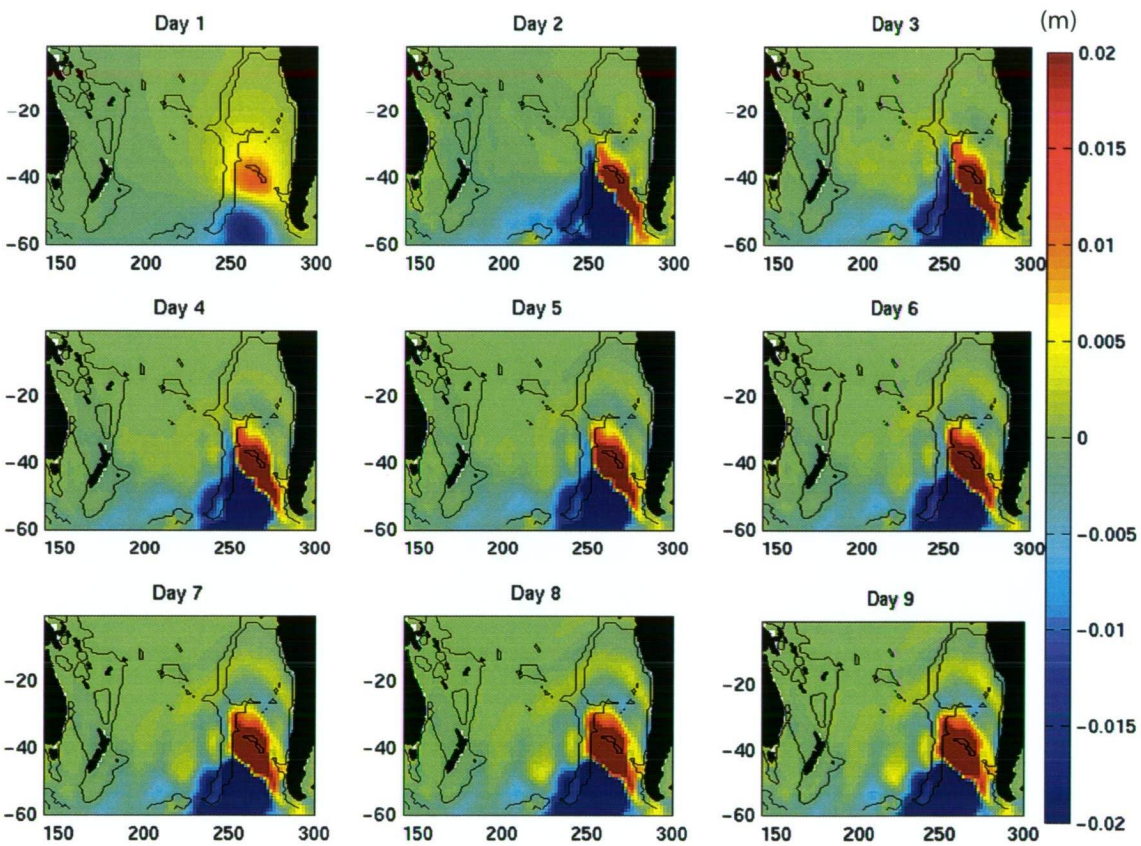

Figure 6.9: Snapshots of SSH anomaly (in metres) for the E5 run from 1-9 days after the initiation of enhanced wind forcing in the eastern South Pacific. The black line represents the 3500m bathymetric contour.

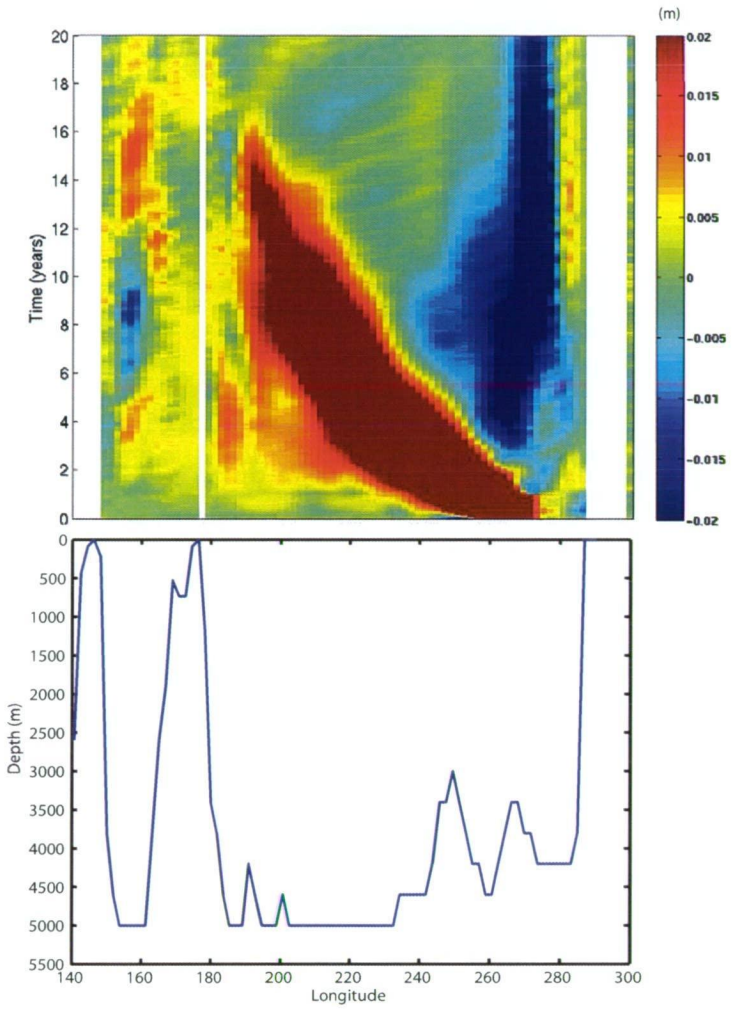

Figure 6.10: A longitude/time plot of SSH anomaly (metres) for E5 year forcing experiment

after being delayed east of the EPR for the first 4 months. After this time, energy is scattered at the ridge and propagates across as fast barotropic waves (2m/s) arriving at the western boundary between 45 months and 4 years.

Further evidence of the barotropic nature of this feature is that it reacts strongly with bathymetry. The SSH anomaly is close to 1.5 cm at 210-220° longitude, it then reduces to 0.5cm by the time it reaches 195°E before increasing to around 1cm on reaching the deep ridges to the east of the NZ coast at around 180-190°E. Such

a strong response is surprising considering the depth of the bathymetry is 4500m. East of NZ, two SSH anomalies result. The first, 3-5 years after the initiation of the forcing anomaly is associated with the scattered barotropic mode being converted into baroclinic Rossby waves via the NZ coastal Kelvin wave (as discussed in section 6.2.1). The second, 12-18 years after the initiation of forcing, is associated with the baroclinic response.

A series of SSH anomaly maps for the E5 run over a period of 15 years provides a spatial picture of the response of the South Pacific to enhanced wind forcing in the east of the basin (see Figure 6.11). The SSH anomaly is mainly confined to the east of the EPR until 6 months after the initiation of forcing when two weak SSH anomalies appear between the EPR and NZ. One at 220°E, which is about 0.7 cm, and one at 190°E, close to the edge of Campbell Plateau, which is about 0.5 cm. The fact that these two anomalies appear at almost the same time is further evidence that they represent a barotropic Rossby wave. These anomalies establish south of 40°S, gain strength and coherence to form a continuous anomaly across the South Pacific by 9 months. The SSH anomaly expands north of 40°S, propagating north of NZ as a coastal anomaly, and into Tasman Sea by 3 years after initiation of the forcing anomaly. By this point, the main SSH anomaly has split, and a large (10 cm) SSH anomaly is advected north up the EPR. The baroclinic anomaly reaches NZ by 13 years. The positive anomaly, which formed along the EPR, has spread out through the northern limb of the South Pacific gyre between 8 and 15 years. A positive SSH anomaly persists in the South Tasman Sea between 6 and 16 years after the start of the experiment.

Variations in transport

Net transport northward through the Tasman Sea for the control and E5 run are compared in Figure 6.12. Transports have been filtered with a 12 month running

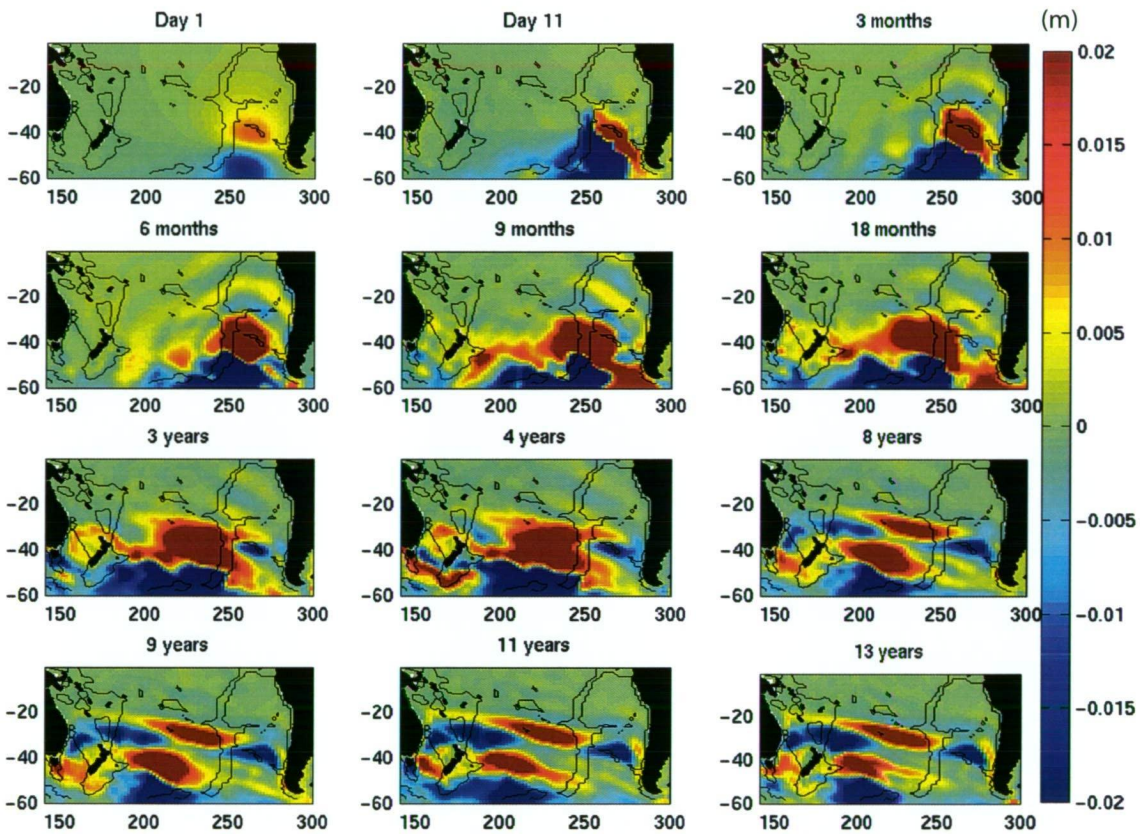

Figure 6.11: Snapshots of SSH anomaly (metres) for the E5 year run after the initiation of enhanced wind forcing in the eastern South Pacific. The Black line represents the 3500m bathymetric contour.

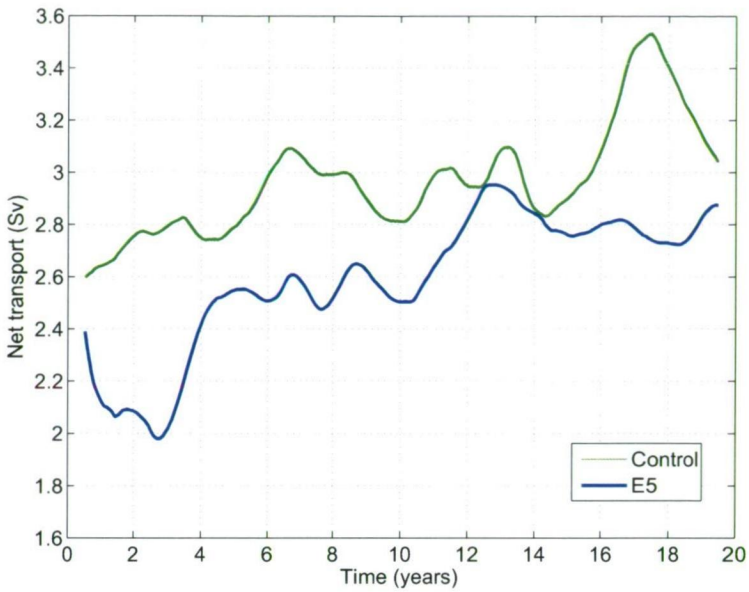

Figure 6.12: Net northward transport (Sv) through the Tasman Sea for Control run and E5 year run

mean to remove the seasonal variability. The control run transports vary by around 0.5 Sv. This raises questions of the significance of the difference in the transports between the control run and the forced run, which are also between 0.5 Sv and 1 Sv. However, as discussed in section 5.4, by removing the control run from the forced run, the impact of the enhanced wind forcing on the ocean is focussed on.

Figure 6.12 shows a weaker northward transport (associated with a stronger EAC Extension) for the E5 run compared to the control run after 3 years, of about -0.8 Sv, followed by a period of prolonged stronger southward transport between year 4 and 11 of about -0.2 to -0.5 Sv and then after 16-20 years of -0.8 Sv. The transport anomaly (E5 run - control run) for the EAC Extension and the Tasman Front shows an anticorrelation (r = -0.54) between the strength of the two currents (Figure 6.13). Three dominant periods where there is a stronger EAC Extension and a weaker Tasman Front are apparent. The first is between 1 and 3 years after the initiation of the perturbation, when the EAC extension is about 0.8 Sv

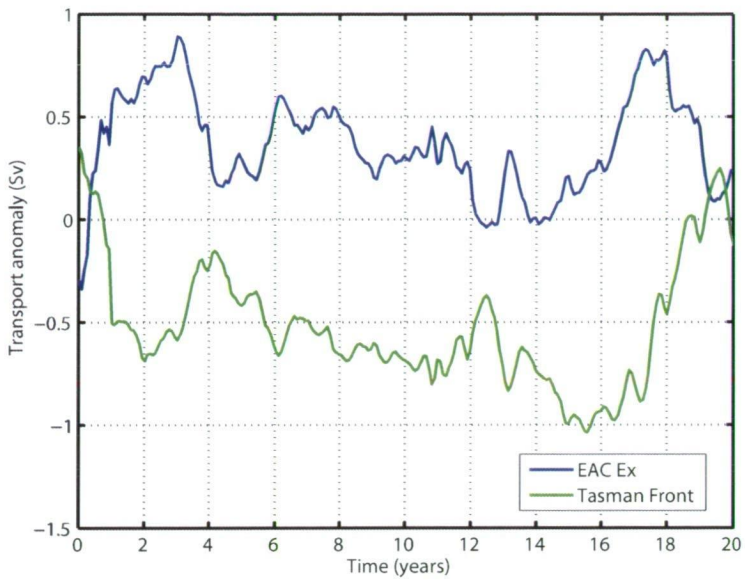

Figure 6.13: Transport anomaly (E5 year run minus control run) for EAC Extension and Tasman Front (Sv)

stronger, and the Tasman Front is about 0.7 Sv weaker which can be related to the delayed barotropic mode propagating into the Tasman Sea, as discussed earlier in this section. The second period is related to a prolonged period of positive SSH anomaly in the South Pacific. The 3rd period appears to be related to the first mode baroclinic Rossby wave reaching NZ and weakening the Tasman Front. The EAC Extension increases 2 to 3 years later, the time it takes for the 1st mode baroclinic Rossby waves to propagate from NZ to the east coast of Australia.

Again, when these periods are compared with the snapshots of SSH anomaly maps (see Figure 6.11) and the Hovmöller diagram of SSH anomaly, these maxima in the EAC and minima in the Tasman Front are not necessarily correlated with the SSH anomaly propagating completely across the Tasman Sea. The timing is often related to when a positive SSH anomaly reaches the Tasman Sea, by propagating around the north of NZ and building up an anomaly along the west coast of NZ, rather than when it completely crosses the Tasman Sea to Australia. For instance, after

18 months - 2 years when the first maximum in the EAC Extension is seen, the faster mode of propagation has only just reached the coast of NZ, and is building up the SSH anomaly around the north coast. As discussed in section 6.2.2, the build up of sea level along the north coast of NZ would reduce this slope, and hence the geostrophic transport of the Tasman Front.

6.3 Discussion

I explored the mechanisms by which the ocean responds to a change in wind forcing using a global ocean model and idealised regional wind forcing experiments. These model runs confirm that the ocean responds to wind forcing by spawning both barotropic and baroclinic Rossby waves, which have very different propagation speeds. These waves interact with topography, resulting in the transfer of energy between wave modes. The result is an ocean which responds at different time lags.

These experiments also demonstrate that the ocean can low frequency decadal ocean variability as a result of a single pulse type wind forcing, due to the multiple ways in which the ocean responds to a change in forcing. The Hovmöller diagrams suggest enhanced wind stress curl produces barotropic waves which propagate rapidly across the Pacific to NZ. The barotropic wave scatters into a coastal Kelvin wave that propagates acround the coast of NZ. The height anomaly associated with the Kelvin wave, in turn, spawns baroclinic waves west of New Zealand. The baroclinic waves take about 2.5 years to cross the Tasman Sea, resulting in a total propagation time of 3 years from the initiation of forcing in the centre of the Pacific. Barotropic Rossby waves take from days to 3 weeks to cross to the east coast of NZ, propagating at around 2 metres per second. There is a stalling at the shelf of NZ, and it takes 5-6 months for this barotropic signal to be converted into a baroclinic signal. As discussed in section 5.3.2, at 45°S, the period of baroclinic Rossby waves is around

300 days (Gill, 1982). This may explain why sustained forcing is needed for a year before barotropic wave energy is converted to baroclinic Rossby waves at the coast of New Zealand. This also accounts for the observed lag of a few months between when barotropic waves reach New Zealand, and baroclinic waves are initiated. and begin to propagate around the north coast of New NZ as a coastal kelvin wave which takes around 10 days to propagate to the west coast, equivalent to a propagation speed of around 1.5m/s. The baroclinic Rossby wave begins to propagate across the Tasman Sea after 1 year, and reaches the east coast of Australia after 3 years. However, this 3 year lag was not clearly reflected in the transport anomalies for the central forcing run (Figure 6.8), which showed a weak response (0.5 Sv) a few years later at 4-6 years. This weak transport response is likely related to unresolved eddy dynamics which govern the EAC, EAC separation, and EAC Extension. The eddy mass transport of the EAC is several times the large as the mean current (Ridgway & Godfrey, 1994; Boland & Church, 1981). The dispersive nature of a model of this resolution is also likely to play a role, by damping the response of the ocean to the wind forcing.

Idealised experiments have demonstrated the role of islands and ocean ridges in converting barotropic energy into baroclinic energy (Liu et al., 1999; Tanaka & Ikeda, 2004). Liu et al. (1999) performed numerical experiments with a 1.5 layer fully non linear reduced gravity box model with an island in the middle. They showed that remote forcing initiates planetary waves which impinge on the eastern side of the island. These planetary waves then interact with the coastal Kelvin wave circulation around the island, spawning baroclinic Rossby waves on the other side. This communication pathway is feasible in the South Pacific, with coastal Kelvin waves communicating the signal around NZ. However, Liu et al. (1999) suggested this is a mechanism by which baroclinic Rossby wave energy can be communicated

around islands. The model results presented in this chapter show that the existence of an island can facilitate the conversion between barotropic and baroclinic modes. Liu et al. (1999) also conclude that along-shore wind stress on the eastern boundary of the island can interact with the coastal Kelvin wave, to spawn baroclinic Rossby waves on the west coast of the island. However, the role of this has been shown to be minor compared to the remote forcing effect (Sasaki et al., 2008), and cross correlations show the strongest correlations between between observed changes in the Tasman Sea properties and wind stress curl in the central south Pacific (see chapter 3). Hence, I focus on the remote forcing dynamics.

Model results presented in this chapter also show interaction of Rossby waves with deep bathymetry, and confirm that many of the processes discussed by Tanaka & Ikeda (2004) in the North Pacific, can also be observed in the South Pacific. North of NZ, the barotropic waves reach the Tonga-Kermadec ridge, then propagate north as a topographic wave. It appears to build up along the ridge before spilling over to propagate across to the east coast of Australia. There is an even longer pause, before the build up of SSH east of NZ propagates around to the north of NZ as a coastal Kelvin wave 7-10 months later. Tanaka & Ikeda (2004) used a North West Pacific regional model with idealised bathymetry and no background wind field. The model was forced with a regional interannual wind stress anomaly of 0.1 Pa (or 0.1 N/m^2) in the central north Pacific centred on 180°E, 30°S. Tanaka & Ikeda (2004) also see a stalling of barotropic energy on ridges. The barotropic waves arrived at the Izu-Ogasawara Ridge just east of Japan within 1 year after the wind forcing was imposed, travelling at greater than 0.5m/s. However, the ridges weren't crossed until after year 4 (Tanaka & Ikeda, 2004). The time lag appears to be much shorter in the model experiments presented in this chapter than those performed by Tanaka & Ikeda (2004). However, the model presented here is forced

with realistic winds, which are then enhanced by 5x background wind forcing in an isolated region, whereas Tanaka & Ikeda (2004) used a model at rest, and forced it with realistic wind stress in an isolated region. This means that in the region of forcing, the model was being perturbed by winds which were around 5 times larger than in the experiments performed by Tanaka & Ikeda (2004). If a critical level of build up is needed before Rossby waves can cross the ridge, this would be reached quicker with this larger perturbation.

Qiu & Chen (2006) used a 1.5 layer reduced gravity model driven by NCEP winds to show that observed low frequency SSH variability in the South Pacific can be explained by first mode baroclinic physics, and are able to successfully recreate a large part of the spatial pattern of the trend in SSH seen during the 1990's in altimeter data. This appears to be at odds with the results presented above. Qiu & Chen (2006) acknowledged that the model showed less skill in the Tasman Sea, where the high sea level trend seen in the altimeter data is not recreated. The maximum sea level trend is also further south and east in the model compared to the altimeter. This analysis is also hampered by the length of the satellite altimeter dataset, which meant that Qiu & Chen (2006) were trying to deduce decadal timescale variability with only one decade (12 years) of data.

Sasaki et al. (2008) also argue that 1st mode baroclinic physics is sufficient to explain the observed variability in the South Pacific, and suggest that the results of Qiu & Chen (2006) can be improved in the Tasman Sea, if the role of NZ is taken into account. The results presented in this chapter confirm the role of NZ in determining variability in the Tasman Sea. However, Sasaki et al. (2008) argue that it is the baroclinic (and not barotropic) Rossby waves interacting with the coastal Kelvin wave around NZ, which then spawns baroclinic waves on the west coast of NZ. Sasaki et al. (2008) compared the first EOF of the Ocean General Circulation Model

(OGCM) for the Earth Simulator (OFES) between 1970 and 2003 and results from a linear 1.5 layer model, incorporating a coastal Kelvin wave around NZ for the same time period. While Sasaki et al. (2008) suggest that the spatial patterns are similar, they acknowledged that large amplitude and small scale SSH anomalies around the north east coast of NZ and the Tasman Front are not reproduced in the model. Other possible mechanisms such as baroclinic Rossby waves generated by a barotropic mode were suggested, in regions where bathymetry plays a significant role in the flow fields. Sasaki et al. (2008) show that large scale sea level variations in the Tasman Sea from OFES and the linear model were highly correlated (r= 0.84), which suggests that it is largely baroclinic Rossby waves which determine the larger scale variability. However, the results presented in this chapter suggest that barotropic Rossby wave propagation has a larger role to play in communicating changes in the ocean; especially in setting timescales of variability.

The results presented here compared with those of Qiu & Chen (2006) and Sasaki et al. (2008) need to be considered in the context of the differences in experiment set up. Qiu & Chen (2006) and Sasaki et al. (2008) compare 7 day interval altimeter data and monthly OFES data respectively with the linear model results, whereas barotropic waves have only been detected in 3 day interval data (Fu, 2004). The linear model used by both Sasaki et al. (2008) and Qiu & Chen (2006) is driven by NCEP winds, with the long term mean removed. Variability in the southern hemisphere westerlies is generally zonally coherent as it is associated with the waxing and waning of the polar vortex, this is seen in wind stress curl as periodic strengthenning of the wind stress curl maximum (see Figure 4.13). As the Rossby waves travel westwards, they integrate the wind forcing along their path, and this wind variability tends to be zonally coherent (see Figure 4.13). If the forcing region is just east of NZ, first mode baroclinic waves could explain the barotropic

response (Qiu & Chen, 2006). If the critical region of forcing is further east, then a faster (barotropic/baroclinic) mechanism is required. The use of a narrow longitude band wind anomaly meant that we could isolate the forcing region and hence the responses of the ocean to this forcing.

Comparison of SSH patterns with transports suggests that the variability in the EAC system can be produced by two mechanisms. First, baroclinic Rossby waves crossing the Tasman Sea to the western boundary can enhance the volume transport south in the EAC extension (Pedlosky, 1979). By bringing more water south through the Tasman Sea, this would reduce the flow across to the north of NZ as the Tasman Front. Second, the build up of SSH around the northern part of NZ in the form of Kelvin wave propagation would act to reduce the slope of the isopycnals, and hence the eastward transport of the Tasman Front. Analysis suggests in both cases, one current is feeling the direct forcing and hence transport change, while the other current is forced indirectly in the opposite sign due to the partitioning of the EAC.

As the focus is on the broad scale oceanic response to forcing, a coarse model was considered an appropriate tool. However, the effect of the resolution on propagating features in the ocean needs to be considered. In the model experiments presented in this chapter, barotropic Rossby waves propagate from 220°E to 180°E within 21 days at 40-50°S. This would give a rough propagation speed of about 1.9-2 m/s, which is comparable with theory presented by Pedlosky (1996) who suggested speeds of 2 m/s for gyre scale waves. The model exhibits baroclinic Rossby wave propagation in agreement with Killworth modified theory (Killworth et al., 1997) with planetary waves propagating at 1-2 cm/s at 40°S. Kelvin wave propagation speeds are related to the baroclinic Rossby radius and the Coriolis parameter. Hence, as the Rossby radius is smaller than the grid spacing in this model, resolution is likely to have an effect on their propagation speed (Hsei et al., 1983). Observations of Kelvin wave

propagation along the south coast of Australia gave speeds of 2.7 m/s (Li & Clarke, 2004). While this is further north than the north coast of NZ studied in this model, the estimated model Kelvin wave speeds of 1.5 m/s are slightly smaller. However, this difference is not large enough to affect the results presented here.

The results suggest that Rossby wave propagation is highly sensitive to even very deep bathymetric features. For instance, the EPR rises to only 3500m, but acts as a barrier, delaying barotropic Rossby wave propagation for 4 months. A delay of 6 months was seen between barotropic waves hitting northern NZ, and the propagation of the Kelvin wave around the north coast of NZ. This delay appears to be related to the conversion from barotropic to baroclinic modes. Interaction was also seen with bathymetric features as deep as 4500m. The stratification of the model was discussed in section 5.2, and compares well with climatology; although some differences were highlighted, especially in the top 500m. Owen et al. (2005) demonstrate that the nature of Rossby wave scattering on ridges depends crucially on the stratification of the model. For instance, if the majority of the density variation is confined to a thin thermocline, a large amount of wave energy can be reflected by a small amplitude ridge.

In addition the model confirms that the observed anti-correlation between the EAC Extension and the Tasman Front is related to variations in the magnitude of the South Pacific wind stress curl maximum, whereby periods of enhanced wind stress curl cause the EAC Extension to be favoured over the Tasman Front. Considering the wind forcing is 5x background wind forcing, the transport response in the Tasman Sea currents was relatively small (0.5-1.5 Sv) compared to observations. Decadal variability in the EAC Extension transport from XBT data is 6-12 Sv (see Figure 4.8) as a result of wind stress curl variability in the South Pacific of 4-6x10^{-8} N/m^3 from NCEP (equivilent to a 1.5x increase). This could be caused by a damped

response of this coarse resolution model as a result of the relatively large dissipation and friction coefficients needed to make the model numerically stable. However, the GECCO model, which is 1x1° resolution (compared to 1.875° x 0.94° for this model), produces EAC extension transport variations of 4-5 Sv in response to the NCEP wind variability (see Figure 4.13). As discussed above, the grid spacing of the model means that the non-linear processes which govern a western boundary current system are not resolved, and this may mean that the model's EAC system responds differently. The design of the wind anomaly could also be a factor. In the real ocean, Rossby waves act as "integrators" of ocean forcing, and are forced as they travel across an ocean basin. This would offset the dissipation of energy. Secondly, the Rossby waves are responding to high frequency variability in the winds, which when smoothed, have a low frequency signature. The relatively slow response of the extratropical oceans in terms of the Rossby wave response means that this low frequency variability dominates. However the wind variability exhibits high frequency, high amplitude variability.

By forcing the ocean with a defined wind anomaly in space as well as time, as opposed to observed wind variability, these model experiments help to elucidate the mechanisms by which the ocean responds to changes in wind forcing can be isolated. The experiments demonstrate the feasibility of a fast combined barotropic/baroclinic mechanism causing a change in the transport of the EAC system on observed timescales. The anti-correlation between the EAC Extension and the Tasman Front can also be created, simply by enhancing the maximum wind stress curl.This study also highlights the many different ways in which the ocean responds to changes in wind forcing. The limitations of the work have also been highlighted. In particular, a large magnitude wind anomaly was required to form a discernible response in the ocean in terms of propagating Rossby waves, and transport anomalies through the

Tasman Sea. Propagation of Rossby waves across the Tasman Sea were not necessarily translated into a enhanced southward transport. This likely related to the resolution of the model as discussed above

Further work could be done utilising a higher resolution eddy resolving model to ensure that the processes at the separation point, and hence transport of the EAC Extension and Tasman Front were more realistic. It could also be used to see if the Kelvin wave propagation characteristics were closer to observed speeds, and to explore whether the efficiency of energy transfer between barotropic and baroclinic modes is improved. Lastly, a higher resolution and hence less diffuse model with a more realistic (stronger) EAC Extension would mean that more realistic increases in wind stress could be explored.

CHAPTER 7

Conclusions

The aim of this thesis is to investigate low frequency variability in the East Australian Current system. This study produces considerable new insight into the nature of decadal variability in the East Australian Current, its relationship with gyre scale circulation and wind forcing and the role of ENSO and SAM. I utilize ocean timeseries observations, atmospheric and ocean reanalyses, and idealised model forcing experiments to build a picture of the drivers of South Pacific decadal variability and related dynamics. I explore the relationship between observed variability in the EAC extension and wind stress (chapter 3), the broader decadal variability in the Tasman Sea/EAC system (chapter 4), and investigate the mechanisms by which the ocean responds to wind forcing (chapter 5/6).

Initial research questions were:

1. What is the relationship between the changes in the South Pacific winds, the South Pacific wind driven gyre, and observed changes in the South Tasman Sea?

2. How is observed EAC variability related to the regional current system? Can we build a picture of regional decadal variability using new 50-year ocean state estimates?

3. What are the mechanisms by which the ocean communicates remote South Pacific wind forcing to changes in the EAC, and how is this achieved within a few years, when the first mode baroclinic response would take 10-20 years?

7.1 Summary of Results

The key findings of this thesis are summarised below.

Chapter 3

- Increased wind stress curl in the South Pacific has caused the East Australia Current to strengthen over 60 years, causing waters off of Tasmania to become gradually warmer and saltier. SST is rising at 2-3 x the rate of global mean SST.

- The EAC also shows strong decadal variability. There is a very close relationship between variability in the South Pacific winds and variability in the EAC current system.

- The variability in SST at Maria Island Coast Station is closely related to decadal ENSO variability. The long term trend is related to the trend in the Southern Annular Mode

- The EAC variability lags wind stress variability in the central South Pacific by 3 years. This is too fast for 1st Mode baroclinic Rossby waves which would take 10-15 years to reach Australia from the central South Pacific.

Chapter 4

- There is an anti-correlation between the EAC Extension and the Tasman Front, caused by a gating at the point of separation of the EAC. When the

EAC Extension is stronger, the southern part of the South Pacific gyre to the east of New Zealand is more pronounced forming a double gyre structure.

- Variability in the magnitude of the wind stress curl causes the anticorrelation between the EAC and the Tasman Front. Enhanced wind stress curl maximum (38-45°S) favours the EAC extension over the Tasman Front.

- The anticorrelation between the EAC and the Tasman Front represents two gyre circulation patterns. An enhanced double gyre structure, with a circulation cell to the east of New Zealand is seen during an EAC Extension favoured state. A gyre confined mostly to the north of New Zealand is seen during a Tasman Front favoured state.

- Decadal variability in South Pacific wind stress curl and hence South Pacific gyre circulation, including the anticorrelation in the transports of the EAC Extension and the Tasman Front have been related to decadal ENSO variability.

Chapter 6

- A Rapid mechanism of adjustment in the South Pacific gyre has been demonstrated, which allows the EAC system to respond to changes in South Pacific winds within a few years. Fast barotropic Rossby waves interact with islands and ridges to spawn baroclinic modes in the Tasman Sea, modifying the strength of the regional currents.

- The anticorrelation between the EAC extension and the Tasman Front has been demonstrated by simply enhancing the wind stress curl maximum in the South Pacific.

- Low frequency variability in the strength of the EAC and Tasman Front has

been demonstrated in model experiments by single pulse of enhanced wind. This shows that the oceans have intrinsic decadal variability, related to a combination of barotropic and baroclinic Rossby waves, and their interaction with ridges and islands causing multiple mechanisms by which the ocean responds to changes in forcing.

These findings all contribute to building a picture of decadal variability in the South Pacific, its forcing, and its manifestation in the western boundary current system.

7.2 Synthesis of ideas: the building blocks of decadal variability in the extratropical South Pacific

Analysis of observations, ocean and atmospheric reanalysis products, and idealised model forcing experiments allows new insights into decadal variability in the South Pacific to be established. Decadal variability in the oceans can be considered in terms of atmospheric and oceanic teleconnections.

Wind stress varies on many timescales. Generally, wind variability is associated with high frequency (weather) timescale events. However, wind patterns also vary on longer timescales. In the subtropical South Pacific, the wind stress has strong interannual and decadal timescale variability.

Low frequency variability in the South Pacific wind stress curl is closely related to low frequency variability in the Southern Oscillation Index, the atmospheric component of the El Niño-Southern Oscillation. The two are connected via an atmospheric teleconnection from the equatorial Pacific to the extratropical South Pacific called the Pacific-South American (PSA) Mode. La Niña-like conditions cause strengthened wind stress curl in the central and eastern South Pacific. The PSA mode shows variability on interannual as well as decadal timescales. Due to the nature and timescale of ocean variability and propagation speed of signals in the extratrop-

ical oceans, the higher frequency variability is filtered out, and the decadal timescale variability dominates.

Much of the research into the relationship between ENSO and the East Australia Current has focused on oceanic teleconnections from the equatorial Pacific. It was argued that the ENSO signal reached the coast of northern Australia, but propagated anti-clockwise around the west coast of Australia as a coastal Kelvin wave, therefore having negligible effects on the East Australia Current System (Feng et al., 2003; Hsieh & Hamon, 1991). However, as discussed above, the main way in which ENSO variability is communicated to the EAC system is via an atmospheric teleconnection to the central South Pacific, and gyre scale response via Rossby waves which propagate to the western boundary of the South Pacific.

Recent literature has focussed on the role of the trend in the Southern Annular Mode (SAM) in spinning up the gyre over the 1990's. However, this study shows that the 1990's spin up is predominantly caused by decadal variability related to ENSO, although this is superimposed on a long term trend, which is likely linked to SAM. Moreover, decadal variability in the gyre seems more related to the shape of the gyre than the absolute strength of the gyre, with two distinct gyre scale circulation patterns being identified on decadal timescales.

The timescales at which the EAC responds to changes in wind stress appears to be related to the interaction of baroclinic and barotropic Rossby waves with islands and ridges. The conversion of barotropic to baroclinic energy around islands and across ocean ridges are necessary for the western boundary current to respond to changes in wind forcing on timescales of 3 years as observed. Pure baroclinic processes would take more than 10 years.

The interaction of Rossby waves with islands and ridges also produces multiple pathways by which the signal is communicated to the western boundary of the

ocean basin. This means that the ocean can produce its own decadal timescale variability, in addition to the external forcing of wind stress variability.

In the EAC current system, this decadal variability communicated as Rossby waves is enhanced by the position of New Zealand. Without New Zealand, the EAC would probably meander back and forth. Due to the position of New Zealand, the EAC is forced to chose between two distinct pathways on separation; either going to the north of New Zealand, or through the Tasman Sea.

7.3 Limitations of this study and further avenues of investigation

The 60 year long time series from the Maria Island coast station is the longest high quality ocean timeseries in the southern hemisphere. This data is a tremendous resource, and the primary inspiration for this thesis. The insight gained from this timeseries highlights the importance of long term monitoring programs for understanding low frequency variability and climate change signals. However, 60 years of data only gave 3-4 realisations of a decadal timescale signal. In Australia, a commitment has been made to continue and enhance this and other time series stations as part of the Integrated Marine Observing System. The importance of understanding decadal climate variability is discussed repeatedly in the Intergovernmental Panel on Climate Change (IPCC) 4th Assesment Report ;

"Many ocean observations are poorly sampled in space and time, and regional distributions often are quite heterogeneous. Furthermore, the observational records only cover a relatively short period of time (e.g., the 1950s to the present). Many of the observed changes have significant decadal variability associated with them, and in some cases decadal variability and/or poor sampling may prevent detection of long-term trends." (Bindoff et al., 2007)

As seen with the EAC, western boundary currents have the potential to amplify background low frequency variability and change, so make useful indicators of the nature of basin scale climate change and variability. It would therefore be useful to explore patterns of decadal variability in other western boundary currents, and explore how this is related to coastline orientation and bathymetry. However the lack of long term (longer than 50 year) observations makes this difficult. In terms of other Southern Hemisphere western boundary currents, very little was known about them. The mean state of the the Aghulas Current was only observed directly during the World Ocean Circulation Experiment (WOCE) in the 1980s and 1990s, and there is not enough data to gain an understanding of decadal variability or long term trends.

Similar to the EAC, variability in the Kuroshio Current, has been related to wind stress variability in the central north Pacific, with a lag of 3 years using a forecast model driven by NCEP-1 winds (Schneider & Miller, 2001). This time lag has been also related to Rossby wave dynamics. However, lack of direct observations also hamper understanding of variability in the Kuroshio Current. The utility of 50 year ocean reanalayses for understanding low frequency variations has been demonstrated in chapter 4. The importance of the PDO to fisheries has been documented in the literature, but little has been written about patterns of gyre scale circulation in the North Pacific. In the coming years, these new long ocean reanalyses have the potential to further our knowledge low frequency ocean processes, in the same way that atmospheric reanalyses have over the last decade.

I am able to determine the broad scale relationships between South Pacific wind forcing and the EAC system, in particular, the anti-correlation between the EAC extension and the Tasman Front, which is caused by variations in the magnitude of the South Pacific wind stress curl maximum (chapters 4 and 6). However, I

was not able to discern how this large scale forcing affects the separation process and hence the partitioning of EAC waters between the EAC Extension and the Tasman Front. Detailed understanding of the dynamics of this region would require a regional process study and high resolution modelling activity.

The results from idealised model experiments opens the door to new perspectives on the mechanisms of decadal variability in the oceans (Chapter 6). While previous studies have suggested that 1st mode baroclinic physics is sufficient to explain patterns of SSH variability, results from this study suggest that it is one of multiple ways in which the ocean can respond to changes in wind stress. Moreover, this study demonstrates that a fast mechanism of response is feasible, with a combination of barotropic and baroclinic Rossby waves interacting with islands and ridges. However, further work is needed to understand how these processes play out in the real ocean. For instance, Tanaka & Ikeda (2004) suggest that the nature of the ocean's response to wind forcing and the relative importance of barotropic and baroclinic energy is dependant on the frequency of the wind forcing. Also, the nature of the interaction of Rossby waves with bathymetry is related to the frequency of forcing, and the size (width and height) of the ridge. Exploration of the response of the ocean to different frequencies of wind forcing was beyond the scope of this project.

The coarse resolution of the model meant that the net transport through the Tasman Sea was northward, rather than southward (as discussed in Chapters 3 and 4). Higher resolution model runs would mean that the EAC system is more realistically represented, and processes at the point of separation could be explored in more detail. Results suggest that the response of the modelled ocean to wind forcing was damped. This is also likely to be related to the model resolution, and the dissipation and friction terms needed to ensure numerical stability. The impact of resolution on propagating features was discussed in Chapter 6 in detail. In particular, Kelvin wave

propagation speeds appear to be slowed slightly by the low resolution of the model. Higher resolution model runs with detailed analysis of the propagation speeds of Kelvin and Rossby waves, and also the magnitude of the ocean's response to wind forcing would be a useful extension of this work.

7.4 Consequences of this work

Changes in the range of species across a number of marine taxa have been related to changes in the strength of the EAC (Edgar, 2000; Thresher et al., 2003). An assessment of the potential impact of climate change on marine life in Australia concludes the projected strengthening EAC and the continued warming of the south Tasman Sea will have a detrimental effect on cold-temperate species in South East Australia, particularly in Tasmanian waters (Poloczanska et al., 2007). Such ecosystem shifts will also impact on commercially important fisheries, such as abalone and rock lobster. Results from this work suggest that observed ecosystem changes are likely linked to changes in ocean circulation driven by changes in basin-scale winds. However, long term observations are needed to distinguish between trends and low frequency variability. To this end, I conclude that both low frequency variability related to decadal ENSO, and a long term trend related to the Southern Annular Mode, are the cause of oberved changes in the EAC system. The recent strengthening of the EAC extension and associated range extension of species is likely related to low frequency variability as well as a long term trend (Qiu & Chen, 2006; Roemmich et al., 2007; Cai et al., 2005). On decadal timescales, the EAC strengthe ned during the mid to late 1990's, peaked in strength in 2002 and has since been weakening. Strategies for management of marine resources in southeastern Australia will need to take into account the response of regional oceanographic conditions to climate variability in the context of climate change.

BIBLIOGRAPHY

Anderson, D. L. T. & Corry, R. A. (1985). Ocean response to low frequency wind forcing with application to the seasonal variation in the Florida Straits - Gulf stream transport. *Progress in Oceanography*, 14, 7–40. article.

Bindoff, N., Willebrand, J., Artale, V., Cazenave, A., Gregory, J., Gulev, S., Hanawa, K., Qur, C. L., Levitus, S., Nojiri, Y., Shum, C., Talley, L., & Unnikrishnan, A. (2007). *Observations: Oceanic Climate Change and Sea Level. In: Climate Change 2007: The Physical Science Basis. Contribution of Working Group I to the Fourth Assessment Report of the Intergovernmental Panel on Climate Change.* Technical report, Cambridge University Press.

Boland, F. M. & Church, J. A. (1981). The East Australian Current, 1978. *Deep Sea Res.*, 28a, 937–957. article.

Boland, F. M. & Hamon, B. V. (1970). The East Australian Current, 1965-68. *Deep Sea Res.*, 17, 777–794. article.

Bostock, H. C., Opdyke, B. N., Gagan, M. K., Kiss, A. E., & Fifield, L. K. (2006). Glacial/Interglacial changes in the East Australian Current. *Climate Dynamics*, (pp. DOI 10.1007/s00382-005-0103-7). article.

Bromwich, D. & Wang, S. (2008). A review of the temporal and spatial variability of Arctic and Antarctic atmospheric circulation based upon ERA-40. *Dynamics of Atmospheres and Oceans*, 44, 213–243.

Bromwich, D. L. & Fogt, R. L. (2004). Strong trends in the skill of the ERA-40 and NCEP-NCAR reanalyses in the high and midlatitudes of the Southern Hemisphere. *Journal of Climate*, 17(23), 4603–4619. article.

Bryan, K. & Lewis, L. J. (1979). A water mass model of the world ocean. *Journal of Geophysical Research*, 84, 2503–2517. article.

Cai, W. (2006). Antarctic ozone depletion causes an intensification of the Southern Ocean super-gyre circulation. *Geophysical Research Letters*, 33(3), L03712. article.

Cai, W., G, G. S., & Cowan, T. (2005). The response of the Southern Annular Mode, the East Australian Current, and the southern mid-latitude ocean circulation to global warming. *Geophysical Research Letters*, 32(23), L23706. article.

Carton, J., Giese, B., & Grodsky, S. (2005). Sea level rise and the warming of the oceans in the Simple Ocean Data Assimilation (SODA) reanalysis. *Journal of Geophysical Research*, 110, doi:10.1029/2004JC002817.

Carton, J. A. & Giese, B. S. (2006). A reanalysis of ocean climate using Simple Ocean Data Assimilation SODA. *Monthly Weather Review*, 136(8), 2999–3017. article.

Casey, K. C. & Cornillion, P. (2001). Global and regional surface temperature trends. *Journal of Climate*, 14, 3801–3818. article.

Chelton, D. B., DeSzoeke, R. A., Schlax, M. G., El Naggar, K., & Siwertz, N. (1998). Geographical variability of the first baroclinic Rossby radius of deformation. *Journal of Physical Oceanography*, 28(3), 433–460.

Cresswell, G. R. (2000). Currents of the continental shelf and upper slope of Tasmania. *Papers and Proceedings of the Royal Society of Tasmania*, 133, 21–30. article.

Dunn, J. & Ridgway, K. (2002). Mapping ocean properties in regions of complex topography. *Deep-sea research part 1 - Oceanographic Research*, 49, 591–604.

Edgar, G. (2000). *Australian marine life : the plants and animals of temperate waters.* Sydney: Reed New Holland, rev. edition.

Feng, M., Meyers, G., Pierce, A., & Wijffels, S. (2003). Annual and interannual variations in the Leeuwin Current at 32°s. *Journal of Geophysical Research*, 108(C11), doi:10.1029/2002JC001763.

Folland, C. K., Parker, D. E., Colman, A. W., & Washington, R. (1998). *Large scale modes of ocean surface temperature since the late nineteenth century.* Climate Research Technical Note CRTN 81, Hadley Centre, UK Meteorological Office. techreport.

Fu, L. (2004). Latitudinal and frequency characteristics of westward propagation of large-scale oceanic variability. *Journal of Physical Oceanography*, 34, 1907–1921.

Fu, L. L. & Davidson, R. (1995). A note on the barotropic response of sea level to time dependant wind forcing. *Journal of Geophysical Research*, 100, 24955 – 24964. article.

Garreaud, R. D. & Battisti, D. S. (1999). Interannual (ENSO) and interdecadal (ENSO-like) variability in the Southern hemisphere tropospheric circulation. *Journal of Climate*, 12, 2113–2123. article.

Gill, A. E. (1982). *Atmosphere-Ocean Dynamics.* New York: Academic Press. book.

Gill, A. E. & Niiler, P. P. (1973). The theory of the seasonal variability in the ocean. *Deep Sea Res.*, 20, 141 –178. article.

Gnanadesikan, A., Dixon, K. W., Griffies, S. M., Balaji, V., Barreiro, M., Beesley, J. A., Cooke, W. F., Delworth, T. L., Gerdes, R., Harrison, M. J., Held, I. M., Hurlin, W. J., Lee, H. C., Liang, Z., Nong, G., Pacanowski, R. C., Rosati, A., Russell, J., Samuels, B. L., Song, Q., Spelman, M. J., Stouffer, R. J., Sweeney, C. O., Vecchi, G., Winton, M., Wittenberg, A. T., Zeng, F., Zhang, R., & Dunne, J. P. (2006). GFDL's CM2 global coupled climate models. part ii: The baseline ocean simulation. *Journal of Climate*, 19(5), 675–697.

Godfrey, J. S. (1989). A sverdrup model of the depth-integrated flow for the world ocean allowing for island circulations. *Geophysical and Astrophysical Fluid Dynamics*, 45, 89–112. article.

Godfrey, J. S., Cresswell, G. R., Golding, T. J., Pearce, A. F., & Boyd, R. (1980). The separation of the East Australian Current. *Journal of Physical Oceanography*, 10, 430–440. article.

Gordon, A. L. (1986). Interocean exchange of thermocline water. *Journal of Geophysical Research*, 91, 5037–5046. article.

Griffies, S., Pacanowski, R., & Rosati, A. (2004). *A technical guide to MOM4*. GFDL Ocean Group Technical Report 5, NOAA/Geophysical Fluid Dynamics Laboratory. techreport.

Grotjan, R. (2008). Different data, different general circulations? a comparison of selected fields in NCEP/DOE AMIP-II and ECMWF ERA-40 reanalyses. *Dynamics of Atmospheres and Oceans*, 44, 108–142.

Hare, S., Mantua, N., & Francis, R. (1999). Inverse production regimes: Alaska and West Coast Pacific salmon. *Fisheries*, 24(1), 6–14.

Harris, G., Nilsson, C., Clementson, L., & Thoman, D. (1987). The watermasses of the east coast of Tasmania: Seasonal and interannual variability and the influence on phytoplankton biomass and productivity. *Aust. J. Mar. Freshwater Res.*, 38, 569–590. article.

Harris, G. P., Davies, P., Nunz, M., & Meyers, G. (1988). Interannual variability in climate and fisheries in Tasmania. *Nature*, 333, 754–756. article.

Helfrich, K., Pedlosky, J., & Carter, E. (1999). The shadowed island. *Journal of Physical Oceanography*, 29, 2559–2577.

Hines, K., D.H.Bromwich, & Marshall, G. (2000). Artificial surface pressure trends in the NCEP-NCAR Reanalysis over the Southern Ocean and Antarctica. *Journal of Climate*, 13, 3940–3952.

Hobday, A. & Hartmann, K. (2006). Near real time spatial management based on habitat predictions for a longline bycatch species. *Fisheries Management and Ecology*, 13, 365–380.

Hsei, W., Davey, M., & Wajsowicz, R. (1983). The free Kelvin wave in finite-difference numerical models. *Journal of Physical Oceanography*, 13, 1383–1397.

Hsieh, W. W. & Hamon, B. V. (1991). The El Niño Southern Oscillation in South Eastern Australian Waters. *Aust. J. Mar. Freshwater Res.*, (pp. 263–275). article.

Johnson, C., Ling, S., Ross, J., Shepherd, S., & Miller, K. (2005). *Establishment of the long-spined sea urchin (Centrostephanus rodgersii) in Tasmania: First assesment of potential threats to fisheries*. Technical Report 2001/044, FDRC Final Report. techreport.

Kalnay, E., Kanamitsu, M., Kistler, R., Collins, W., D.Deavern, L.Gandin, Iredell, M., S.Saha, G.White, J.Woolen, Y.Zhu, M.Chelliah, Ebisuzaki, W., Higgins, W., J.Janowiak, K.C.Mo, Ropelewski, C., J.Wang, Leetma, W., Reynolds, R., Jenne, R., & Joseph, D. (1996). The NCEP/NCAR 40-year reanalysis project. *Bull. Amer. Met. Soc.*, 77, 347–471. article.

Karoly, D. J. (1989). Southern hemisphere circulation features associated with El nino - Southern Oscillation events. *Journal of Climate*, 2, 1239–1252. article.

Kessler, W. S. & Taft, B. A. (1987). Dynamic heights and zonal geostrophic transports in the central tropical Pacific during 1979-1984. *Journal of Physical Oceanography*, 17, 97–122. article.

Killworth, P., Chelton, D., & DeSzoeke, R. (1997). The speed of observed and theoretical long extratropical planetary waves. *Journal of Physical Oceanography*, 27(9), 1946–1966.

Kilworth, P. & Blundell, J. (2005). The dispersion relation for planetary waves in the presence of mean flow and topography. part ii: Two dimensional examples and global results. *Journal of Physical Oceanography*, 35(11), 2110–2133.

Kistler, R., Kalnay, E., Collins, W., Saha, S., White, G., Woollen, J., Chelliah, M., Ebisuzaki, W., Kanamitsu, M., Kousky, V., van den Dool, H., Jenne, R., & Fiorino, M. (2001). NCEP-NCAR 50 year reanalysis: Monthly means CD-ROM and documentation. *Bulletin of the American Meteorological Society*, 82, 247–267. article.

Koehl, A., Dommenget, D., Ueyoshi, K., & Stammer, D. (2006). *The Global ECCO 1952-2001 Ocean Synthesis.* Technical Report 40, Institut fur Meerseskunde University of Hamburg.

Koehl, A. & Stammer, D. (2007). *Decadal sea level changes in the 50-year GECCO ocean synthesis.* Technical Report 44, Institut fur Meereskunde Zentrum fur Meeres- und Klimaforschung Universitat Hamburg.

Kushner, P. J., Held, I. M., & Delworth, T. L. (2001). Southern Hemisphere atmospheric circulation response to global warming. *Journal of Climate*, 14, 2238–2246. article.

Latif, M. & Barnett, T. (1996). Decadal climate variability in the North Pacific and North america: Dynamics and predictability. *Journal of Climate*, 9, 2407–2423.

L'Heureux, M. L. & Thompson, D. W. J. (2006). Observed relationships between the El Nino-Southern Oscillation and the extratropical zonal mean circulation. *Journal of Climate*, 19, 276–287. article.

Li, J. & Clarke, A. (2004). Coastline direction, interannual flow and the strong El Niño currents along Australia's nearly zonal southern coast. *Journal of Physical Oceanography*, 34, 2373–2381.

Ling, S. (2008). Range expansion of a habitat-modifying species leads to loss of taxonomic diversity: a new and impoverished reef state. *Oecologica*, 156(4), 883–894.

Ling, S., Johnson, C., Frusher, S., & King, C. (2008). Reproductive potential of a marine ecosystem engineer at the edge of a newly expanded range. *Global Change Biology*, 14, doi.

Liu, Z., Wu, L., & Hurbert, H. (1999). Rossby wave - coastal Kelvin wave interaction in the extratropics. part ii: Formation of island circulation. *Journal of Physical Oceanography*, 29, 2405–2418.

Lu, Y. & Stammer, D. (2004). Vorticity balance in coarse-resolution global ocean simulations. *Journal of Physical Oceanography*, 34(3), 605–622.

Lyne, V., Thresher, R., & Rintoul, S. (2005). Regional impacts of climate change and variability in South East Australia.

Mantua, N., Hare, S., Zhang, Y., Wallace, J., & Francis, R. (1997). A pacific interdecadal climate oscillation with impacts on salmon production. *Bulletin of the American Meteorological Society*, 78, 1069–1079.

Mata, M. M., Tomczak, M., Wijffels, S., & Church, J. A. (2000). East Australian Current volume transports at 30°S: Estimates from the World Ocean Circulation Experiment hydrographic sections PR11/P6 and the PCM3 current meter array. *Journal of Geophysical Research*, 105(C12), 28509 - 28526. article.

Matano, R. P., Beier, E. J., Strub, P. T., & Tokmakian, R. (2002). Large-scale forcing of the Agulhas variability: The seasonal cycle. *Journal of Physical Oceanography*, 32, 1228 - 1241. article.

McCreary, J. (1984). Equatorial beams. *Journal of Marine Research*, 42, 395–430. article.

Mo, K. C. (2000). Relationships between low-frequency variability in the Southern Hemisphere and sea surface temperature anomalies. *Journal of Climate*, 13(20), 3599–3610.

Moore, M. & Wilkin, J. (1998). Variability in the South Pacific deep western boundary current from current meter observations and a high resolution global model. *Journal of Geophysical Research*, 103(C5), 5439–5457.

Morris, M., Roemmich, D., & Cornuelle, B. (1996). Observations of variability in the South Pacific subtropical gyre. *Journal of Physical Oceanography*, 26, 2359–2379. article.

Mulhearn, P. (1987). The Tasman Front - A study using satellite infrared imagery. *Journal of Physical Oceanography*, 17(8), 1148–1155.

Nilsson, C. S. & Cresswell, G. R. (1980). The formation and evolution of East Australian Current warm core eddies. *Progress in Oceanography*, 9, 133–183. article.

Oke, P., Brassington, G., Griffin, D., & Schiller, A. (2008). The BlueLINK ocean data assimilation system. *Ocean Modelling*, 21, 46–70.

Oke, P. R. & England, M. H. (2004). Oceanic response to changes in tthe latitude of the southern hemisphere subpolar westerly winds. *Journal of Climate*, 17, 1040 – 1054. article.

Owen, G., Wilmot, A., Abrahams, I., & Mansley, H. (2005). The scattering of Rossby waves from finite abrupt topography. *Geophysical and Astrophysical fluid dynamics*, 99(3), 219–239.

Pedlosky, J. (1979). *Geophysical Fluid Dynamics.* New York: Springer-Verlag. book.

Pedlosky, J. (1996). *Ocean Circulation Theory.* New York: Springer. Book.

Poloczanska, E. S., Babcock, R. C., Butler, A., Hobday, A. J., Hoegh-Guldberg, O., Kunz, T. J., Matear, R., Milton, D., Okey, T. A., & Richardson, A. J. (2007). Climate change and Australian marine life. *Oceanography and Marine Biology: an annual review*, 45, 407–478. article.

Pond, S. & Pickard, G. L. (1983). *Introductory Dynamical Oceanography, 2nd Edition.* Jordon Hill, Oxford: Butterworth-Heinemann. book.

Power, S., Casey, T., Folland, C., Colman, A., & Mehta, V. (1999). Interdecadal modulation of the impact of ENSO on Australia. *Climate Dynamics*, 15, 319–324. article.

Power, S., Haylock, M., Colman, R., & Wang, Z. (2006). The predictability of inter-decadal changes in ENSO activity and ENSO teleconnections. *Journal of Climate*, 38(18), 4755–4771.

Pratt, L. & Pedlosky, J. (1998). Barotropic circulation around islands with friction. *Journal of Physical Oceanography*, 28.

Pratt, L., Spall, M., & Helfrich, K. (1997). Circulation around islands and ridges. *Journal of Marine Research*, 55, 1199–1251.

Qiu, B. & Chen, S. (2006). Decadal variability in the large-scale sea surface height field of the South Pacific Ocean: Observations and Causes. *Journal of Physical Oceanography*, 36(9), 1751–1762. article.

Qu, T. & Lindstrom, E. J. (2002). A climatological interpretation of the circulation in the western South Pacific. *Journal of Physical Oceanography*, 32, 2492–2508.

Rabe, B., Schott, F., & Koehl, A. (2008). Mean circulation variability of the tropical Atlantic during 1952-2001 in the GECCO assimilation fields. *Journal of Physical Oceanography*, 38, 117–1192.

Reid, J. L. (1986). On the total geostrophic circulation of the South Pacific Ocean: Flow patterns, tracers and transports. *Progress in Oceanography*, 16, 1–61. article.

Renwick, J. A. (2004). Trends in the Southern Hemisphere subpolar vortex in NCEP and ECMWF reanalyses. *Journal of Geophysical Research*, 31(7), art. no. L07209. article.

Ridgway, K. (2008). Decadal variability of East Australian Current transport inferred from repeat high density XBT transects, a CTD survey and satellite Altimetry. *Journal of Geophysical Research*.

Ridgway, K., Dunn, J., & Wilkin, J. (2002). Ocean interpolation by 4-dimensional weighted least squares - application to the waters around Australasia. *Journal of Atmospheric and Oceanic Technology*, 19(9), 1357–1375.

Ridgway, K. R. (2007). Long term trend and decadal variability of the southward penetration of the East Australia Current. *Geophysical Research Letters*, 34(L13613), doi: 10.129/2007GL030393.

Ridgway, K. R. & Dunn, J. R. (2003). Mesoscale structure of the East Australian Current system and its relationship with topography. *Progress in Oceanography*, 56, 189 – 222.

Ridgway, K. R. & Godfrey, J. S. (1994). Mass and heat budgets in the East Australian Current: A direct approach. *Journal of Geophysical Research*, 99, 3231–3248.

Ridgway, K. R. & Godfrey, J. S. (1997). Seasonal cycle of the East Australian Current. *Journal of Geophysical Research*, 102, 22921 – 22936.

Roemmich, D. & Cornuelle, B. (1990). Observing the fluctuations of gyre-scale ocean circulation: A study of the subtropical South Pacific. *Journal of Physical Oceanography*, 20, 1919–1934.

Roemmich, D., Gilson, J., Davies, R., Sutton, P., Wijffels, S., & Riser, S. (2007). Decadal spin up of the deep subtropical gyre in the South Pacific. *Journal of Physical Oceanography*, 37, 162 – 173.

Roemmich, D., Gilson, J., Willis, J., Sutton, P., & Ridgway, K. (2005). Closing the time-varying mass and heat budgets for large ocean areas: The Tasman Box. *Journal of Climate*, 18, 2330–2343.

Sasaki, Y., Minobe, S., Kagimoto, T., Nonaka, M., & Sasaki, H. (2008). Decadal sea level variability in the South Pacific in a global eddy resolving model. *Journal of Physical Oceanography*, 38, 1731–1747.

Schiller, A., Oke, P., Brassington, G., Entel, M., Fiedler, R., Griffin, D., & Mansbridge, J. (2008). Eddy resolving ocean circulation in the Asian-Australian region from an ocean reanalysis effort. *Progress in Oceanography*, 76, 309–316.

Schneider, N. & Cornuelle, B. D. (2005). The forcing of the Pacific Decadal Oscillation. *Journal of Climate*, 18(21), 4355–4373.

Schneider, N. & Miller, A. J. (2001). Predicting western North Pacific climate. *Journal of Climate*, 14, 2997–4002.

Schneider, N., Miller, A. J., & Pierce, D. W. (2002). Anatomy of North Pacific Decadal variability. *Journal of Climate*, 15, 586 – 605.

Schott, F., Lee, T., & Zantopp, R. (1988). Variability in the structure and transport of the florida current in period range of days to seasonal. *Journal of Physical Oceanography*, 18, 1209–1234.

Smith, T. M. & Reynolds, R. W. (2004). Improved extended reconstruction of SST based on COADS data (1854-1997). *Journal of Climate*, 17, 2466–2477.

Smith, W. H. F. & Sandwell, D. T. (1997). Global seafloor topography from satellite altimetry and ship depth soundings. *Science*, 277, 1957–1962.

Sprintall, J., Roemmich, D., Stanton, B., & Bailey, R. (1995). Regional climate variability and ocean heat transport in the south-west Pacific Ocean. *J. Geophys. Res.*, 100(C8), 15865–15871.

Sutton, P., Bowen, M., & Roemmich, D. (2005). Decadal temperature changes in the Tasman Sea. *New Zealand Journal of Marine and Freshwater Research*, 39, 1321–1329.

Tanaka, K. & Ikeda, M. (2004). Propagation of Rossby waves over ridges excited by interannual wind forcing in a Western North Pacific mode. *Journal of Oceanography*, 60, 329–340.

Tennant, W. (2004). Considerations when using pre-1979 NCEP/NCAR reanalyses in the Southern Hemisphere. *Journal of Geophysical Research*, 31(11), art. no. L11112.

Thompson, D. W. J. & Solomon, S. (2002). Interpretation of recent Southern Hemisphere climate change. *Science*, 296, 895–899.

Thresher, R., Proctor, C., Ruiz, G., Gurney, R., MacKinnon, C., Walton, W., Rodriguez, L., & Bax, N. (2003). Invasion dynamics of the European shore crab, *Carcinus maenas*, in Australia. *Marine Biology*, 142(5), 867–876.

Thresher, R., Rintoul, S. R., Koslow, A. J., Weidman, C., Adkins, J., & Proctor, C. (2004). Oceanic evidence of climate change in southern Australia over the last 3 centuries. *Geophysical Research Letters*, 31, L07212, doi:10.1029/2003GLO18869.

Thresher, R. E. (2002). Solar correlates of Southern Hemisphere mid latitude climate variability. *International Journal of Climatology*, 22, DOI:10.10002/joc.768.

Tilburg, C. E., Hurlburt, H. E., O'Brien, J. J., & Shriver, J. F. (2001). The dynamics of the East Australian Current system: the Tasman Front, the East Auckland Current and the East Cape Current. *Journal of Physical Oceanography*, 31, 2917 – 2943.

Torrence, C. & Compo, G. (1998). A practical guide to Wavelet analysis. *Bulletin of the American Meteorological Society*, 79(1), 61–78.

Trenberth, K. (1984). Signal verses noise in the Southern Oscillation. *Monthly Weather Review*, 112, 326–332.

Uppala, S. M., Kllberg, P. W., Simmons, A. J., Andrae, U., da Costa Bechtold, V., Fiorino, M., Gibson, J. K., Haseler, J., Hernandez, A., Kelly, G. A., Li, X., Onogi, K., Saarinen, S., Sokka, N., Allan, R. P., Andersson, E., Arpe, K., Balmaseda, M. A., Beljaars, A.

C. M., van de Berg, L., Bidlot, J., Bormann, N., Caires, S., Chevallier, F., Dethof, A., Dragosavac, M., Fisher, M., Fuentes, M., Hagemann, S., Hlm, E., Hoskins, B. J., Isaksen, L., Janssen, P. A. E. M., Jenne, R., McNally, A. P., Mahfouf, J. F., Morcrette, N. A., Rayner, N. A., Saunders, R. W., Simon, P., Sterl, A., Trenberth, K. E., Untch, A., Vasiljevic, D., Viterbo, P., & Woollen, J. (2005). The ERA-40 Reanalysis. *Quarterly Journal of the Royal Meteorological Society*, 131, 2961–3012.

Veronis, G. & Stommel, H. (1956). The action of variable wind stresses on a stratified ocean. *Journal of Marine Research*, 15, 43–75.

Wajsowicz, R. C. (1993). The circulation of the depth-intergrated flow around an island with application to the indonesian throughflow. *J. Phys. Oceanog.*, 23, 1470–1484.

Weijer, W. & Gille, S. (2005). Adjustment of the Southern Ocean to wind forcing on synoptic timescales. *Journal of Physical Oceanography*, 35, 2076–2089.